Pertanika Journal of

SCIENCE & TECHNOLOGY

JST

VOL. 34 (S2) 2026

A Special Issue devoted to

Innovating Sustainable Materials and Technologies for a Greener, Resilient, and Sustainable Future

Guest Editors

Rohana Hassan, Mohd Fadzil Arshad, and Fauzi Baharudin

PERTANIKA JOURNALS

A scientific journal published by Universiti Putra Malaysia Press

Pertanika Journal of Science & Technology
Pertanika Journal of Science & Technology

PERTANIKA JOURNAL OF SCIENCE & TECHNOLOGY

About the Journal

Overview

Pertanika Journal of Science & Technology is an official journal of Universiti Putra Malaysia. It is an open-access online scientific journal. It publishes original scientific outputs. It neither accepts nor commissions third party content.

Recognised internationally as the leading peer-reviewed interdisciplinary journal devoted to the publication of original papers, it serves as a forum for practical approaches in improve quality on issues pertaining to science and engineering and its related fields.

Pertanika Journal of Science & Technology currently publishes 6 issues a year (*February, April*, *June, August, October, and December*). It is considered for publication of original articles as per its scope. The journal publishes in **English** and it is open for submission by authors from all over the world.

The journal is available world-wide.

Aims and Scope

Pertanika Journal of Science & Technology aims to provide a forum for high quality research related to science and engineering research. Areas relevant to the scope of the journal include: bioinformatics, bioscience, biotechnology and bio-molecular sciences, chemistry, computer science, ecology, engineering, engineering design, environmental control and management, mathematics and statistics, medicine and health sciences, nanotechnology, physics, safety and emergency management, and related fields of study.

History

Pertanika Journal of Science & Technology was founded in 1993 and focusses on research in science and engineering and its related fields.

Vision

To publish a journal of international repute.

Mission

Our goal is to bring the highest quality research to the widest possible audience.

Quality

We aim for excellence, sustained by a responsible and professional approach to journal publishing. Submissions can expect to receive a decision within 90 days. The elapsed time from submission to publication for the articles averages 180 days. We are working towards decreasing the processing time with the help of our editors and the reviewers.

Abstracting and Indexing of Pertanika

Pertanika Journal of Science & Technology is now over 33 years old; this accumulated knowledge and experience has resulted the journal being abstracted and indexed in SCOPUS (Elsevier), Journal Citation Reports (JCR-Clarivate), EBSCO, ASEAN CITATION INDEX, Microsoft Academic, Google Scholar, and MyCite.

Citing Journal Articles

The abbreviation for Pertanika Journal of Science & Technology is *Pertanika J. Sci. & Technol.*

Publication Policy

Pertanika policy prohibits an author from submitting the same manuscript for concurrent consideration by two or more publications. It prohibits as well publication of any manuscript that has already been published either in whole or substantial part elsewhere. It also does not permit publication of manuscript that has been published in full in proceedings.

Code of Ethics

The *Pertanika* journals and Universiti Putra Malaysia take seriously the responsibility of all of its journal publications to reflect the highest in publication ethics. Thus, all journals and journal editors are expected to abide by the journal's codes of ethics. Refer to *Pertanika*'s **Code of Ethics** for full details, or visit the journal's web link at http://www.pertanika.upm.edu.my/code_of_ethics.php

Originality

The author must ensure that when a manuscript is submitted to *Pertanika*, the manuscript must be an original work. The author should check the manuscript for any possible plagiarism using any programme such as Turnitin or any other software before submitting the manuscripts to the Editorial Office, *Pertanika* Journal Publication Section.

All submitted manuscripts must be in the journal's acceptable similarity index range:

≤ 20% – PASS; > 20% – REJECT.

International Standard Serial Number (ISSN)

An ISSN is an 8-digit code used to identify periodicals such as journals of all kinds and on all media–print and electronic.

Pertanika Journal of Science & Technology: e-ISSN 2231-8526 (Online).

Lag Time

A decision on acceptance or rejection of a manuscript is reached in 90 days (average). The elapsed time from submission to publication for the articles averages 180 days.

Authorship

Authors are not permitted to add or remove any names from the authorship provided at the time of initial submission without the consent of the journal's Chief Executive Editor.

Manuscript Preparation

For manuscript preparation, authors may refer to Pertanika's **INSTRUCTION TO AUTHORS**, available on the official website of *Pertanika*.

Editorial Process

Authors who complete any submission are notified with an acknowledgement containing a manuscript ID on receipt of a manuscript, and upon the editorial decision regarding publication.

Pertanika follows a **double-blind peer-review** process. Manuscripts deemed suitable for publication are sent to reviewers. Authors are encouraged to suggest names of at least 3 potential reviewers at the time of submission of their manuscripts to *Pertanika*, but the editors will make the final selection and are not, however, bound by these suggestions.

Notification of the editorial decision is usually provided within 90 days from the receipt of manuscript. Publication of solicited manuscripts is not guaranteed. In most cases, manuscripts are accepted conditionally, pending an author's revision of the material.

The Journal's Peer Review

In the peer-review process, 2 to 3 referees independently evaluate the scientific quality of the submitted manuscripts. At least 2 referee reports are required to help make a decision.

Peer reviewers are experts chosen by journal editors to provide written assessment of the **strengths** and **weaknesses** of the written research, with the aim of improving the reporting of research and identifying the most appropriate and highest quality material for the journal.

Operating and Review Process

What happens to a manuscript once it is submitted to *Pertanika*? Typically, there are 7 steps to the editorial review process:

1. The journal's Chief Executive Editor and Editor-in-Chief examine the paper to determine whether it is relevant to the journal's needs in terms of novelty, impact, design, procedure, language as well as presentation and allow it to proceed to the reviewing process. If it is not appropriate, the manuscript is rejected outright and the author is informed.

2. The Chief Executive Editor sends the article-identifying information having been removed, to 2 to 3 reviewers. They are specialists in the subject matter of the article. The Chief Executive Editor requests that they complete the review within 3 weeks.

   Comments to authors are about the appropriateness and adequacy of the theoretical or conceptual framework, literature review, method, results and discussion, and conclusions. Reviewers often include suggestions to strengthening of the manuscript. Comments to the editor are in the nature of the significance of the work and its potential contribution to the research field.

Pertanika Journal of Science & Technology
Pertanika Journal of Science & Technology

Pertanika Journal of Science & Technology
Pertanika Journal of Science & Technology

3. The Editor-in-Chief examines the review reports and decides whether to accept or reject the manuscript, invite the authors to revise and resubmit the manuscript, or seek additional review reports. In rare instances, the manuscript is accepted with almost no revision. Almost without exception, reviewers' comments (to the authors) are forwarded to the authors. If a revision is indicated, the editor provides guidelines to attend to the reviewers' suggestions and perhaps additional advice on how to revise the manuscript.

4. The authors decide whether and how to address the reviewers' comments and criticisms and the editor's concerns. The authors return a revised version of the paper to the Chief Executive Editor along with specific information describing how they have addressed' the concerns of the reviewers and editor, usually in a tabular form. The authors may also submit a rebuttal if there is a need especially when the authors disagree with certain comments provided by the reviewers.

5. The Chief Executive Editor sends the revised manuscript out for re-review. Typically, at least 1 of the original reviewers will be asked to examine the article.

6. When the reviewers have completed their work, the Editor-in-Chief examines their comments and decides whether the manuscript is ready to be published, needs another round of revisions, or should be rejected. If the decision is to accept, the Chief Executive Editor is notified.

7. The Chief Executive Editor reserves the final right to accept or reject any material for publication, if the processing of a particular manuscript is deemed not to be in compliance with the S.O.P. of *Pertanika*. An acceptance letter is sent to all the authors.

   The editorial office ensures that the manuscript adheres to the correct style (in-text citations, the reference list, and tables are typical areas of concern, clarity, and grammar). The authors are asked to respond to any minor queries by the editorial office. Following these corrections, page proofs are mailed to the corresponding authors for their final approval. At this point, **only essential changes are accepted**. Finally, the manuscript appears in the pages of the journal and is posted online.

Pertanika Journal of

SCIENCE & TECHNOLOGY

Vol. 34 (S2) 2026

A Special Issue devoted to
Innovating Sustainable Materials and Technologies for a Greener, Resilient, and Sustainable Future

Guest Editors
Rohana Hassan, Mohd Fadzil Arshad, and Fauzi Baharudin



A scientific journal published by Universiti Putra Malaysia Press

PJST
Pertanika Journal of Science & Technology
AN INTERNATIONAL PEER-REVIEWED JOURNAL

UNIVERSITY PUBLICATIONS COMMITTEE

CHAIRMAN
Zamberi Sekawi

EDITOR-IN-CHIEF
Mohamed Thariq Hameed Sultan
SEARCA Chair of Agriculture Technology and Innovation

JOURNAL SECTION
Head of Section:
Navaneetha Krishna Chandran

Journal Officers:
Ain Haziqah Ab Razak
Nur Izni Shafiqah Mohd Hamidi
Saundarya Saran

Editorial Assistants:
Zulinaardawati Kamarudin

Pre-press Officers:
Aisyah Umairah Jasmin
Engku Erina Zahirah Engku Mohd Suhaimi
Ku Ida Mastura Ku Baharom

IT Officer:
Kiran Raj Kaneswaran

Journal Section Office
Putra Science Park
1st Floor, IDEA Tower II
UPM-MTDC Technology Centre
Universiti Putra Malaysia
43400 UPM Serdang
Selangor, Malaysia

General Enquiry
Tel. No: +603 9769 1622
E-mail:
pertanika.proceeding@upm.edu.my
URL:
http://www.pertanika.upm.edu.my/

PUBLISHER
UPM Press Centre
Universiti Putra Malaysia
43400 UPM Serdang
Selangor, Malaysia
Tel: +603 9769 3606
E-mail: dir.penerbit@upm.edu.my
URL: http://penerbit.upm.edu.my

ASSOCIATE EDITOR
2024-2026

Miss Laiha Mat Kiah
Security Services Sn: Digital Forensic, Steganography, Network Security, Information Security, Communication Protocols, Security Protocols
Universiti Malaya, Malaysia

Saidur Rahman
Renewable Energy, Nanofluids, Energy Efficiency, Heat Transfer, Energy Policy
Sunway University, Malaysia

EDITORIAL BOARD
2024-2026

Abdul Latif Ahmad
Chemical Engineering
Universiti Sains Malaysia, Malaysia

Hsiu-Po Kuo
Chemical Engineering
National Taiwan University, Taiwan

Mohd. Ali Hassan
Bioprocess Engineering, Environmental Biotechnology
Universiti Putra Malaysia, Malaysia

Ahmad Zaharin Aris
Hydrochemistry, Environmental Chemistry, Environmental Forensics, Heavy Metals
Universiti Putra Malaysia, Malaysia

Ivan D. Rukhlenko
Nonliner Optics, Silicon Photonics, Plasmonics and Nanotechnology
The University of Sydney, Australia

Nor Azah Yusof
Biosensors, Chemical Sensor, Functional Material
Universiti Putra Malaysia, Malaysia

Azlina Harun@ Kamaruddin
Enzyme Technology, Fermentation Technology
Universiti Sains Malaysia, Malaysia

Lee Keat Teong
Energy Environment, Reaction Engineering, Waste Utilisation, Renewable Energy
Universiti Sains Malaysia, Malaysia

Norbahiah Misran
Communication Engineering
Universiti Kebangsaan Malaysia, Malaysia

Bassim H. Hameed
Chemical Engineering: Reaction Engineering, Environmental Catalysis & Adsorption
Qatar University, Qatar

Mohamed Othman
Communication Technology and Network, Scientific Computing
Universiti Putra Malaysia, Malaysia

Roslan Abd-Shukor
Physics & Materials Physics, Superconducting Materials
Universiti Kebangsaan Malaysia, Malaysia

Biswajeet Pradhan
Digital image processing, Geographical Information System (GIS), Remote Sensing
University of Technology Sydney, Australia

Mohd Shukry Abdul Majid
Polymer Composites, Composite Pipes, Natural Fibre Composites, Biodegradable Composites, Bio-Composites
Universiti Malaysia Perlis, Malaysia

Sodeifian Gholamhossein
Supercritical technology, Optimisation, nanoparticles, Polymer nanocomposites
University of Kashan, Iran

Ho Yuh-Shan
Water research, Chemical Engineering and Environmental Studies
Asia University, Taiwan

Mohd Zulkifly Abdullah
Fluid Mechanics, Heat Transfer, Computational Fluid Dynamics (CFD)
Universiti Sains Malaysia, Malaysia

Wing Keong Ng
Aquaculture, Aquatic Animal Nutrition, Aqua Feed Technology
Universiti Sains Malaysia, Malaysia

INTERNATIONAL ADVISORY BOARD
2024-2027

Hiroshi Uyama
Polymer Chemistry, Organic Compounds, Coating, Chemical Engineering
Osaka University, Japan

Mohini Sain
Material Science, Biocomposites,Biomaterials
University of Toronto, Canada

Mohamed Pourkashanian
Mechanical Engineering, Energy, CFD and Combustion Processes
Sheffield University, United Kingdom

Yulong Ding
Particle Science & Thermal Engineering
University of Birmingham, United Kingdom

ABSTRACTING AND INDEXING OF PERTANIKA JOURNALS

Pertanika Journal of Science & Technology is indexed in Journal Citation Reports (JCR-Clarivate), SCOPUS (Elsevier), EBSCO, ASEAN Citation Index, Microsoft Academic, Google Scholar and MyCite.

The publisher of Pertanika will not be responsible for the statements made by the authors in any articles published in the journal. Under no circumstances will the publisher of this publication be liable for any loss or damage caused by your reliance on the advice, opinion or information obtained either explicitly or implied through the contents of this publication.
All rights of reproduction are reserved in respect of all papers, articles, illustrations, etc., published in Pertanika. Pertanika provides free access to the full text of research articles for anyone, web-wide. It does not charge either its authors or author-institution for refereeing/publishing outgoing articles or user-institution for accessing incoming articles.
No material published in Pertanika may be reproduced or stored on microfilm or in electronic, optical or magnetic form without the written authorisation of the Publisher.
Copyright ©2026 Universiti Putra Malaysia Press. All Rights Reserved.

Pertanika Journal of Science & Technology
Vol. 34 (S2) 2026

Contents

Preface xi
Rohana Hassan, Mohd Fadzil Arshad, and Fauzi Baharudin

Removal of Methylene Blue Using Durian Peel: A Column Experiment 1
Jurina Jaafar, Nur Azwa Zulkefli, Zulhafizal Othman, Siti Rashidah Mohd Nasir, Shariff Ibrahim, and Nur Qudus

Self-Healing Ability of Steel Fibre Asphalt Mixture Using Microwave Heating and Semi-Circular Bending Test 15
Ekarizan Shaffie, Fionna Shiong, Ahmad Kamil Arshad, Mohd Khairul Afzan Mohd Lazi, Muhammad Ibrahim Khalili Abd Rahim, and Ramadhansyah Putra Jaya

Hybrid Solar PV-Micro-Hydro System for Sustainable Electrification of Remote Communities in Arunachal Pradesh, India 29
Somila Hashunao, Taken Nguri, A.S Shimreiwung, Ngayaiwon Hashunao, and Ram Krishna Mehta

Correlation Between Compressive and Flexural Properties in Steel Fibre Reinforced Concrete (SFRC) Beam Using Regression Analysis 37
Md Yushairi Kamarul Effendy Mohd Yusof, Anizahyati Alisibramulisi, Muhd Norhasri Muhd Sidek, Nadiah Saari, and Suraya Hani Adnan

Evaluation of the Causes of On-Farm Food Loss in Cabbage Production: A Case Study in the Large-Scale Farming Group of Hot District, Chiang Mai, Thailand 51
Pichayapak Channiyamathorn, Suraphol Sreshthaputra, Ruth Sirisanyaluck, and Juthathip Chalermphol

Influence of Tree Canopy Characteristics on Rainfall Interception, Throughfall and Stemflow in a Tropical Forest 65
Azinoor Azida Abu Bakar and Muhammad Khairudin Khalil

Experimental and Finite Element Analysis of Shear Strength in Melunak and Mengkulang Glulam Using Shear Block Test 75
Nor Jihan Abd Malek, Rohana Hassan, Mohd Nizam Shakimon, Nurharniza Abdul Rahman, Nazrul Azmi Ahmad Zamri, and Khaled M.H. Alreqeb

Enhancing Health and Safety Practices by Complying with SOP Requirements at Construction Sites During the Pandemic 89
Siti Rashidah Mohd Nasir, Sulaiman Hasim, and Eleanna Guan

Strength and Durability Performance of Three-Layered Leucaena Leucocephala Cement-Bonded Particleboard 101
Marzuki Ab. Rahman, Mohd Fakri Muda, Mohd Razmi Zainudin, Muhammad Isha Ismail, Farah Wahida Mohd Latib, Amminudin Ab Latif, Noor Safwan Muhamad, Wan Zukri Wan Abdullah, Herlien Dwiarti Setio, and Mohd Hisbany Mohd Hashim

Review Article 117
The Use of Lignin as Bio-Binder for Sustainable Asphalt Pavement - A Recent Review
Amminudin Ab Latif, Mohd Fakri Muda, Noor Safwan Muhamad, Marzuki Ab. Rahman, Muhammad Isha Ismail, Mohd Razmi Zainudin, Farah Wahida Mohd Latib, and Wan Zukri Wan Abdullah

Preface

The transition towards a more sustainable and resilient future requires engineering materials and technologies that address environmental challenges while responding to the evolving needs of society. Green Engineering Materials and Technologies brings together a collection of research contributions that explore innovative materials, sustainable technologies, environmental management, and engineering practices from diverse perspectives.

This book presents ten research papers covering a broad range of topics related to green engineering and sustainable development. The contributions demonstrate how natural and renewable resources can be transformed into useful engineering materials, how innovative technologies can improve the performance and durability of infrastructure, and how engineering solutions can contribute to environmental protection and community well-being.

Several chapters focus on the development and application of sustainable materials, including durian peel for the removal of methylene blue, Leucaena leucocephala cement-bonded particleboard, glulam manufactured from Melunak and Mengkulang, and the use of lignin as a bio-binder for sustainable asphalt pavement. Other contributions investigate innovative approaches to infrastructure materials, including the self-healing performance of steel fibre asphalt mixtures, the mechanical behaviour of steel fibre reinforced concrete, and the application of experimental and finite element techniques in timber engineering.

The scope of the book also extends beyond material development to wider environmental and sustainability challenges. Studies on rainfall interception, food losses in cabbage production, and the experiences of communities in un-electrified remote areas highlight the importance of understanding the interaction between engineering, natural systems, resources, and society. In addition, the discussion of health and safety practices at construction sites demonstrates that sustainability must encompass not only materials and technologies, but also safe and responsible practices throughout the construction process.

Collectively, these contributions reflect the multidisciplinary nature of green engineering. They demonstrate that sustainable engineering requires an integrated approach in which material innovation, environmental stewardship, technological advancement, structural performance, resource efficiency, and human well-being are considered together. The research presented in this book also illustrates the importance of combining experimental investigation, numerical modelling, field

studies, statistical analysis, and review of existing knowledge to develop practical and scientifically grounded solutions.

We hope that Green Engineering Materials and Technologies will serve as a useful reference for researchers, academics, engineers, postgraduate students, practitioners, and other professionals interested in sustainable materials, green construction, environmental engineering, and emerging engineering technologies. More importantly, we hope the collection will encourage further research, collaboration, and innovation towards a more sustainable built environment and a greener future.

Guest Editors
Rohana Hassan (Prof. Ir. Ts. Dr.)
Mohd Fadzil Arshad (Prof. Ts. Dr.)
Fauzi Baharudin (Dr.)

Pertanika J. Sci. & Technol. 34 (S2): 1 - 14 (2026)

PERTANIKA JOURNALS

SCIENCE & TECHNOLOGY

Journal homepage: http://www.pertanika.upm.edu.my/

Removal of Methylene Blue Using Durian Peel: A Column Experiment

Jurina Jaafar[1]*, Nur Azwa Zulkefli[1], Zulhafizal Othman[1], Siti Rashidah Mohd Nasir[1], Shariff Ibrahim[2], and Nur Qudus[3]

[1]Faculty of Civil Engineering, Universiti Teknologi MARA, 40450 Shah Alam, Selangor, Malaysia
[2]Faculty of Applied Sciences, Universiti Teknologi MARA, 40450 Shah Alam, Selangor, Malaysia
[3]Department of Civil Engineering, Faculty of Engineering, Universitas Negeri Semarang, 50229 Semarang, Central Java, Indonesia

ABSTRACT

The increasing demand for sustainable, low-cost alternatives to activated carbon has spurred the use of agricultural waste, such as durian peel (DP), in wastewater treatment. This study evaluates the performance of DP, a lignocellulosic material rich in cellulose, hemicellulose, and lignin, for the removal of Methylene Blue (MB) from aqueous solutions using a fixed-bed column. Experiments were conducted in a column of 1.5 cm diameter at bed depths of 2, 3, and 4 cm and flow rates of 3, 4, and 5 mL/min, with an initial MB concentration of 50 mg/L. The treated volumes increased with bed depth, achieving 294, 594, and 1044 mL for 2, 3, and 4 cm, respectively. At a constant bed depth of 3 cm, lower flow rates improved adsorption efficiency, with treated volumes of 940, 594, and 230 mL at flow rates of 3, 4, and 5 mL/min, respectively. Breakthrough occurred within 2–3 h, indicating near saturation of the adsorption zone. The experimental breakthrough curves exhibited typical adsorption profiles and were well described by the Thomas and Yoon–Nelson models (R^2 = 0.95-1.00), with predicted breakthrough times closely matching experimental values. The findings demonstrate that DP is an effective and environmentally friendly adsorbent for dye removal from wastewater.

ARTICLE INFO

Article history:
Received: 18 June 2026
Accepted: 06 August 2026
Published: 30 September 2026

DOI: https://doi.org/10.47836/pjst.34.S2.01

E-mail address:
jurina@uitm.edu.my (Jurina Jaafar)
azwazulkefli@gmail.com (Nur Azwa Zulkefli)
zulhafizal445@uitm.edu.my (Zulhafizal Othman)
sitir015@uitm.edu.my (Siti Rashidah Mohd Nasir)
sha88@salam.uitm.edu.my (Shariff Ibrahim)
nurqudus@mail.unnes.ac.id (Nur Qudus)
* Corresponding author

Keywords: Adsorption, breakthrough curve, durian peel, fixed-bed column, methylene blue, Thomas and Yoon-Nelson models

INTRODUCTION

Water is essential to our daily lives. According to the U.S. Geological Survey, about 96.5% of Earth's water is saltwater and is not suitable for human consumption

e-ISSN: 2231-8526

© Universiti Putra Malaysia Press

without further treatment. About 3.5% of the total water is fresh water. Only 0.8% of freshwater is available to humans, agriculture, and industry, and it is mainly stored in polar ice and underground sources. Due to the increasing global population and industrial activity, the demand for water is also rising. The fresh water sources from rivers, lakes, and aquifers were meant to supply water for agriculture, industry, and households; however, these supplies have increased greatly in the last decade, from 600 km3 to more than 4000 km3 per annum (Dawood, 2013). By 2025, it was estimated that about 60% of the world's population would live in places experiencing moderate-to-extreme water-resource-based vulnerability (Kulshreshtha, 1998).

With urbanisation and industrialisation over the years, water is becoming polluted. Dyes are an important class of pollutants that, once they enter water bodies, can harm ecosystems. Several industries use dyes in their production, including textiles, dyestuffs, paper, printing, plastics, food, and cosmetics. All these dyes will be left as industrial waste and directly discharged into the water body. In Malaysia, the same problem is currently being faced and has been a major problem for environmental management (Hameed & Hakimi, 2008). Dyes can be classified into cationic, anionic and non-ionic dyes. Out of those classes of dyes, the removal of anionic dyes is known to be the most challenging task, as they are water-soluble and produce very bright colours in water with acidic properties. It has been estimated that the total dye consumption in the textile industry worldwide exceeds 10,000 tons per year, and about 10-15% of these dyes are released as effluents during dyeing processes (Gupta et al., 2013).

Various methods have been developed to remove dye wastewater, such as adsorption, anaerobic treatment, coagulation, electrocoagulation, flotation, filtration, ion exchange, membrane separation, and advanced oxidation (Robinson et al., 2001). However, there are many limitations to those treatments, including low efficiency, high operational costs, corrosion, recontamination, incomplete removal of coloured effluent (for dyes), and more. Additionally, adsorption is a separation method for removing dye-bearing wastewater, as reported by Kumar et al. Furthermore, activated carbon is a widely used adsorbent. It is not an economical way to use activated carbon, especially for treating dye wastewater (Wang et al., 2005); hence, many researchers have actively explored alternative, cheaper materials in recent years.

Various low-cost adsorbent materials derived from agricultural waste have been studied over the past few decades (Yagub, 2013). There are many advantages to agricultural wastes, such as being cheap and abundantly available, requiring simple technology, having relatively low running costs, and being biodegradable. Durian peels, an agricultural waste or by-product, have been selected as adsorbents in this study. The utilisation of durian peels as an adsorbent has been studied by several researchers, and it has been shown that they are promising sorbents for removing dyes from aqueous solutions (Hameed & Hakimi, 2008).

In this study, methylene blue (MB), a basic dye, is selected as a model compound to evaluate the capacity of durian peels (DP) to remove MB from solutions. MB, the most common dye in its category, is generally used to dye cotton and silk. Even though MB is not highly hazardous, it can still cause harmful effects. Acute exposure to MB can cause increased heart rate, vomiting, shock, Heinz body formation, cyanosis, jaundice, quadriplegia, and tissue necrosis in humans (Vadivelan & Vasanth Kumar, 2005).

This study assesses the feasibility of using durian peels as an adsorbent for removing dyes from wastewater. The study was conducted with specific objectives: to determine the effect of column parameters on MB removal by durian peels and to simulate the experimental data using column kinetic models, such as the Thomas and Yoon-Nelson models.

This study was established to achieve its objectives. Furthermore, it is a promising approach for developing an environmentally sustainable adsorbent to treat wastewater and remove MB. On top of that, this study aims to analyse the effects of parameters such as bed heights (2-4 cm) and flow rates (3-5 mL/min). This study used a column design to investigate breakthrough plots for these parameters. Thomas and Yoon-Nelson mathematical models were applied in this study to analyse the breakthrough curves (BTCs) on the MB adsorption.

The absorbance of dyes depends on dye characteristics, including molecular structure and the type, number, and position of substituents. Agricultural by-products, which are cheaper than activated carbon, are readily available and can be used directly as adsorbents or for partial treatment. The advantages of using agricultural by-products as adsorbents include lower cost, high efficiency, the ability to minimise chemical and biological sludge, and the possibility of dye recovery.

Thus, the importance of this study is also to identify or explore another environmentally friendly and economically beneficial agricultural by-product for use as an adsorbent, given its ease and affordability in treating wastewater. The purpose of this research is to use durian peels to efficiently remove MB. Moreover, conducting research on this will raise public awareness of the environment and strengthen the urge to protect the quality of water and wastewater in the future.

MATERIALS AND METHOD

Preparation of Durian Peel

Durian Peel (DP) was collected from the local market in Shah Alam, Selangor. The biomass was rinsed repeatedly with distilled water to remove dirt and dust, but the colour persisted. The cleaned biomass was first dried in sunlight and then oven-dried overnight at 80°C. The dried biomass was ground with a domestic blender and lastly sieved to obtain a particle size range of 500 to 1000 μm. The prepared biomass was stored in a plastic container and used for further adsorption experiments.

Preparation of Aqueous Dye Solution

The cationic dye Methylene Blue (MB), with a λmax of 665 nm, was selected as the model adsorbate in this study. It has the formula of C16H18ClN3S and a molecular weight of 319.85 g. The analytical grade was obtained from Friendemann Schmidt with 99% purity. A stock solution of dye was prepared by dissolving 50 mg of MB in 500 mL of distilled water.

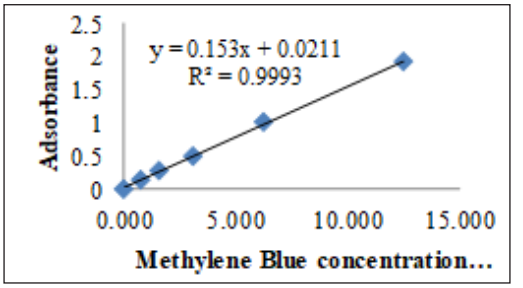

Figure 1. UV Calibration curve plot for MB adsorption

Spectrophotometer

The DR2800 spectrophotometer was used to measure the concentration of the MB dye in solution. It was measured at ʎ max. The maximum adsorption of the dye solution was measured at λmax = 665 nm using a spectrophotometer.

Calibration Curve

Figure 1 shows the calibration curve for the adsorption of MB dye at concentrations ranging from 0.00 to 12.50 ppm, with a regression coefficient of 0.9993.

Column Design Experiment

The adsorption of MB dye on durian peels was carried out in a fixed-bed column design. The experimental arrangement consists of a peristaltic pump, a reservoir containing dye stock solution, a 14 mm-diameter silicon tube delivery line to convey the dye solution from the reservoir to the column, an adsorbent-packed column, and vials serving as the sampling point, as shown in Figure 2. A fixed-bed column study was performed using polypropylene

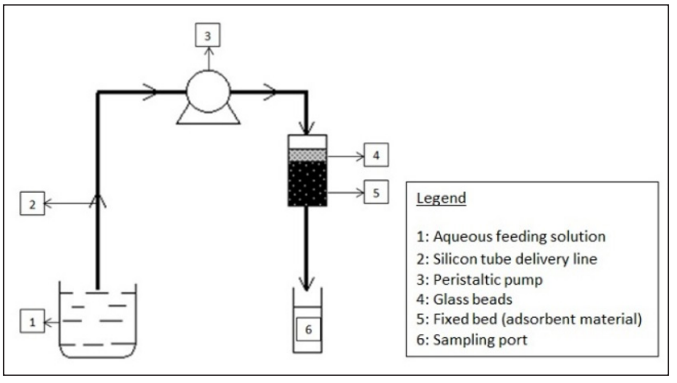

Figure 2. Column system schematic drawing

cylindrical columns with diameters and heights of 1.5 cm and 7.5 cm, respectively. The column was then occupied with a net cloth bed of 1 mm at the bottom and top sections to hold the adsorbent, whilst ensuring a homogeneous distribution of the feed solution. Using a 14-gauge silicon tube with a Cole-Palmer Masterflex peristaltic pump, a 50-ppm dye stock solution was pumped into the down-flow mechanism at the desired flow rate. Samples of column runoff were collected in intervals using vials and were examined for absorbance. The column operation is stopped once the effluent MB concentration exceeds 99.5%, as suggested by Uddin et al. (2009).

Effect Column of Parameters

Two operating parameters were studied. In the bed-depth study, different volumes of adsorbent were packed into the column in each run to provide bed depths of 2, 3, and 4 cm, while the flow rate and MB concentration were constant at 4 mL/min and 50 ppm, respectively. As for the flow-rate study, the analogous fixed-bed experiment was repeated at flow rates of 3, 4, and 5 mL/min, with the bed depth and MB concentration held constant at 3 cm and 50 ppm, respectively.

Thomas Model

The Thomas model was used to characterise the performance of the fixed bed for MB removal and to predict the concentration-time profile, or breakthrough curve, of the effluent. The input data were nonlinear plots of effluent concentration versus sampling time from experimental findings for both bed-depth and flow-rate studies. The output data of this model were the Thomas rate constant (kTh), equilibrium adsorbate uptake (q0) and regression coefficient (R2). Only R2 was discussed in this column study.

Yoon-Nelson Model

A simple theoretical model developed by Yoon–Nelson was applied to investigate the breakthrough behaviour of MB on durian peel. The input data were nonlinear plots of effluent concentration versus sampling time from experimental findings for both bed-depth and flow-rate studies. The output data for this model were the Yoon-Nelson rate constant (kYN), the time needed for 50% adsorbate breakthrough (τ) and the regression coefficient (R2). Only τ and R2 were discussed further in this column study. The τ values from the model represent the time required for 50% adsorbate breakthrough and are used to compare with the time required for 50% adsorbate breakthrough from experimental findings. While the R2 value was the regression coefficient.

RESULTS AND DISCUSSIONS

Effect of Bed Depth on Breakthrough Curve

To study the effect of bed depth on the breakthrough curve, a column experiment was carried out at bed depths of 2, 3, and 4 cm, whilst the MB concentration and the flow rate were held constant at 50 ppm and 4 mL/min, respectively.

As shown in Figure 3, the adsorption bed was exhausted within 1 to 3 hours after breakthrough, indicating that the adsorption zone was almost saturated at the time of exhaustion. These types of breakthrough curves are highly desirable. The breakthrough times, corresponding to C/C0 = 0.200, were 1.25, 13.75, and 26.25 minutes for bed depths of 2, 3, and 4 cm, respectively. The exhausted times, corresponding to C/C0 = 0.995, as suggested by Uddin et al. (2009), were 58.75, 118.75, and 208.75 minutes, respectively. The corresponding volumes of wastewater treated at the breakthrough point were 6.25, 68.75, and 131.25 mL, respectively, and at the exhaust point were 293.75, 593.75, and 1043.75 mL, respectively.

In Figure 3, the breakthrough curves showed that as the bed depth increases, MB has more time to contact durian peels, resulting in improved MB ion removal performance in the column. Therefore, the solute concentration in the effluent decreased simultaneously with the increment in the bed column results. A wider mass-transfer zone resulted from the decreasing slope of the breakthrough curve as bed depth increased. As a result of the increase in the adsorbent surface area, additional adsorption sites were created, as evidenced by the high uptake observed at the topmost bed depth (Han et al., 2007).

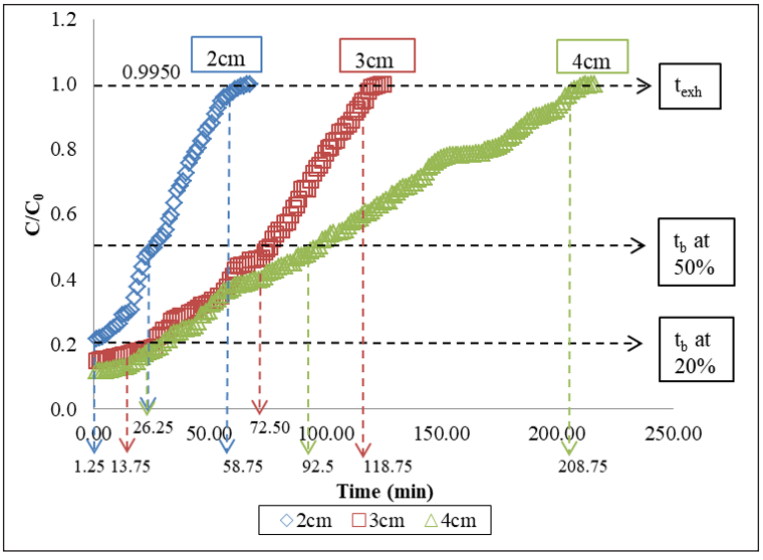

Figure 3. Bed depth effect on breakthrough curve on durian peels mb adsorption at C0 = 50 mg/L and 4 mL/min flow rate

Table 1
Column experiment breakthrough parameters on bed depth

Bed Depth	HRT (min)	T_b (min)	V_b (mL)	t_{exh} (min)	V_{exh} (mL)	% Removal
2 cm	0.8837	1.25	6.25	58.75	293.75	49.05
3 cm	1.3255	13.75	68.75	118.75	593.75	80.93
4 cm	1.7674	26.25	131.25	208.75	1043.75	82.49

As illustrated in Figure 3, a common breakthrough curve was plotted to investigate the effect of bed depth on MB removal. From this parameter study, the column parameters information was gathered and tabulated in Table 1. According to Table 1, the longest breakthrough time was observed at a bed depth of 4 cm (26.25 minutes), compared to 2 cm and 3 cm, which were only 1.25 and 13.75 minutes, respectively, thereby providing more contact time with the adsorbent to adsorb a larger volume of MB. This indicates that the lower bed depth reached breakthrough sooner than the higher bed depth, and that the column exhaustion time increased significantly with bed depth. It was observed that the breakthrough curves became steeper as the bed depth reduced. Although MB adsorption was rapid, diffusion effects were reduced due to insufficient dye residence time in the column at lower bed depths. These results show that higher bed depth yields better MB removal performance than lower bed depth in column mode.

As shown in Table 3, the column reached the exhaustion condition more slowly at a 4 cm bed depth (208.75 minutes) than at 3 cm (118.75 minutes) or 2 cm (58.75 minutes), respectively. In addition, higher bed depth produced a larger volume of treated effluent and a longer column service time. The percentage removal of MB was calculated, and it shows that a 4 cm bed depth has 82.49%, the highest compared to 3 and 2 cm, at 80.93% and 49.05%, respectively. This indicates that a higher bed depth is more effective at absorbing more MB than a lower bed depth.

Effect of Flow Rate on Breakthrough Curve

The influent MB concentration and bed depth were held constant at 50 ppm and 3 cm, respectively, to study the effect of flow rate on MB removal. Column operation was then performed at three different flow rates: 3, 4, and 5 mL/min. The results obtained were plotted for breakthrough curves as shown in Figure 4.

As shown in Figure 4, the adsorption bed was exhausted within 1 to 3 hours after breakthrough, indicating that the adsorption zone was almost saturated at the time of exhaustion. These types of breakthrough curves are highly desirable. The breakthrough times (corresponding to C/C0 = 0.200) were 63.40, 13.75, and 0.5 minutes at flow rates of 3, 4, and 5 mL/min, respectively. The exhausted times (corresponding to C/C0 = 0.995) were 188, 118.75 and 46 minutes, respectively. The corresponding volumes of wastewater

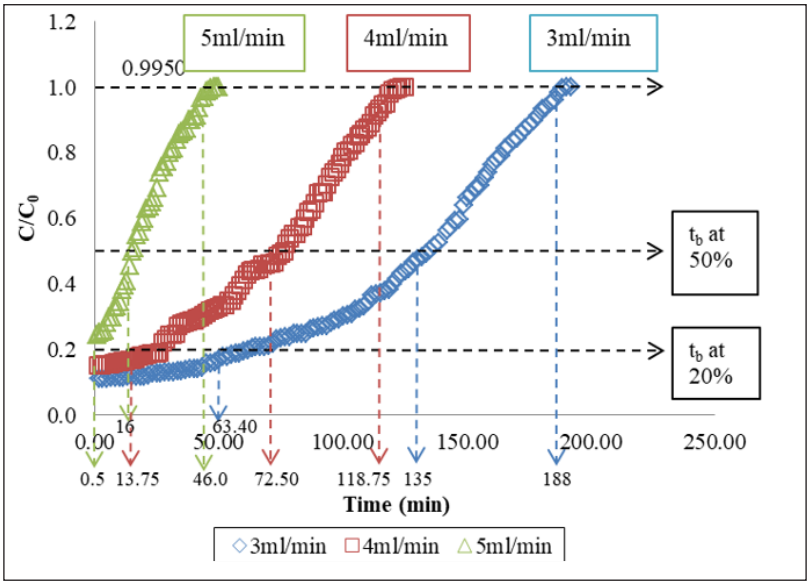

Figure 4. Flow rate effect on the breakthrough curve on durian peels MB adsorption at c0 = 50 mg/l and 3 cm bed depth

treated at the breakthrough point were 317, 68.75, and 2.5 mL, respectively, and at the exhaust point were 940, 593.75, and 230 mL, respectively.

Figure 4 indicates that the higher flow rate reached breakthrough faster than the lower flow rate, and the column exhaustion time increased significantly with reduced flow rate. At a low influent rate, the contact time between MB and durian peel was longer, resulting in higher MB ion removal in the column. It was observed that the breakthrough curves became steeper as the flow rate increased. The column system's exhaustion point increased at lower flow rates. Although MB adsorption was rapid, diffusion effects were reduced due to insufficient dye residence time in the column at higher flow rates. Hence, lower flow rates were desirable for effective MB removal in the column design.

In mass transfer fundamentals, capacity can be inferred from the diversity of breakthrough curve slopes, along with adsorption capacity. According to Ko et al. (2000), the mass transfer rate increased with flow rate, increasing the amount of dye adsorbed onto the adsorbent bed; therefore, the column is exhausted faster at higher flow rates. As shown in Table 2, the column reached the exhaustion condition faster at 5 mL/min (within 46 minutes) than at 3 mL/min (188 minutes). The percentage removal of MB was calculated, and it shows that a flow rate of 3 mL/min yields 89.56%, the highest compared to 4 and 5 mL/min, at 80.93% and 44.37%, respectively. This indicates that a lower flow rate is more effective at absorbing more MB than a higher flow rate.

Table 2
Column breakthrough parameters on flow rate

Flow Rate	HRT (min)	T_b (min)	V_b (mL)	t_{exh} (min)	V_{exh} (mL)	% Removal
3 mL/min	1.7674	63.4	317	188	940	89.56
4 mL/min	1.3255	13.75	68.75	118.75	593.75	80.93
5 mL/min	1.0604	0.5	2.5	46	230	44.37

Table 3
Thomas model parameters

Dye	Adsorbent	Parameter		K_{Th} (mL mg-1 min-1)	q_0 (mg g-1)	R^2
MB	DP	bed depth	2 cm	0.2011	79.113	0.9969
			3 cm	0.0399	264.343	0.9968
			4 cm	0.0031	821.816	0.9926
		flow rate	3 mL/min	0.0092	1268.712	0.9943
			4 mL/min	0.0399	264.343	0.9968
			5 mL/min	0.3910	17.584	0.9968

Thomas Model

Generally, to determine the solid-phase concentration corresponding to the adsorbent's maximum adsorption capacity and to obtain a concentration-time profile or breakthrough curve, column experiments should be conducted (Yan et al., 2001). According to Ibrahim (2010), a widely used model for regulating the ultimate solid-phase concentration of solute on the sorbent and the rate constant in an adsorption column is the Thomas model, developed by Thomas.

As tabulated in Table 3, the number of R2 values was significantly high for all column system simulations at a range of 0.99-1.00. This indicates that all breakthrough curves were well predicted by the Thomas model, as shown in Figures 5 and 6. The phenomenon of axial dispersion was reduced by the uniform size of the adsorbent, and the dye solution was distributed evenly, making the Thomas model suitable.

The Thomas model parameters obtained were tabulated in Table 4, where kTh and q0 represent the Thomas rate constant and the equilibrium MB uptake, respectively. Column adsorption capacity was recorded as q0, and the operation with the highest bed depth yielded the largest q0, 821.816 mg g-1 at a bed depth of 4 cm. As for the flow-rate effect, the highest q0 was recorded at the lowest flow rate, 3 mL/min, at 1268.712 mg g-1.

As the flow rate increased, q0 decreased, while kTh increased. As the bed depth increased, the value of q0 increased significantly, while the value of kTh decreased significantly. Thus, a lower flow rate and a higher bed depth increased MB adsorption on durian peels.

Table 4
Yoon-Nelson model parameters

Dye	Adsorbent	Parameter		K_{Th} (mL mg-1 min-1)	τ (min)	$t_{50\%}$exp (min)	R^2
MB	DP	bed depth	2 cm	0.00020	26.25	26.25	0.9942
			3 cm	0.00008	72.50	76.25	0.9970
			4 cm	0.00006	96.25	97.50	0.9951
		flow rate	3 mL/min	0.00005	133.60	135.27	0.9961
			4 mL/min	0.00008	72.50	76.25	0.9970
			5 mL/min	0.0029	16.00	15.00	0.9966

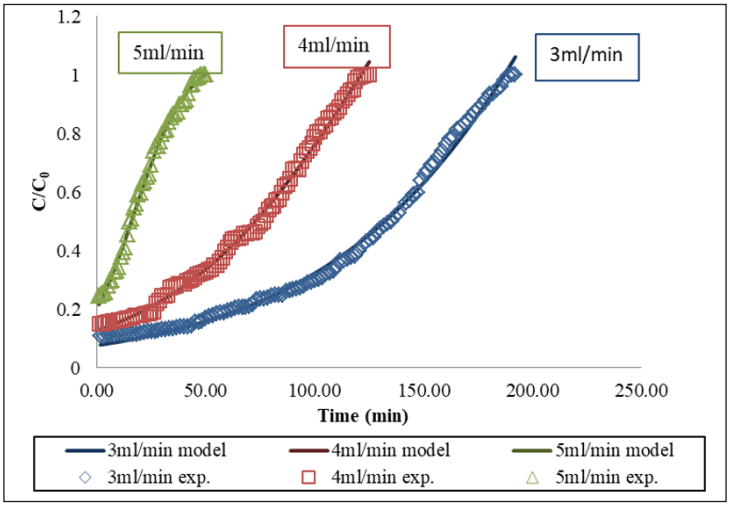

Figure 5. Nonlinear Thomas model curves on various bed depths

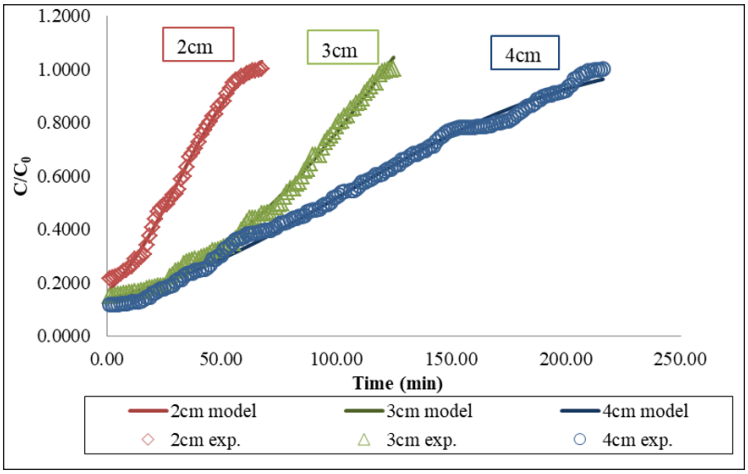

Figure 6. Nonlinear Thomas model curves on various flow rates

Yoon-Nelson Model

This uncomplicated theoretical model was formulated by Yoon-Nelson to investigate column breakthrough characteristics. Assuming that the reduction in the probability of each absorber being adsorbed is comparable to the feasibility of adsorption and breakthrough in the adsorbent, the Yoon-Nelson model is very simple in form (Xu et al., 2013). This model is also reliable, as is the Thomas model, since it provided an acceptable fit to the empirical data. Additionally, this model is expected to yield identical R2 values, since it predicts similar uptake capacity and Ct/Ci values for a given data set.

As tabulated in Table 4, the number of R2 values was significantly high for all column system simulations at a range of 0.99-1.00. This indicates that all breakthrough curves were well predicted by the Yoon-Nelson model, as shown in Figures 7 and 8. In Table 4, the Yoon-Nelson parameters were denoted as kYN (the Yoon-Nelson rate constant), while the time required for 50% breakthrough was denoted by τ. The time required for 50% breakthrough was highest at the lowest flow rate, 133.60 minutes at 3 mL/min, compared to 72.50 and 16 minutes at 4 and 5 mL/min, respectively. This model prediction was like the 50% breakthrough time from the bed-depth experimental findings, which were 135, 72.50, and 16 minutes at flow rates of 3, 4, and 5 mL/min, respectively.

The significant outputs from the Yoon-Nelson model were the regression coefficient value (R2) and the time required for 50% breakthrough (τ). The nonlinear plots of the Yoon-Nelson model yielded the best fit, with R2 values of 0.99-1.00 across all column systems. The R2 values were important in showing that the experimental data were well predicted. The τ values were compared with the experimentally obtained time to 50% breakthrough.

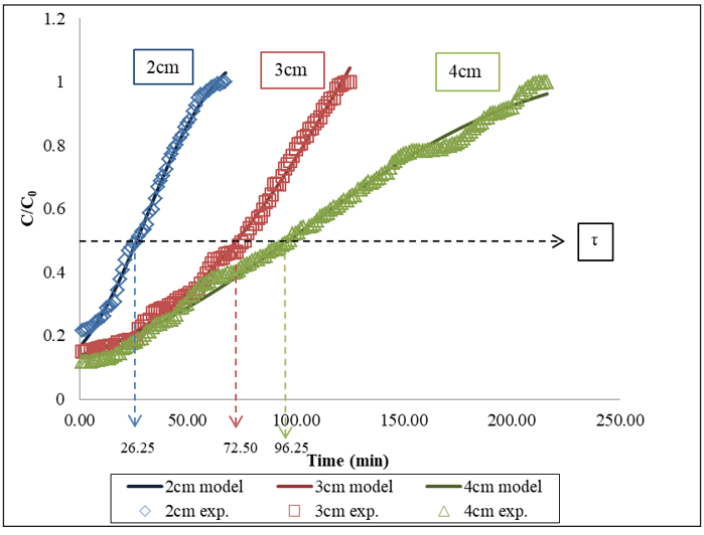

Figure 7. Nonlinear Yoon-Nelson model curves on various bed depths

As presented in Table 4, the τ values for the bed depth study were 26.25, 72.50, and 96.25 minutes for bed depths of 2, 3, and 4 cm, respectively. Similar values were recorded from experimental findings: 26.25, 72.50, and 92.5 minutes for bed depths of 3, 5, and 7 cm, respectively. As for the flow rate study, the τ values matched the experimental flow rate findings: 133.60, 72.50, and 16 minutes for 3, 4, and 5 mL/min, respectively.

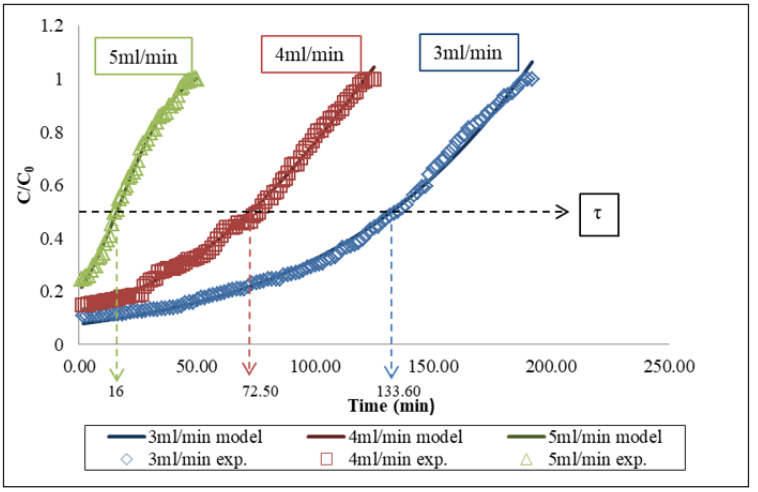

Figure 8. Nonlinear Thomas Model curves on various flow rates

CONCLUSION

In this study, two parameters were considered in the column design. The main parameters in this column experiment are bed depth and flow rate. The objectives of this study have been successfully attained, as durian peels are effective as absorbents for removing dyes from wastewater. This is evident from the results, which show that the breakthrough curves of each experimental data set are very similar to the suggested or standard pattern for breakthrough curves in adsorption studies. The other objective of this study has also been achieved: simulating the experimental data using the column mathematical models implemented here, namely the Thomas and Yoon-Nelson models. From this study, it was concluded that:

Bed depth parameters can be improved by increasing the adsorbent bed depth in the column design. This action will result in a higher amount of MB volume that can be removed. This is because the higher the bed height, the greater the adsorbent's capacity to adsorb MB.

As for flow rate parameters, they contrasted with bed depth: the lower the flow rate used in the column designs, the greater the MB volume removed. Hydraulic retention time (HRT) is highest at the lower flow rate, indicating that the contact time between the

adsorbent and the dye is longer. This allows molecules and particles to adhere, thereby increasing the volume of MB removal.

The mathematical models, Thomas, can be well equipped with experimental data once applied to them. It was a convenient way to determine whether the experimental data were studied efficiently. The coefficient of determination (R2) values ranged from 0.99 to 1.00. This demonstrates that the dynamic model fitted well with experimental breakthrough curves. As Nainamalai et al. (2018) noted, the R2 values ranging from 0.797 to 0.970 indicate that the model fits well.

As for the Yoon-Nelson model application, it shows that the model fitted experimental data as well. The coefficient of determination (R2) values ranged from 0.99 to 1.00. This demonstrates that the dynamic model fitted well with experimental breakthrough curves. As Nainamalai et al. (2018) noted, the R2 values ranging from 0.797 to 0.970 indicate that the model fits well. In addition, the τ value obtained from the Yoon-Nelson model represents the time to 50% breakthrough and was nearly equal to the 50% breakthrough time from the experimental findings for both bed depth and flow rate studies.

Generally, durian peels, as an agricultural solid waste, can be found abundantly disposed of mostly in the countryside. Because of that, it was inconvenient to implement an economical method for using durian peels as an adsorbent without chemical processing. The industrial sector that currently uses dyes for discharge can implement this design as one way to filter before directly discharging into waterways. A pre-treatment process may be implemented to enhance performance and meet the industry standard.

ACKNOWLEDGEMENT

The authors wish to thank the School of Civil Engineering, College of Engineering, Universiti Teknologi MARA.

REFERENCES

Dawood, S. A. (2013). *Development and characterization of biomass based novel adsorbent in the removal of Congo red dye by adsorption* [Master's thesis, Curtin University]. Curtin University eSpace.

Gupta, V. K., Kumar, R., Nayak, A., Saleh, T. A., & Barakat, M. A. (2013). Adsorptive removal of dyes from aqueous solution onto carbon nanotubes: A review. *Advances in Colloid and Interface Science, 193-194*, 24-34. https://doi.org/10.1016/j.cis.2013.03.003

Hameed, B. H., & Hakimi, H. (2008). Utilization of durian (*Durio zibethinus* Murray) peel as low cost sorbent for the removal of acid dye from aqueous solutions. *Biochemical Engineering Journal, 39*(2), 338-343. https://doi.org/10.1016/j.bej.2007.10.005

Han, R., Wang, Y., Yu, W., Zou, W., Shi, J., & Liu, H. (2007). Biosorption of methylene blue from aqueous solution by rice husk in a fixed-bed column. *Journal of Hazardous Materials, 141*(3), 713-718. https://doi.org/10.1016/j.jhazmat.2006.07.031

Ko, D. C. K., Porter, J. F., & McKay, G. (2000). Optimised correlations for the fixed-bed adsorption of metal ions on bone char. *Chemical Engineering Science, 55*(23), 5819-5829. https://doi.org/10.1016/S0009-2509(00)00416-4

Kulshreshtha, S. N. (1998). A global outlook for water resources to the year 2025. *Water Resources Management, 12*(3), 167-184. https://doi.org/10.1023/A:1007957229865

Nainamalai, M., Palani, M., Soundarajan, B., & Allwin, A. E. (2018). Decolourisation of synthetic dye wastewater using packed bed electro-adsorption column. *Chemical Engineering and Processing: Process Intensification, 130*, 160-168. https://doi.org/10.1016/j.cep.2018.06.013

Robinson, T., McMullan, G., Marchant, R., & Nigam, P. (2001). Remediation of dyes in textile effluent: A critical review on current treatment technologies with a proposed alternative. *Bioresource Technology, 77*(3), 247-255. https://doi.org/10.1016/S0960-8524(00)00080-8

Uddin, M. T., Islam, M. A., Mahmud, S., & Rukanuzzaman, M. (2009). Adsorptive removal of methylene blue by tea waste. *Journal of Hazardous Materials, 164*(1), 53-60. https://doi.org/10.1016/j.jhazmat.2008.07.131

Vadivelan, V., & Vasanth Kumar, K. (2005). Equilibrium, kinetics, mechanism, and process design for the sorption of methylene blue onto rice husk. *Journal of Colloid and Interface Science, 286*(1), 90-100. https://doi.org/10.1016/j.jcis.2005.01.007

Wang, S., Boyjoo, Y., Choueib, A., & Zhu, Z. H. (2005). Removal of dyes from aqueous solution using fly ash and red mud. *Water Research, 39*(1), 129-138. https://doi.org/10.1016/j.watres.2004.09.011

Xu, Z., Cai, J., & Pan, B. (2013). Mathematically modelling fixed-bed adsorption in aqueous systems. *Journal of Zhejiang University-SCIENCE A, 14*(3), 155-176. https://doi.org/10.1631/jzus.A1300029

Yagub, M. T. A. (2013). *Removal of methylene blue contaminant by natural and modified low cost agricultural by-product* [Doctoral thesis, Curtin University]. Curtin University eSpace. http://hdl.handle.net/20.500.11937/1468

Yan, G., Viraraghavan, T., & Chen, M. (2001). A new model for heavy metal removal in a biosorption column. *Adsorption Science & Technology, 19*(1), 25-43. https://doi.org/10.1260/0263617011493953

Pertanika J. Sci. & Technol. 34 (S2): 15 - 28 (2026)

PERTANIKA JOURNALS

SCIENCE & TECHNOLOGY

Journal homepage: http://www.pertanika.upm.edu.my/

Self-Healing Ability of Steel Fibre Asphalt Mixture Using Microwave Heating and Semi-Circular Bending Test

Ekarizan Shaffie[1,2]*, Fionna Shiong[2], Ahmad Kamil Arshad[2], Mohd Khairul Afzan Mohd Lazi[3], Muhammad Ibrahim Khalili Abd Rahim[4,5], and Ramadhansyah Putra Jaya[6]

[1]Faculty of Civil Engineering, Universiti Teknologi MARA, 40450 Shah Alam, Selangor, Malaysia
[2]Institute for Infrastructure Engineering and Sustainable Management (IIESM), Universiti Teknologi MARA, 40450 Shah Alam, Selangor, Malaysia
[3]Faculty of Civil Engineering, Universiti Teknologi Malaysia, 81310 Skudai, Johor, Malaysia
[4]Department of Civil Engineering, School of Engineering, Monash University Malaysia, Jalan Lagoon Selatan, 47500 Bandar Sunway, Selangor, Malaysia
[5]Monash Climate-Resilient Infrastructure Research Hub (M-CRInfra), School of Engineering, Monash University Malaysia, Jalan Lagoon Selatan, 47500 Bandar Sunway, Selangor, Malaysia
[6]Faculty of Civil Engineering Technology, Universiti Malaysia Pahang, Al-Sultan Abdullah, 26300 Kuantan, Pahang, Malaysia

ABSTRACT

The durability of asphalt pavements is a critical concern in civil engineering due to frequent cracking and deterioration, which often necessitate costly, disruptive maintenance. To address these issues and extend pavement lifespan, the development of self-healing asphalt materials has gained increasing attention. One promising approach involves incorporating steel fibres into asphalt mixtures to enhance both mechanical performance and self-healing capability. However, the relationship between steel fibre content and healing efficiency, particularly under microwave heating, remains insufficiently understood. This study investigates the self-healing performance of Steel Fibre Asphalt Mixture (SFAM) using microwave heating and the Semi-Circular Bending (SCB) test. SFAM samples were prepared with varying steel fibre contents (0%, 0.3%, 0.5%, and 0.7% by total mixture weight) and a bitumen content of 6.0% PEN 60/70. Mechanical properties and healing performance were evaluated using Marshall Stability and Flow, Cantabro Loss, and SCB tests. Results indicate that the inclusion of steel fibres significantly improves mixture stability, flow, and wear resistance compared to conventional asphalt. SFAM also demonstrates

ARTICLE INFO

Article history:
Received: 18 June 2026
Accepted: 06 August 2026
Published: 30 September 2026

DOI: https://doi.org/10.47836/pjst.34.S2.02

E-mail address:
eka@uitm.edu.my (Ekarizan Shaffie)
fionnashiong@gmail.com (Fionna Shiong)
drahmadkamil@gmail.com (Ahmad Kamil Arshad)
mohdkhairulafzan@utm.my (Mohd Khairul Afzan Mohd Lazi)
ibrahimkhalii014@gmail.com (Muhammad Ibrahim Khalili Abd Rahim)
ramadhansyah@umpsa.edu.my (Ramadhansyah Putra Jaya)
* Corresponding author

e-ISSN: 2231-8526

© Universiti Putra Malaysia Press

enhanced crack resistance and load-bearing capacity. Furthermore, self-healing capability is confirmed through observable recovery in SCB measurements after crack initiation. Overall, the incorporation of steel fibres and microwave-assisted healing shows strong potential to reduce pavement deterioration and maintenance needs, thereby supporting the development of more durable infrastructure.

Keywords: Crack healing, microwave heating, semi-circular bending, self-healing, steel fibre, stone mastic asphalt

INTRODUCTION

The implementation of road construction plays a crucial role in facilitating Malaysia's advancement in both society and the economy. The civil sector undergoes constant evolution, adopting dynamic infrastructure developments that prioritise the integration of cost-effective, sustainable, and environmentally friendly technologies. Robust economic growth depends on well-maintained road networks that effectively serve road users. Most Malaysian roads are built on flexible pavements, specifically bituminous hot-mix asphalt. Nevertheless, continuous exposure to traffic-related stress and the surrounding environment can lead to mechanical weakness and durability issues, including ageing, moisture damage, and temperature-induced cracking. Therefore, routine maintenance is crucial to extend the road's lifespan.

Self-healing asphalt pavement is a new concept that is becoming increasingly popular in the effort to achieve durable and environmentally friendly infrastructure. Conventional asphalt mixes largely rely on expensive, labour-intensive maintenance and repair operations to minimise deterioration. In contrast, asphalt mixes enhanced with steel fibres have the remarkable ability to self-repair minor damage and fractures, thereby reducing maintenance needs and prolonging the lifespan of asphalt pavements. The utilisation of fibres has gained significant recognition as an efficient means of enhancing road pavements (Serin et al., 2012; Haikal Mohd Ghazali et al., 2021; Sun et al., 2018; Zhang et al., 2020).

Furthermore, asphalt mixes have the distinct capability to self-repair when they sustain damage, as the bitumen within them flows into cracks in response to higher temperatures (Norambuena-Contreras & Garcia, 2016). The use of steel fibres in pavement engineering materials demonstrates their importance in asphalt, as they improve self-repair and reduce problems such as potholes, ravelling, and sliding in wet conditions (Shiong & Shaffie, 2021). The correlation between the incorporation of steel fibres and the self-healing properties of asphalt mixes using microwave heating remains poorly understood, despite extensive research. The objective of this study is to examine the effect of microwave heating on the ability of fibre asphalt mixtures to self-heal.

Microwave heating is increasingly recognised as an effective method for accelerating the healing of asphalt mixtures containing microwave-absorbing materials (Lou et al.,

2021; Song et al., 2021). Several types of fibres, including carbon fibre, steel fibre, and steel wool, have been utilised in the production of self-healing asphalt mixes. The mechanical characteristics and self-healing abilities of the material were assessed by the Semi-Circular Bending (SCB) test (Loureiro et al., 2023; Haikal Mohd Ghazali et al., 2021).

Recent studies have explored the potential of microwave heating to facilitate the self-healing of cracks in asphalt mixes. Zhang et al. (2023) highlighted the advantages of incorporating coal gangue powder (CGP) and basalt in this method, emphasising that the presence of metal oxides in coal gangue enhances microwave heating efficiency and improves asphalt healing. Another investigation provided evidence of the efficacy of incorporating steel slag aggregates (SSA) and steel wool fibres (SWF) into asphalt mixtures. This resulted in notable enhancements in asphalt's self-healing ability, as well as a substantial 150% increase in the asphalt's lifespan after healing. These findings highlight the considerable potential of these materials in asphalt engineering (Liu et al., 2017; Garcia et al., 2013).

These findings are consistent with prior research demonstrating that appropriate heating methods can facilitate self-healing in asphalt mixtures containing steel fibres or slags. Significantly, specimens subjected to microwave heating exhibited improved healing outcomes compared with those subjected to induction heating (González et al., 2018). The study's findings demonstrated that incorporating steel fibres into the asphalt mixture can improve stability, wear resistance, and self-healing. Overall, incorporating steel fibres into asphalt mixes, especially when combined with microwave heating, has the potential to improve the performance of road pavements. These findings support current initiatives to create durable road infrastructure, thereby promoting sustained economic growth and societal progress.

MATERIALS AND METHODS

Materials

The asphalt mixes were produced using granite aggregates obtained from the Kajang Rocks Quarry. The aggregates undergo careful drying and sieving to ensure they meet the specified 20 mm size range, in accordance with JKR Malaysia's SMA20 standards, as shown in Table 1. To ascertain the appropriateness of the materials for the combinations, a range of tests was carried out on the aggregate materials, following the procedures outlined in the ASTM standards, to establish their physical and mechanical properties.

The asphalt mixtures were produced using a Penetration Grade (PEN 60/70) asphalt binder. The SMA was enhanced by using steel fibres obtained from Gardner Global Enterprise, as shown in Figure 1, in different contents. For this study, two types of SMA20 asphalt mixes were prepared: the steel fibre asphalt mixture (SFAM) and conventional asphalt mixtures, which served as control samples.

The study used Steel Fibre Asphalt Mixture (SFAM) samples with steel fibres at concentrations of 0%, 0.3%, 0.5%, and 0.7% to assess their mechanical properties and healing capacity. The percentages provided are derived from previous research, which demonstrates that a decrease in fibre content (below 1%) improves performance while maintaining the quality of the mixture (Zhao et al., 2020). High percentages may lead to problems with fibre dispersion and mix consistency (Garcia et al., 2013). The chosen percentages are both cost-effective and practicable for large-scale applications, while also enabling an in-depth analysis of the correlation between fibre content and mixture performance (Sun et al., 2017). The characteristics of the steel fibres are specified in Table 2.

Marshall Specimen Preparation

Twelve (12) Marshall specimens were created in accordance with the requirements outlined in ASTM D 1559. The SMA mixes were formed by heating a mixture of 1100 g of aggregate

Table 1
SMA aggregate gradation

Sieve Size (mm)	Lower Gradation	Upper Gradation	Percentage Passing	Percentage Retained	Mass Passing (g)	Mass Retained (g)
19.0	100	100	100	0.0	1200.0	0
12.5	85	95	90	10.0	1080.0	120
9.5	65	75	70	20.0	840.0	360
4.75	20	28	24	46.0	288.0	912
2.36	16	24	20	4.0	240.0	960
0.60	12	16	14	6.0	168.0	1032
0.30	12	15	13.5	0.5	162.0	1038
0.075	8	10	9	4.5	108.0	1092
Pan	-	-	-	9.0	-	108



Table 2
Properties of steel fibres

Description	Straight
Length (mm)	13
Diameter (mm)	0.2
Density (Kg/m^3)	7800
Tensile strength (Mpa)	2600
Aspect Ratio	65

Figure 1. Steel fibre

and filler to 160 °C. The required amount of bitumen was also heated to 160 °C to achieve the acceptable viscosity for the mixture's manufacture. The mixture contained 6.0% bitumen by weight. The steel fibre, at 0%, 0.3%, 0.5%, and 0.7% of the total weight of the mix, was dry-mixed directly into the mix prior to bitumen addition. Each test specimen was subjected to 50 blows per surface using a conventional Marshall compactor. Afterwards, all twelve (12) Marshall specimens underwent additional assessments for Marshall stability, flow test, and Cantabro test in accordance with specific standards.

Marshall Stability and Flow Test

The Marshall stability and flow test was conducted in accordance with the guidelines set by ASTM D 6927. The procedure involved immersing the test specimens in a water bath maintained at 60 °C for 30 minutes. Afterwards, each specimen was removed and immediately placed in the loading head of the Marshall Stability Machine. The flow meter was zeroed by inserting a metal cylinder with a diameter of 101.6 mm into the loading head.

The specimens were subjected to a constant strain rate of 50.8 mm/min until they reached their maximum capacity (peak load). Marshall stability was determined by measuring the maximum load the specimens could withstand before failure. During the stability test, the flowmeter was firmly held above the guide bar and withdrawn as the load started to decrease. The flow value of the specimen was determined based on the deformation observed at the maximum load.

Cantabro Loss Test

This test was conducted in accordance with ASTM D 7064, using specimens produced with steel fibre proportions of 0%, 0.3%, 0.5%, and 0.7% by weight of the mixture. The test specimens were held at 25 °C for 6 hours. Following this, their weight was measured and recorded as the sample's original weight before testing. The recorded weight was then entered into the machine. The drum underwent 300 revolutions at a velocity ranging from 188 to 208 radians per second, with no steel balls present. The Cantabro Loss value is expressed as a percentage, calculated using Equation 1:

$$\text{Cantabro Loss (\%)} = \frac{(M_0 - M_1)}{M_0} \times 100 \quad [1]$$

Where M_0 is denoted as the initial mass of the sample before testing (g), and M1 is the final mass of the sample in grams.

Semi-Circular Bending (SCB)

The Semi-Circular Bend (SCB) test is a laboratory test employed to measure the fracture resistance of asphalt mixes. The test follows the ASTM D8044 criteria for intermediate temperatures. The process involves measuring two important parameters: Strain Energy (kJ) and Peak Load (N). These parameters are crucial for understanding the mechanical properties and carrying capacity of materials, particularly in applications such as pavements, concrete, and other structural elements.

Four sets of cylindrical asphalt specimens were prepared: one control group without steel fibre, and three groups with varying amounts of steel fibre (0.3%, 0.5%, and 0.7% by weight of the total mixture). The asphalt mixtures were prepared using standard procedures and included steel fibres as required for each specific group. The mixes were compacted into cylindrical moulds to produce standardised specimens. The notches for each sample were cut at depths of 25 mm, 32 mm, and 38 mm, as shown in Figure 2.

The tests were performed with a multispeed universal loading testing machine, as depicted in Figure 3. After achieving equilibrium, a preload was applied for 30 seconds to ensure the specimen was securely positioned, while maintaining a constant temperature of 25 °C throughout the operation. Subsequently, the load was released, and the test began in displacement-control mode at a velocity of 0.5 mm/min.

The variables of time, force, and displacement were recorded at a sample frequency of 10 Hz. The test was terminated when the applied load decreased to 25% of the maximum load. Simultaneously, the crack development in the SCB asphalt specimen was continuously monitored. Following cracking, the specimens were subjected to microwave heating for a predetermined duration.



Figure 2. SCB samples



Figure 3. SCB equipment

Microwave Healing Conditions Test

The methodology for assessing the self-healing rate of the asphalt mixture consisted of a sequence of experiments designed to induce and assess the formation and recovery of cracks. The samples were first subjected to the Semi-Circular Bending (SCB) test utilising a Universal Testing Machine (UTM) to induce cracks. The test was conducted on all specimens until a specific deformation length was reached to measure the peak load (kN) and the strain energy required to crack the sample. Each sample was subjected to the SCB test twice: once to assess early cracking and once after receiving microwave-induced healing.

The healing process was accelerated by employing a microwave oven with a power output of 1000 Watts and a frequency of 2.45 GHz. Microwave energy was used to stimulate binder movement and crack closure in damaged samples, thereby promoting self-healing. Following microwave treatment, the specimens were cooled and subsequently retested using the SCB test to evaluate the rate of self-healing. Load-displacement curves were measured, and self-healing efficiency was determined by assessing the recovered stiffness and load-bearing capacity.

The initial SCB test was performed on each specimen under control conditions at 25 °C. The test measured the Peak Load (Fi) and Strain Energy (kJ) required to induce cracking. Following the initial test, the damaged samples were conditioned in a chamber at 20 °C for 2 hours. Subsequently, each conditioned sample was subjected to microwave heating for 40 seconds, with temperature monitored using either a thermocouple or an infrared thermometer. This was done to ensure consistent, controlled heating while preventing an excessive increase in temperature.

After heating, the specimens were allowed to cool to 20 °C in the conditioning chamber. After the specimens cooled, the SCB test was repeated to measure the peak load (Fb) and Strain Energy (kJ) required to induce cracking after the healing process. The self-healing rate was determined by using Equation 2, which accurately represented the recovered mechanical properties of the specimens:

$$Sh = \frac{F_b}{F_i} \times 100 \qquad [2]$$

Where,
Fb is the maximum peak load after heating and
Fi is the maximum peak load before heating.

RESULTS AND DISCUSSIONS

Stability and Flow

Three specimens were produced for each steel fibre proportion category to evaluate stability (kg) and flow (mm). The average values were then calculated. The stability and flow tests are conducted to assess the ability of bituminous materials to withstand deformation, displacement, rutting, and shearing loads. Internal friction and cohesion are the primary variables that contribute to stability. Internal friction refers to the resistance that arises from the interlocking and friction between aggregates, whereas cohesion refers to the binding force exerted by the binder material. The bituminous material must possess high stability and flow characteristics to withstand the substantial traffic loads that bituminous pavement is subjected to.

Figure 4 illustrates the correlation between the stability and flow of the specimens and the different proportions of steel fibres. The results demonstrate that incorporating steel fibres into the asphalt mixture improves stability, as seen by the considerably lower value of the control sample. The improvement in performance can be attributed to the presence of steel fibres in the asphalt mixture, which decreases the internal friction of the asphalt properties (Shaffie et al., 2021).

The specimen with a steel fibre proportion of 0.3% exhibits the highest stability value of 1089.7 kg among all specimens. It is followed by specimens with proportions of 0.5%, 0.7%, and 0%. The stability of the mix decreases progressively as the steel proportion exceeds 0.3%, possibly due to an uneven distribution of steel fibres in the mixture.

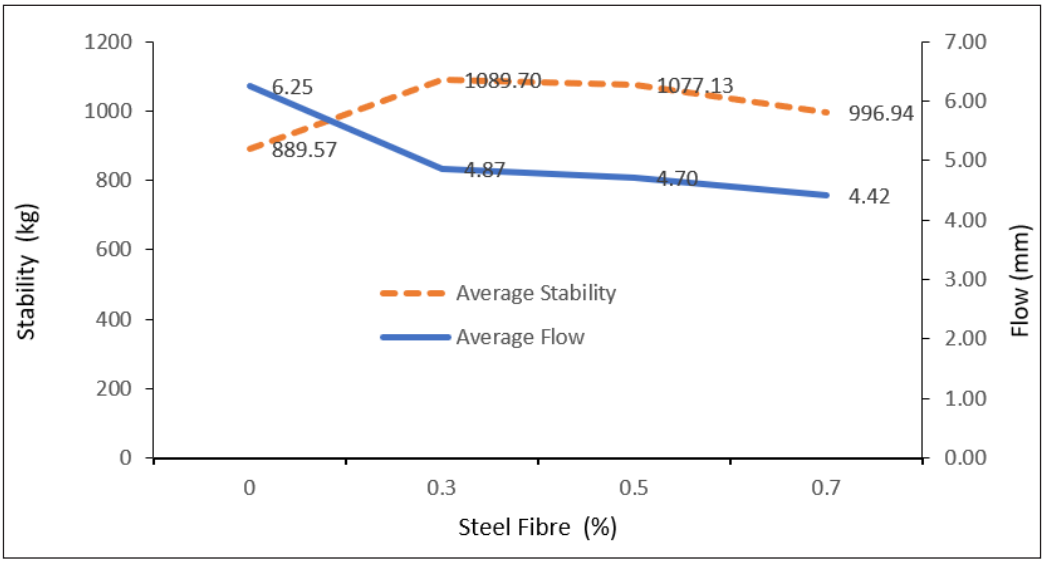

Figure 4. Stability and flow against steel fibre (%)

This uneven distribution can result in voids or weak areas, which negatively affect stability measures.

Conversely, the flow data consistently demonstrates a pattern: as the proportion of steel fibres increases, the flow value decreases. These flow numbers indicate the extent of deformation in the mixture as the load decreases. The sample with a 0% steel fibre proportion exhibits the highest flow value of 6.25 mm, whilst the sample with the highest steel fibre proportion of 0.7% indicates the lowest flow value of 4.42 mm. Introducing steel fibres into the mixture limits the sample's flexibility and free movement, reducing flow values as the amount of steel fibres increases.

Cantabro Loss and Air Voids

According to Figure 5, the air void content decreases as the steel fibre content increases, reaching a maximum at 0.5% of the total asphalt mixture. This occurrence may be attributed to the infiltration of steel fibres into the gaps between the aggregates in the asphalt mixture. The steel fibres used in the experiment were thin strips, allowing them to easily penetrate the spaces between the aggregates (Shiong et al., 2023). Nevertheless, the air void content increases to 7.8% when the steel fibre percentage reaches 0.7%, falling within the desirable range for the specified air void content.

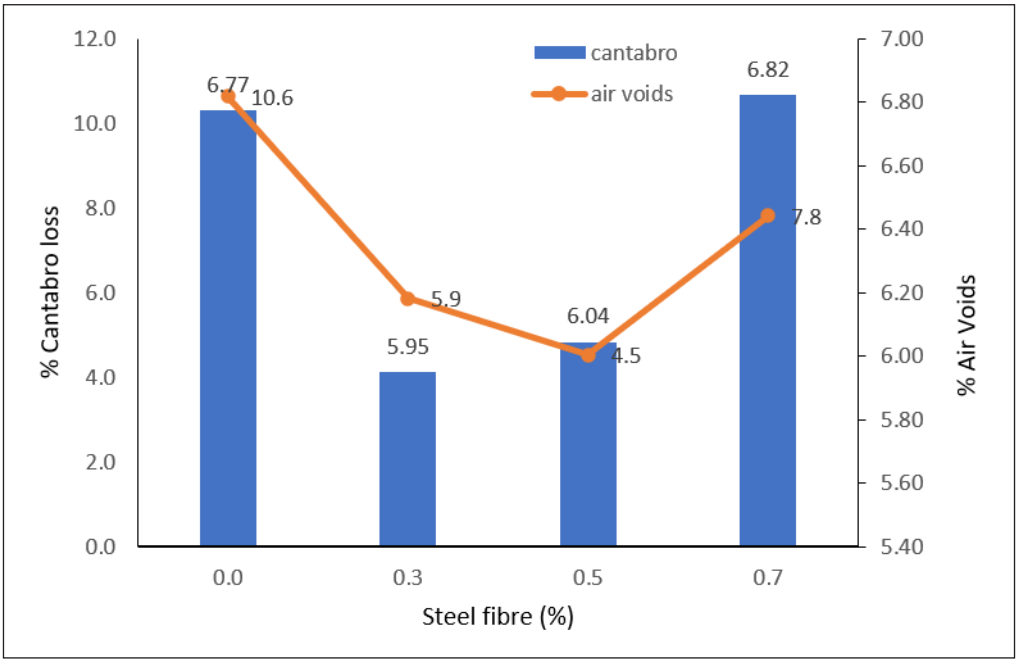

Figure 5. Air voids & cantabro loss values against steel fibre (%)

Figure 5 displays the Cantabro loss data. It is evident that the SMA combination with 0.3% steel fibre content had the lowest abrasion loss percentage, at 5.95%. This was followed by mixtures with steel fibre contents of 0.5%, 0%, and 0.7%. On the other hand, the SMA mixture containing 0.7% steel fibre achieved the highest Cantabro loss of 6.82% compared with the other proportions. The variations in abrasion loss seen for each proportion can be attributed to the abrasion force exerted between the mixture specimens and the drum, resulting in the disintegration of the mixture and a corresponding quantity of abrasion loss.

The inclusion of 0.3% steel fibre in the SMA mixture resulted in a notable decrease of up to 13% in abrasion loss. However, the addition of 0.5% and 0.7% steel fibre later led to an increase in abrasion loss. The addition of 0.7% steel fibre is causing the control mixture's abrasion loss to exceed that of the 0.7% steel fibre mixture. This suggests that using a large quantity of steel fibre does not improve the abrasion resistance of the SMA combination. The changes in the abrasion values may be influenced by several factors, such as the angularity of coarse particles and unequal compaction force. It has been demonstrated that adding steel fibres to SMA is an effective method for minimising abrasion loss when used in appropriate proportions.

The relationship between Cantabro loss and air voids in hot mix asphalt (HMA) is crucial for assessing the long-term resilience of asphalt pavements. Cantabro loss quantifies an asphalt's ability to withstand deterioration from traffic and environmental factors, whilst air voids refer to the empty spaces within the compacted mixture. Experimental data indicate that an increased air-void content typically leads to greater Cantabro loss, as it reduces aggregate interlocking and binder cohesion.

The mix containing 0.3% steel fibre had the lowest abrasion loss, indicating that bitumen quality in this mixture affects the relationship between Cantabro loss and air voids. An excellent binder can reduce Cantabro loss, even when air void levels are within acceptable limits. Adequate compaction and uniform void dispersion are essential for maintaining the long-term durability of asphalt pavement (Ahmad et al., 2020).

Semi-Circular Bending

The Semi-Circular Bending (SCB) test is an important method used in materials testing and engineering, particularly in mechanics and fracture mechanics. This study aimed to assess the self-healing rate of pavement specimens by preparing 12 SCB specimens, with three specimens allocated for each steel fibre proportion.

Figure 6 demonstrates a strong correlation between the addition of steel fibres to asphalt mixtures and the capacity of these mixtures to self-heal when exposed to microwave heating. Before cracking, the asphalt's strength is indicated by its initial peak load. Analysis indicated that specimens containing 0.3% steel fibre exhibited the highest initial peak load, surpassing those of other samples. After inducing cracks and subjecting the specimens to

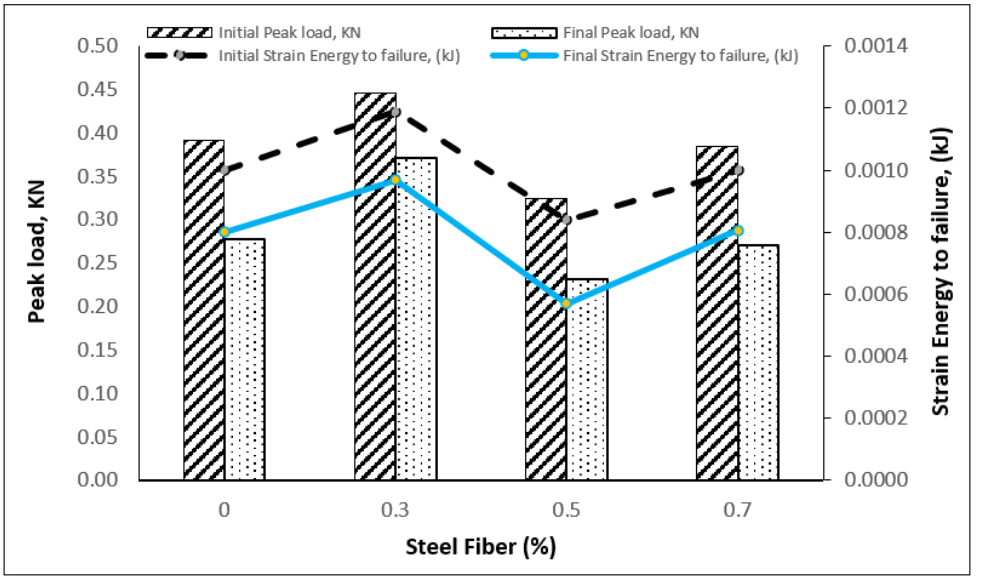

Figure 6. Peak load & strain energy-to-failure values for steel fibre (%)

microwave heating for self-healing, the steel fibre specimens with a 0.3% fibre content exhibited the highest ultimate peak load, indicating excellent self-healing effectiveness.

Steel fibres, particularly at higher concentrations, improve asphalt's ability to return to its original form after cracking. More precisely, the addition of 0.3% steel fibres and the application of microwave treatment enhance the self-healing capability of asphalt pavements, thereby increasing durability.

The results demonstrate a consistent correlation between peak load and strain energy, suggesting their interrelation in assessing a material's mechanical properties. Peak load refers to the maximum amount of force that a material can withstand, which indicates its strength and ability to resist deformation. Strain energy quantifies the energy absorbed during deformation, thereby indicating a material's toughness. A higher peak load indicates superior energy absorption and more resistance to deformation.

The emergence of this tendency can be attributed to the material's inherent mechanical properties, whereby higher strength is associated with stronger molecular bonding and greater structural integrity. The relationship between the maximum load and the energy stored in a material emphasises the balance between its strength and toughness, which is essential for its overall longevity and effectiveness.

Self-Healing Rate of Pavement

The Semi-Circular Bending (SCB) Test measures the Strain Energy and Peak Load of samples, indicating their ability to withstand loads before fracturing. The test exerts

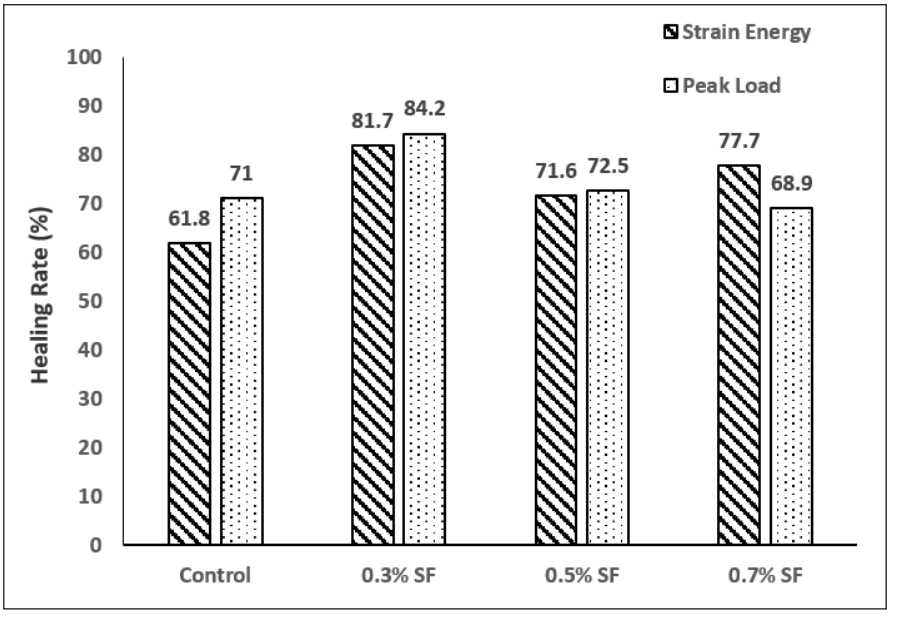

Figure 7. Healing rate of the asphalt mixture

pressure until a predetermined deformation length is achieved. The average healing rate is calculated by comparing the numbers before and after the healing test.

Figure 7 illustrates a percentage comparison of healing rates, showing data for strain energy (kJ) and peak load (N). Data indicate that the inclusion of steel fibre in SMA typically enhances the rate of self-healing. More precisely, a steel fibre content of 0.3% yields the maximum self-healing rate, reaching 81.7% in terms of Strain Energy. In contrast, the control sample with 0% steel fibre has the lowest self-healing rate, measuring 61.8%.

The healing rate varies, suggesting possible anomalies in the mixing or compaction process. The peak load data provide additional evidence of the superiority of the 0.3% steel fibre content, which has a healing rate of 84.2%. In contrast, the steel fibre content of 0.7% has the lowest healing rate at 68.9%.

CONCLUSION

This study examined the impact of adding steel fibre to an asphalt mixture in line with SMA20 requirements. The aim was to identify differences in the mixture's physical properties and its potential for self-healing after performing SCB testing. The following findings are formed based on the outcomes of the experimental work and the extensive analysis:

1. The highest level of stability is attained when the steel fibre percentage is 0.3%, resulting in a weight of 1089.7 kg. Stability decreases beyond this proportion because

of the uneven distribution of fibres. As the steel fibre content increases, the flow values decrease, indicating reduced deformation under load.

2. Air voids decrease with up to 0.5% steel fibre, enhancing density. The 0.3% steel fibre mixture exhibits the lowest abrasion loss, hence enhancing durability. An excessive amount of steel fibre (0.7%) increases abrasion loss and air voids.
3. The 0.3% steel fibre mixture demonstrates the highest initial and ultimate peak loads after self-healing, indicating superior effectiveness. The highest self-healing rates are achieved at a steel fibre content of 0.3%.
4. A steel fibre content of 0.3% maximizes the stability, flow, durability, and self-healing properties of asphalt pavements, leading to improved performance and longevity. Steel fibres, when used in conjunction with microwave heating, greatly enhance the self-healing ability of the asphalt mixture, resulting in stronger and longer-lasting road surfaces.

ACKNOWLEDGEMENT

The authors extend their deepest gratitude to the School of Civil Engineering, College of Engineering, UiTM Shah Alam, for providing the facilities. Additionally, they thank the Ministry of Higher Education for financial support under the Fundamental Research Grant Scheme (600-IRMI/FRGS 5/3(379/2019)), which made writing this paper possible

REFERENCES

Ahmad, N., Haroon, W., & Abid, M. M. (2020). Effect of air voids on permeability and durability of hot mix asphalt. *Journal of the National Science Foundation of Sri Lanka, 48*(4), 463-474. https://doi.org/10.4038/jnsfsr.v48i4.10246

García, A., Norambuena-Contreras, J., Partl, M. N., & Schuetz, P. (2013). Uniformity and mechanical properties of dense asphalt concrete with steel wool fibres. *Construction and Building Materials, 43*, 107-117. https://doi.org/10.1016/j.conbuildmat.2013.01.030

González, A., Norambuena-Contreras, J., Storey, L., & Schlangen, E. (2018). Self-healing properties of recycled asphalt mixtures containing metal waste: An approach through microwave radiation heating. *Journal of Environmental Management, 214*, 242-251. https://doi.org/10.1016/j.jenvman.2018.03.001

Haikal Mohd Ghazali, M. F., Mohd Hasan, M. R., Seman, A. A., Dorett, D. D., Mukhtar, N., & Jaya, R. P. (2021). A review of asphaltic crack healing approaches and its mechanism. *Advances in Materials Science and Engineering, 2021*(1), Article 1093224. https://doi.org/10.1155/2021/1093224

Liu, Q., Li, B., Schlangen, E., Sun, Y., & Wu, S. (2017). Research on the mechanical, thermal, induction heating and healing properties of steel slag/steel fibres composite asphalt mixture. *Applied Sciences, 7*(10), Article 1088. https://doi.org/10.3390/app7101088

Lou, B., Sha, A., Barbieri, D. M., Liu, Z., & Zhang, F. (2021). Microwave heating properties of steel slag asphalt mixture using a coupled electromagnetic and heat transfer model. *Construction and Building Materials, 291*, Article 123248. https://doi.org/10.1016/j.conbuildmat.2021.123248

Loureiro, C. D. A., Silva, H. M. R. D., Oliveira, J. R. M., Costa, N. L. S., & Palha, C. A. O. (2023). The effect of microwave radiation on the self-healing performance of asphalt mixtures with steel slag aggregates and steel fibres. *Materials, 16*(10), Article 3712. https://doi.org/10.3390/ma16103712

Norambuena-Contreras, J., & Garcia, A. (2016). Self-healing of asphalt mixture by microwave and induction heating. *Materials & Design, 106*, 404-414. https://doi.org/10.1016/j.matdes.2016.05.095

Serin, S., Horan, R., & McQuillan, J. (2012). The role of fibres in improving road pavements. *Journal of Pavement Engineering, 13*(2), 165-175.

Shaffie, E., Rashid, H. A., Shiong, F., Arshad, A. K., Ahmad, J., Hashim, W., Jaya, R. P., & Masri, K. A. (2021). Performance characterisation of stone mastic asphalt using steel fibre. *Journal of Advanced Industrial Technology and Application, 2*(2), 22-33. https://doi.org/10.30880/jaita.2021.02.02.003

Shiong, F., & Shaffie, E. (2021). Application of steel fibre to improve the self-healing mechanism of bituminous mixtures: A review. *IOP Conference Series: Earth and Environmental Science, 920*(1), Article 012013. https://doi.org/10.1088/1755-1315/920/1/012013

Shiong, F., Shaffie, E., & Mohamad Rais, N. (2023). Evaluation on volumetric properties of stone mastic asphalt mix containing steel fibre using response surface method. In U. R. Hashim, A. K. Arshad, N. H. Abdul Hamid, R. Hassan, E. Shaffie, A. Alisibramulisi, N. M. Bhkari, & M. N. M. Sidek (Eds.), *Green infrastructure: Materials and sustainable management* (pp. 331–350). Springer. https://doi.org/10.1007/978-981-99-7003-2_19

Song, Y., Wang, Z., Zhou, Y., & Hu, R. (2021). Research on microwave heating performance of modified steel slag asphalt mixture. *Advances in Mechanical Engineering, 13*(4), Article 1687814021990479. https://doi.org/10.1177/1687814021990479

Sun, D., Lin, J., Zhu, X., & Guo, Z. (2017). Investigation on the self-healing behaviour of asphalt mixtures under microwave irradiation. *Road Materials and Pavement Design, 18*(1), 52-70.

Sun, D., Sun, G., Zhu, X., Guarin, A., Li, B., Dai, Z., & Ling, J. (2018). A comprehensive review on self-healing of asphalt materials: Mechanism, model, characterisation and enhancement. *Advances in Colloid and Interface Science, 256*, 65-93. https://doi.org/10.1016/j.cis.2018.05.003

Zhang, B., Gao, X., Xu, S., Yang, X., Tian, Q., & Liu, J. (2023). Microwave heating healing of asphalt mixture with coal gangue powder and basalt aggregate. *Sustainability, 15*(17), Article 12986. https://doi.org/10.3390/su151712986

Zhang, W., Wang, D., & Han, B. (2020). Self-healing concrete-based composites. In A. Khan, M. Jawaid, S. N. Raveendran, & A. M. A. Asiri (Eds.), *Self-healing composite materials: From design to applications* (pp. 259-284). Woodhead Publishing. https://doi.org/10.1016/B978-0-12-817354-1.00015-6

Zhao, H., Zeng, M., & Guo, Y. (2020). Influence of steel fibre content on the mechanical properties and self-healing ability of asphalt mixtures. *Journal of Cleaner Production, 258*, Article 120836.

Pertanika J. Sci. & Technol. 34 (S2): 29 - 36 (2026)

PERTANIKA JOURNALS

SCIENCE & TECHNOLOGY

Journal homepage: http://www.pertanika.upm.edu.my/

Hybrid Solar PV-Micro-Hydro System for Sustainable Electrification of Remote Communities in Arunachal Pradesh, India

Somila Hashunao[1]*, Taken Nguri[1], A.S Shimreiwung[2], Ngayaiwon Hashunao[3], and Ram Krishna Mehta[1]

[1]Department of Electrical Engineering, Northeastern Regional Institute of Science and Technology (NERIST), 791109 Nirjuli (Itanagar), Arunachal Pradesh, India
[2]Department of Sociology, Tezpur University, Napaam, 784028 Sonitpur, Assam, India
[3]Department of Electrical Engineering, Manipur Technical University, Government Polytechnic Campus, Takyelpat, 795004 Imphal West, Manipur, India

ABSTRACT

Existence is challenging without power. The load demand indicates the condition or benchmark for that specific zone/region. It is a metric that represents the standard of living. Natural, clean, renewable resources abound in Arunachal Pradesh, particularly in the state's rural areas, where electricity demand remains unmet. This study focuses on resources that could be used to generate small-scale energy to meet the electrical needs of economically disadvantaged rural areas with dispersed populations and low living standards. Field observations, conversations with locals, and other data were gathered throughout the site study to help sketch out a workable off-grid technology. Additionally, the paper addresses barriers to entry, as well as the implications and opportunities that come with sustainable energy technology. It concludes that in areas with lower population densities and remote locations from grid-connected systems, it makes more sense and is more cost-effective to focus on a modest-scale renewable energy system using locally available natural resources.

Keywords: Hydro Energy, rural areas, solar PV, sustainable development

ARTICLE INFO

Article history:
Received: 18 June 2026
Accepted: 25 September 2026
Published: 30 September 2026

DOI: https://doi.org/10.47836/pjst.34.S2.03

E-mail address:
susonao@gmail.com (Somila Hashunao)
shimreiwung@gmail.com (A.S Shimreiwung)
ng.hashunao@gmail.com (Ngayaiwon Hashunao)
takennguri1998@gmail.com (Taken Nguri)
rkm@nerist.ac.in (Ram Krishna Mehta)
* Corresponding author

INTRODCUTION

Electricity is a necessity of life. To narrow the gap between well-being and livelihoods, the only measure is to find the most economical and feasible way. Exploring the renewable resources will encapsulate the difficulties. Renewable resources are an alternative for isolated areas with smaller populations, where off-grid power is more

e-ISSN: 2231-8526

© Universiti Putra Malaysia Press

economical. Furthermore, the cost of renewable energy (RE) technologies has dropped significantly in recent years, coinciding with a significant decline in the price of electricity produced by wind, photovoltaics (PV), hydropower, and concentrated solar power between 2010 and 2018 (Figure 1). Over 80% of solar photovoltaic (PV) and 75% of wind projects scheduled for commissioning in 2020 will generate energy at a lower cost than any natural gas, coal, or oil option, according to a report from the International Renewable Energy Agency (2019). For low-load power and remote locations, solar photovoltaics (PV) and wind turbines (WT) are the most popular green energy alternatives (Javed et al., 2019; Roberts & Mosey, 2014; St. Croix Tribal Council, 2005). Yet, as demonstrated by a recent work by Fasihi and Breyer (2020), these RE resources' inherent intermittency, volatility, and randomness typically render them unsuitable for direct integration to the grid.

Arunachal Pradesh is one of the 7th northeastern-most states of India. It shares international borders with Bhutan; Myanmar is separated from China in the north by the McMahon Line and the state border with Assam and Nagaland. This state consists of 25 districts, with more districts proposed and in development. Itanagar is the capital of the state. Geographically, it is the largest state among the Northeastern states. Arunachal Pradesh consists of the sub-mountainous and mountainous ranges. With 94% of the area rural, life is scattered across 3,257 villages under the umbrella of 48 integrated rural development blocks. Off-grid generation must be considered to meet electrical demand at a reasonable cost (Rehman et al., 2012). Due to geographical features and current grid restrictions, which make grid extension economically infeasible in many places, it is frequently technically difficult (Nouni et al., 2006). National policy documents commit to the long-term objective of ensuring that everyone has access to clean energy by 2030 and acknowledge that environmental concerns are also very real. They also state that off-grid energy provision is necessary to raise the living conditions of the rural poor (Ministry of Population and Environment, 2016). The lives of the rural can be improved with respect to primary health care and education centres if alternative means, such as the use of more renewable energy, are embedded in people's minds through awareness camps and seminars, or by interacting with the well-being. The people of Arunachal Pradesh are abundant in natural resources, including hydropower, and are among the largest generators of hydropower, but many places remain inaccessible due to dense forests, creating a significant gap in transportation and communication facilities. Some districts, such as East Siang and Lower Subansiri, have been 99% electrified.

Study on the Selected Site

The selected site area has a population of 600 and 150 households, two primary schools, and 10 mini commercial local utility centres. People's livelihoods depend solely on farming. To fulfil the basic requirement, a power plant with a generating capacity of 27 kW is to be installed. The most economically feasible approach is to adopt a hybrid system (Come Zebra et al., 2021). In the current context, research studies emphasise raising awareness

and facilitating access to off-grid renewable energy sources, particularly in isolated regions (Ma & Javed, 2019; Khodayar, 2017). In their evaluation of the importance of remote places, Liu et al. (2019) found that hybrid RES systems can significantly increase off-grid electricity output (Jithendranath et al., 2021). It is important to consider a cost-benefit analysis for energy sector interconnection.

A comprehensive cost-benefit analysis of energy sector interconnection should consider a range of economic, technical, and environmental benefits. These include reductions in the value of lost load, improvements in energy security, and environmental benefits from increased utilisation of cleaner energy sources. Greater interconnection may also enhance competition within the energy sector, potentially resulting in lower electricity prices for consumers. Furthermore, access to interconnected energy systems can defer the need for additional investments in generation capacity required to meet domestic demand. Transmission and distribution costs may also be reduced when lower-cost and geographically closer generation sources are utilised in place of more expensive alternatives. In addition, improvements in power system stability and reliability can contribute to local economic development by supporting commercial activities and essential public services. Reduced electricity expenditure may increase households' and businesses' disposable income, thereby generating positive spillover effects on the local economy, infrastructure development, and public service provision. Moreover, the integration of neighbouring energy markets through enhanced interconnection may stimulate further investment in domestic power generation facilities and strengthen the overall resilience of the energy system.

Objectives of the Study

The installation of small hydropower plants is a growing focus because they are more reliable, have lower environmental impact, and, most importantly, can supply energy at low cost (Patel, 2018). It has been found that a Pico Hydro Power plant can provide power in the most efficient way to small, scattered populations and remote communities that require power only for lighting. Pico-hydro setups are typically run-of-stream, as water runs downhill, it has potential energy that can be captured. The advantages of a steady stream of flowing water over solar and wind power systems are substantial (Islam et al., 2013; Javed et al., 2020). Because Micro-Hydro systems only require a steady flow of water through the turbine, they can operate day or night and in any kind of weather. The objective is to identify un-electrified villages, survey potential renewable energy sources in remote, un-electrified villages where grid connection is not feasible or economical and provide basic household lighting systems to improve the quality of life (Javed et al., 2021).

Identification of Un-Electrified Villages

Still, around the globe, many efforts and steps are being taken by governments, NGOs, and even private firms. Many rural homes lack power, according to government statistics

(as of October 12, 2018) derived from the Saubhagya dashboard. The goal of Saubhagya, which was introduced in September 2017, was to electrify 35 million homes by March 2019. Subsequently, the government announced that it would electrify every home by December 31, 2018, pushing the deadline forward. However, as of October 12, 2018, data from the Saubhagya Dashboard shows that approximately 25-30% of rural households in four states, Uttar Pradesh, Arunachal Pradesh, Nagaland, and Meghalaya, still lack electricity (Indian Express, 2018; Singh, 2016). According to a recent government release, 2,217 villages in India lacked electricity. Arunachal Pradesh made up 1,069, or 48%, of this total. It is important to note that the rugged terrain and the scattered nature of communities across hills and forested areas make comprehensive village electrification appear to be a daunting endeavour (Aquino et al., 2011). In Arunachal, a state with a total land area of 83,743 square kilometres, roughly 82% is covered in dense evergreen forests. Nevertheless, village electrification has accelerated recently, particularly since the announcement of the goal of achieving universal village electricity (Rehman et al., 2012). According to the survey, villages such as Norbing in Lower Subansiri District, Machang in Papumpare District, Sijirarkhsap in West Siang District, and Lokpeng in East Siang District are yet to be electrified. Dwellings in a cluster of disconnected, unelectric homes, images taken during the research fieldwork for the site study, are shown in Figures 1 and 2.



Figure 1. Unelectrified village of Norbing, District- Lower Subansiri. Circle –Raga



(a) (b)

Figure 2. Unelectrified at (a) Sibe village, Lower Siang and (b) Sijirarkhsap village of West Siang

METHODOLOGY

The analysis was done in Sibe village (under Gensi circle) in Lower Siang district of Arunachal Pradesh, India. It is located about 60 km away from the main state road and about 40 km from the last electrified point. The study area is administered by the Circle Officer (CO). Most of the population belongs to the Galo tribe community. Solar irradiance data were obtained from a survey conducted in the study area and surrounding regions, and the river flow rate was calculated from it.

Energy Demand Estimation

The total electrical demand for the study area is estimated based on the community's actual needs and divided into categories such as domestic, commercial, and community, as shown in Table 1. The LED-based lighting scheme is considered in the analysis due to its advantages over incandescent and CFL lamps. The power demand is estimated for the average daily demand of the entire village, which is about 270100 watts. The daily energy demand profile is shown in Table 2.

Table 1
Number of lights/ fans/tv/computer

Sl. No.	Quantity	No. of Lights	No. of Fans	No. of Computers
	Residential	300	300	Nil
	Shop	10	10	Nil
	School	20	20	8

Table 2
Estimated daily energy demand profile

Serial Number	Category and Sector (with Quantities) of Load	Appliance	Hours/ Day	Rating (W)	No. of Points (in Each House)	Total No. of Points	Wattage
1	Domestic:						
	Households (150)	LED lamp	5	12	2	300	3600
		Fan	6	45	2	300	13500
		TV	6	70	1	100	7000
2	Commercial:						
	Shops (10)	LED lamp	4	12	1	10	120
		Fan	6	45	1	10	450
3	Community:						
	School	LED lamp	4	12	10	20	240
		Fan	6	45	10	20	900
		Computer	4	150	4	8	1200

Resource Estimation

Arunachal Pradesh is hilly and rich in renewable energy sources such as hydropower and solar power. To estimate the potential of the sources, an extensive survey was conducted in the study area and surrounding regions. According to Synergy Environ Engineers (Indian Express, 2018), the average global solar radiation on a horizontal surface is 4.01 kWh/m^2/day, with a peak of 4.5 kWh/m^2/day in May and a minimum of 3.39 kWh/m^2/day in January. Table 3 shows the daily isolation corresponding to the clearness index of the study area. The village also has many streams that flow year-round, and the flow rate of each stream has been determined using the conventional flow-meter method; therefore, a micro-hydro power plant has been considered in addition to the solar PV system.

Table 3
Solar radiation and clearance index

Sr. No.	Month	Monthly Average Daily Solar Radiation (kWh/m^2/day)	Clearness Index
1	January	3.39	0.53
2	February	3.46	0.51
3	March	3.65	0.57
4	April	4.03	0.53
5	May	4.50	0.57
6	June	4.03	0.49
7	July	3.88	0.33
8	August	4.20	0.41
9	September	4.20	0.22
10	October	4.17	0.51
11	November	4.07	0.29
12	December	3.65	0.54

CONCLUSION

A study has been conducted to evaluate the economic and technical feasibility of combining a micro hydropower plant with a 27-kW integrated solar PV power plant to meet the energy needs of Sibe village in the Gensi circle of Arunachal Pradesh's Lower Siang district. The PV system consists of 60 PV modules, with two connected in series and 30 such series-connected in parallel, three 2400W inverters, and a 2285 Ah battery bank. A centralised battery bank and inverter are connected to the PV modules. The PV system can generate 77.67kWh of energy daily. A 15 kW micro-hydro power plant, along with the PV system, has been analysed to meet the total demand for basic well-being needs.

Thus, most villages with small, scattered populations can be electrified using available renewable energy. Resources are readily available, but due to a lack of transportation and unexplored areas, they cannot utilise the full range of available resources uniformly, leading

to a non-uniform standard of living. Hence, with proper planning and the selection of renewable resources, improvements in their lifestyles and healthcare will be facilitated, which are among the basic and foremost requirements for a healthy life. Exploring more small-scale renewable power plants will be the primary driver to eradicate differences based on geographical region or zone and bring 100% electrification to every corner of the people, regardless of the geographical region or population.

ACKNOWLEDGEMENT

The authors would like to sincerely thank our supervisors for their valuable guidance, encouragement, and continuous support throughout this research. Their insightful suggestions, constructive feedback, and patience greatly contributed to the successful completion of this work. The authors are also grateful to all for their constant encouragement and support, whether direct or indirect, throughout this study.

REFERENCES

Aquino, A., Bosscher, D., Schnoor, W., & Ziegler, D. (2011). *Project proposal and feasibility study: Sim Escape*. Calvin College Engineering Department.

Come Zebra, E. I., van der Windt, H. J., Nhumaio, G., & Faaij, A. P. C. (2021). A review of hybrid renewable energy systems in mini-grids for off-grid electrification in developing countries. *Renewable and Sustainable Energy Reviews, 144*, Article 111036. https://doi.org/10.1016/j.rser.2021.111036

Fasihi, M., & Breyer, C. (2020). Baseload electricity and hydrogen supply based on hybrid PV-wind power plants. *Journal of Cleaner Production, 243*, Article 118466. https://doi.org/10.1016/j.jclepro.2019.118466

Icaza, D., Pulla Galindo, S., Flores-Vázquez, C., & Sangurima Paute, F. (2021). Artistic creations supplied by renewable energy located in the most attractive mountains of Azuay: Case study: Cultural heritage of Quingeo. In M. Botto Tobar, H. Cruz, & A. Díaz Cadena (Eds.), *Recent advances in electrical engineering, electronics and energy: Proceedings of the CIT 2020* (pp. 273–287). Springer. https://doi.org/10.1007/978-3-030-72212-8_20

International Renewable Energy Agency. (2019). *Renewable power generation costs in 2018*. https://www.irena.org/publications/2019/May/Renewable-power-generation-costs-in-2018

Islam, M. S., Islam, A., Hasan, M. M., & Khan, A. H. (2013). Feasibility study of wind power generation in Bangladesh: A statistical study in the perspective of wind power density and plant capacity factor. *International Journal of Renewable Energy Research, 3*(3), 476-487.

Javed, M. S., Ma, T., Jurasz, J., & Amin, M. Y. (2020). Solar and wind power generation systems with pumped hydro storage: Review and future perspectives. *Renewable Energy, 148*, 176-192. https://doi.org/10.1016/j.renene.2019.11.157

Javed, M. S., Ma, T., Jurasz, J., Canales, F. A., Lin, S., Ahmed, S., & Zhang, Y. (2021). Economic analysis and optimization of a renewable energy based power supply system with different energy storages for a remote island. *Renewable Energy, 164*, 1376-1394. https://doi.org/10.1016/j.renene.2020.10.063

Javed, M. S., Song, A., & Ma, T. (2019). Techno-economic assessment of a stand-alone hybrid solar-wind-battery system for a remote island using genetic algorithm. *Energy, 176*, 704-717. https://doi.org/10.1016/j.energy.2019.03.131

Jithendranath, J., Das, D., & Guerrero, J. M. (2021). Probabilistic optimal power flow in islanded microgrids with load, wind and solar uncertainties including intermittent generation spatial correlation. *Energy, 222*, Article 119847. https://doi.org/10.1016/j.energy.2021.119847

Khodayar, M. E. (2017). Rural electrification and expansion planning of off-grid microgrids. *The Electricity Journal, 30*(4), 68–74. https://doi.org/10.1016/j.tej.2017.04.004

Liu, L., Sun, Q., Li, H., Yin, H., Ren, X., & Wennersten, R. (2019). Evaluating the benefits of integrating floating photovoltaic and pumped storage power system. *Energy Conversion and Management, 194*, 173-185. https://doi.org/10.1016/j.enconman.2019.04.071

Ma, T., & Javed, M. S. (2019). Integrated sizing of hybrid PV-wind-battery system for remote island considering the saturation of each renewable energy resource. *Energy Conversion and Management, 182*, 178-190. https://doi.org/10.1016/j.enconman.2018.12.059

Ministry of Population and Environment. (2016). *Renewable energy subsidy policy, 2073 BS*. Government of Nepal.

Nouni, M. R., Mullick, S. C., & Kandpal, T. C. (2006). Techno-economics of micro-hydro projects for decentralized power supply in India. *Energy Policy, 34*(10), 1161-1174. https://doi.org/10.1016/j.enpol.2004.10.016

Patel, D. (2018, January 29). Rural electrification: Arunachal a major hurdle in achieving May 1 deadline. *The Indian Express*. https://indianexpress.com/article/business/budget/union-budget-rural-electrification-arunachal-a-major-hurdle-in-achieving-may-1-deadline-5042809/

Rehman, S., Mahbub Alam, M., Meyer, J. P., & Al-Hadhrami, L. M. (2012). Feasibility study of a wind–PV–diesel hybrid power system for a village. *Renewable Energy, 38*(1), 258-268. https://doi.org/10.1016/j.renene.2011.06.028

Roberts, J. O., & Mosey, G. (2014). *Economic and technical feasibility study of utility-scale wind generation for the New York Buffalo River and South Buffalo Brownfield Opportunity Areas* (NREL/TP-5000-60440). National Renewable Energy Laboratory. https://doi.org/10.2172/1129276

St. Croix Tribal Council. (2005). *Feasibility study for biomass electrical generation on tribal lands*. St. Croix Chippewa Indians of Wisconsin.

Synergy Environ. (n.d.). *Solar irradiance: Yupia, Arunachal Pradesh, India*. Retrieved September 25, 2026, from https://www.synergyenviron.com/tools/solar-irradiance/india/arunachal-pradesh/yupia

Pertanika J. Sci. & Technol. 34 (S2): 37 - 50 (2026)

PERTANIKA JOURNALS

SCIENCE & TECHNOLOGY

Journal homepage: http://www.pertanika.upm.edu.my/

Correlation Between Compressive and Flexural Properties in Steel Fibre Reinforced Concrete (SFRC) Beam Using Regression Analysis

Md Yushairi Kamarul Effendy Mohd Yusof[1], Anizahyati Alisibramulisi[2,3]*, Muhd Norhasri Muhd Sidek[2,3], Nadiah Saari[2], and Suraya Hani Adnan[4]

[1]ARUP Jururunding Sdn. Bhd., Level 26, 1 Powerhouse, No. 1 Persiaran Bandar Utama, Bandar Utama, 47800 Petaling Jaya, Selangor, Malaysia

[2]Faculty of Civil Engineering, Universiti Teknologi MARA, 40450 Shah Alam, Selangor, Malaysia

[3]Institute for Infrastructure Engineering and Sustainable Management (IIESM), Universiti Teknologi MARA, 40450 Shah Alam, Selangor, Malaysia

[4]Department of Civil Engineering Technology, Faculty of Engineering Technology, Universiti Tun Hussein Onn Malaysia, 84600 Pagoh, Johor, Malaysia

ABSTRACT

This study evaluated Ground-Penetrating Radar (GPR) to assess steel fibre distribution in Steel Fibre Reinforced Concrete (SFRC) beams and correlated non-destructive and mechanical strength properties. High-Performance Concrete (C60) beam specimens (100 mm × 100 mm × 500 mm) were prepared with steel fibre volume fractions of 0.5%, 1.0%, and 1.5%. Non-destructive testing (GPR, Rebound Hammer) and destructive testing (3000 kN compressive and 1000 kN flexural strength) were conducted at 7, 21, and 28 days. GPR radargrams displayed hazy patterns with overlapping hyperbolas, confirming uniform fibre distribution. Haze intensity increased at 1.5% fibre content. Compressive strength peaked at a 0.5% fibre fraction, whereas flexural strength reached its optimum at 1.5%. Linear Regression Analysis (NCSS 2021) demonstrated a strong R2 fit between compressive and flexural strengths. Overall, GPR proves effective for non-destructive fibre evaluation, aiding quality assessment in high-performance concrete structures.

Keywords: Compressive, flexural, Ground Penetrating Radar (GPR), regression analysis, Steel Fibre Reinforced Concrete (SFRC)

ARTICLE INFO

Article history:
Received: 18 June 2026
Accepted: 19 August 2026
Published: 30 September 2026

DOI: https://doi.org/10.47836/pjst.34.S2.04

E-mail addresses:
mdyushairi@gmail.com (Md Yushairi Kamarul Effendy Mohd Yusof)
aniza659@uitm.edu.my (Anizahyati Alisibramulisi)
muhdnorhasri@uitm.edu.my (Muhd Norhasri Muhd Sidek)
nadiahsaari@uitm.edu.my (Nadiah Saari)
suraya@uthm.edu.my (Suraya Hani Adnan)
* Corresponding author

INTRODUCTION

Steel Fibre Reinforced Concrete (SFRC) is a structural reinforcing technology that aims to reduce the demand for reinforcement while simultaneously increasing the flexural toughness, flexural strength,

e-ISSN: 2231-8526

© Universiti Putra Malaysia Press

fatigue resistance, impact resistance, and post-fracture strength of the concrete. The Non-Destructive Testing (NDT) method has been used to investigate a variety of concrete issues. Although SFRC beams may exhibit higher compressive and flexural strength, there is a dearth of research on the use of Ground-Penetrating Radar (GPR) to analyse concrete quality in relation to SFRC beam strength, compared with conventional reinforced concrete. Additionally, there is a dearth of studies about the uniformity of steel fibres in SFRC beams. It is observed that most published empirical relationships have been reported for conventional concrete and SFRC; however, few have been studied for SFRC using regression and Pearson correlation analyses.

Bibliometric studies are defined as statistical evaluations and tools used to achieve quantitative research of published journal papers, proceedings, scholars, scientific articles or books, and are an effective method to assess the influence of journal papers, authors' research areas, citation networks, topics, and documents (Briones-Bitar et al., 2020; Van Eck & Waltman, 2020). VOSviewer software was used to construct and visualise the bibliometric networks of journal papers related to GPR.

GPR is a non-destructive testing technique that uses a scanning method and is currently in wide use in the civil engineering field, with a potential application in concrete testing (Dinh et al., 2013; Giannopoulos, 2005; Lakshmi et al., 2016; Sultan et al., 2020; Warren & Giannopoulos, 2016).

According to early research by Bachiri et al. (2018), Morcous and Erdogmus (2009), and Sun et al. (2018), the GPR method achieves 98%- 99% accuracy in detecting rebar position, delamination, and corrosion defects. Lakshmi et al. (2016), Leucci (2012), Rathod et al. (2019), and He et al. (2009) have demonstrated in their studies that the difference in rebar radius estimates is about 2.5% to 6% when using the GPR method on bridge decks and reinforced concrete slabs. The use of GPR in reinforced concrete can detect concrete delamination and rebar corrosion at an early stage (Shamsudin et al., 2015; Sun et al., 2018; Zaki et al., 2018) and assess the thickness of concrete pavement (Morcous & Erdogmus, 2009). Other researchers have used the GPR technique to detect air void size and depth (Razak et al., 2015) and to estimate the volumetric water content in reinforced concrete (Leucci, 2012).

For steel fibre fractions of 0%, 0.5%, 1.0%, and 1.5%, there is a marginal improvement in compressive strength from 0.5% to 1.0%, followed by a decrease from 1.0% to 1.5%. The compressive strength increased with increasing steel fibre volume fraction from 0% to 3.0%, reaching a maximum at 3.0%. Findings from Al-Ameeri (2013) indicate that compressive strength increases with age and with the steel fibre volume fraction up to 0.75% and decreases when the steel fibre volume fraction exceeds 0.75%. As the steel fibre volume fraction increases from 0% to 3.0%, the compressive strength of concrete increases progressively owing to the balling effect, and inappropriate bonding occurs

beyond 3.0% (Al-Ameeri, 2013). Harle (2019) discovered that the optimal steel fibre content for compressive cube strength is 1.0%.

Increasing the steel fibre volume fraction from 0% to 3.0% was found to increase flexural strength and improve resistance to cracking (Kumar Athithan et al., 2017). According to Al-Ameeri (2013), flexural strength increases continuously with increasing steel fibre volume fraction up to 1.5%. According to studies conducted by Al-Ameeri (2013), the addition of steel fibre to concrete increases the flexural strength continuously as the steel fibre fraction volume increases from 0% to 3.0%, but as the steel fibre fraction volume increases above 3.0%, the flexural strength appears to decrease gradually due to the balling effect and improper bonding with the concrete.

Incorporating steel fibres reduces the workability of new concrete and increases the likelihood of non-uniform dispersion. The water-cement ratio may be increased, or water-reducing admixtures may be used. According to Eurocode 2, steel fibres don't change the tensile strength of the concrete itself. They can, however, reduce cracking and help concrete parts be more ductile (Al-Ameeri, 2013; Jhatial et al., 2018; Neville, 2012; Shetty, 2012).

In this study, the correlation between compressive strength and flexural strength was explored using Linear Regression Analysis and Pearson Correlation. Correlation analysis quantifies the degree and direction of the linear relationship between two variables, while basic linear regression estimates parameters in a linear equation that can be used to forecast one variable from the other (Profillidis & Botzoris, 2019). A total of 878 authors, with a minimum of 5 documents per author, are repeated in the publication and conduct studies related to ground-penetrating radar. Only 17 authors with publications in ground penetrating radar meet the threshold. The total strength of the co-authorship links with other authors was calculated by Vos viewer, and the greatest total link strength was selected. In total, the 17 authors who conducted studies on the application of ground-penetrating radar to existing structures can be clustered into 9 groups, indicating a strong bond among them, as shown in Figure 1.

There was a total of 24 authors, each of whom has at least one paper related to the publication, who undertake research on ground-penetrating radar and steel fibre-reinforced concrete. The 24 authors with publications on ground-penetrating radar in steel fibre-reinforced concrete that meet the threshold. Figure 2 shows that the 24 authors have strong bond links and co-occurrence in studies on the application of GPR to steel fibre-reinforced concrete, with eight clusters of co-authorship that are linked to each other. Some of the 24 authors in the network are not connected to each other (Van Eck & Waltman, 2020). Based on the schematic literature, GPR is most widely used on existing concrete structures and is also used abroad.

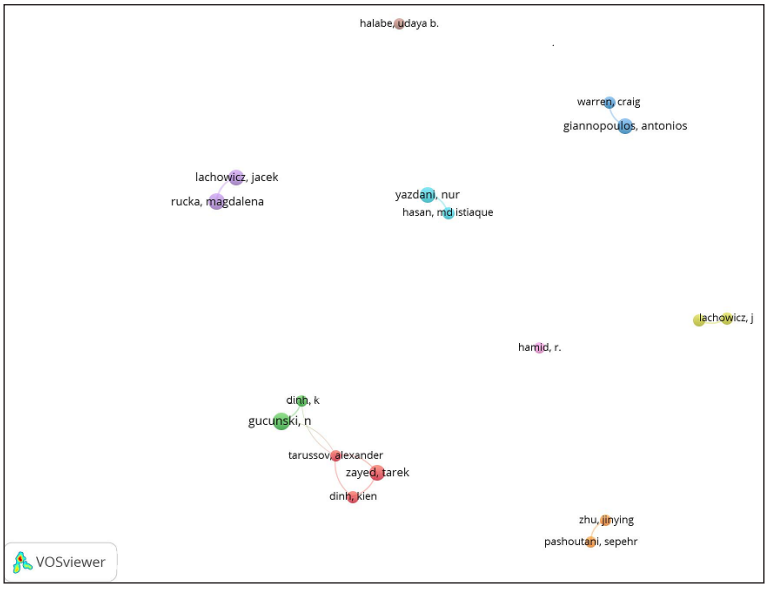

Figure 1. Authors are grouped into 9 clusters, as reported in GPR studies



Figure 2. A total of 24 authors linked studies on GPR applications to steel fibre-reinforced concret

METHODOLOGY

A comprehensive method and methodology will aid in understanding the underlying principle and the experimental procedure. This research methodology describes the experimental setup, test procedures for non-destructive and destructive tests, linear

regression analysis, and Pearson correlation for conducting the test regime undertaken in the present research topic. Data collection for this experimental study shall be collected by using GPR equipment IDS GeoRadar TR-HF with antenna 2.0 GHz, Rebound Hammer Test and Flexural Test for scanning and testing the specimen sample SFRC beam and RC beam prepared in laboratory environment condition and field test data of GPR, Rebound Hammer Test, Flexural Test and Cube Compressive Test/Broken Beam Compressive Test to specimen sample SFRC beam and RC beam shall be process for evaluation, analysis and modelled in linear regression analysis using NCSS 2021 software (Hintze, 2007). The experimental work that will be used in this study is to determine the application and effectiveness of the GPR application and to study the strength of SFRC using GPR, with a correlation of the Rebound Hammer Test and the behaviour of the SFRC beam using the Flexural Test Method from the experimental work, as shown in Figure 3.

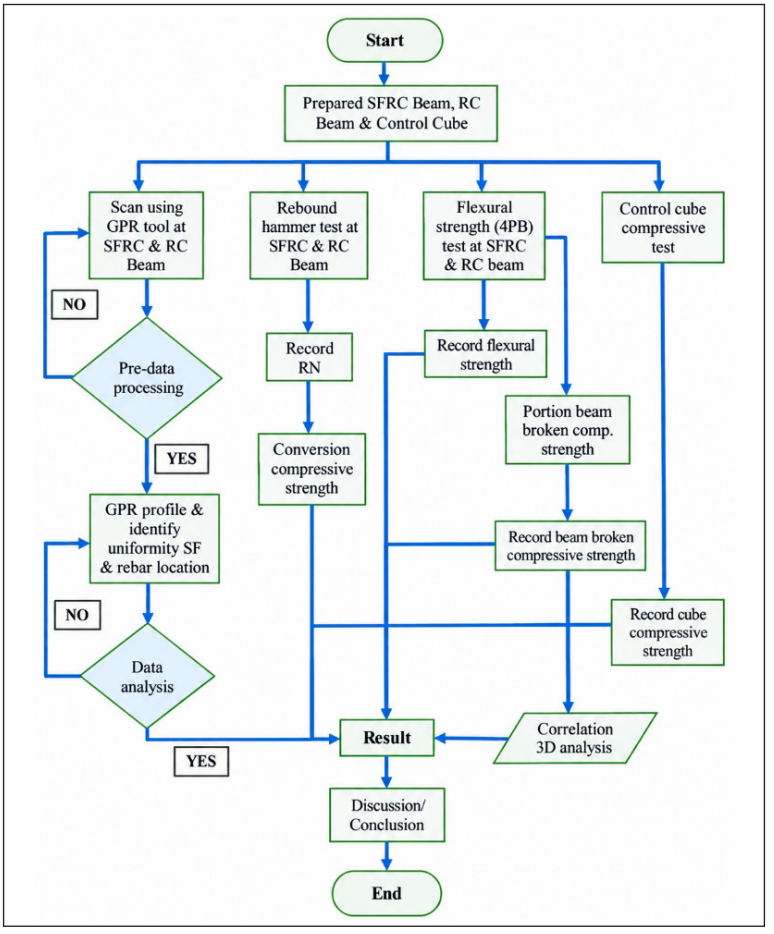

Figure 3. Methodology in this study

RESULTS AND DISCUSSION

GPR - Radargram

Figure 4a shows the radargram B-scan image section of the reinforced concrete beam control sample in X-plane and Y-plane, where the target formed a hyperbolic shape to represent the reinforcement bar detected embedded in the control samples. This finding is in line with other researchers' (Gehrig, 2004; Hasan & Yazdani, 2016; Jaya, 2013; Lakshmi et al., 2016; Leucci, 2012; Liu et al., 2020; Rathod et al., 2019; Wiwatrojanagul et al., 2018; Zhou et al., 2018) efforts to identify the location and reinforcement bar diameter. Figure 4b shows the radargram B-scan image section of the SFRC beam sample with a different steel fibre fraction volume. It can be observed that for the steel fibre mix, the radargram does not show the expected result of the hyperbola shape found in the RC beam (Maierhofer, 2003); instead, the radargram image shows a hazy image like a radio static wave and multiply hyperbola with overlapping each other, with no distinct apparent reflection of individual hyperbolas as embedded reinforcement bars. This shows the uniformity of steel fibre in the SFRC beam. The radargram image for the SFRC beam, under hazy conditions, has become heavier and more sophisticated as the steel fibre volume fraction increased from 0.5% to 1.5%.

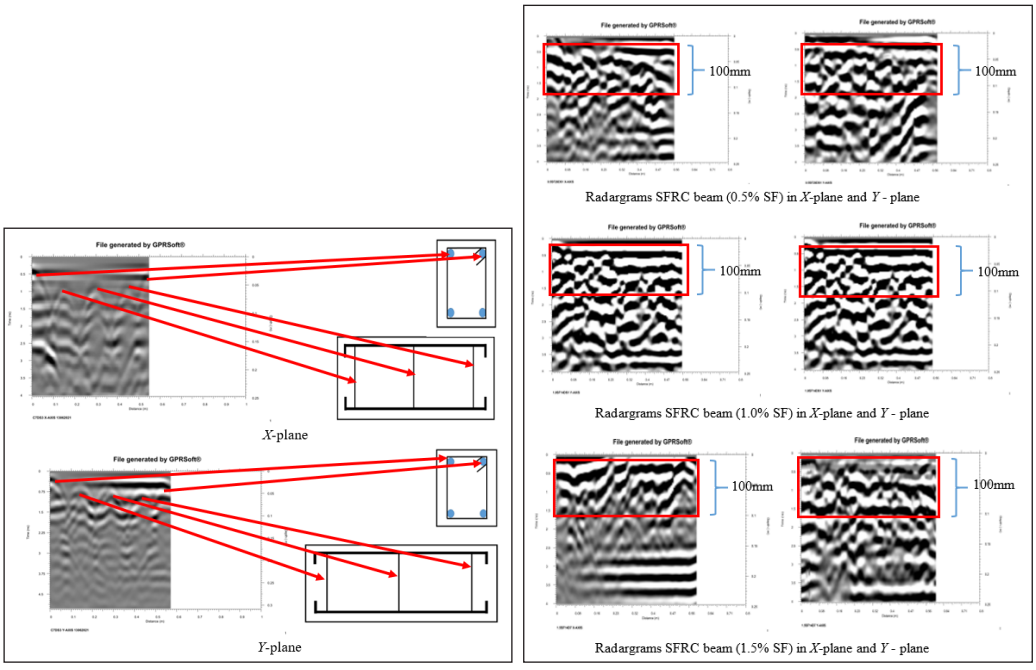

Figure 4. Tabulation of (a) Radargrams RC beam size 100mm × 100mm × 500mm in X-plan and Y-plane (b) Radargrams SFRC beam (0.5%, 1.0%, and 1.5% steel fibre) in X-plane and Y-plane

Compressive and Flexural Strength

From Figure 5, the cube compressive strength test result, it is shown that the addition of steel fibres in the concrete helps to increase the concrete strength when 0.5% steel fibre and 1.5% steel fibre fraction volume are added to the concrete, given the compressive values of 181.2 N/mm^2 and 88.1 N/mm^2 at 28 days of concrete age. When a 1.0% steel fibre volume fraction is added to the concrete, the concrete's compressive strength decreases from 139.5 N/mm^2 at 7 days to 98.2 N/mm^2 at 28 days of ageing. Based on the cube compressive strength test result at 28 days of concrete age, the optimum fibre content for SFRC was found to be 0.5% steel fibre, given a compressive strength of 181.2 N/mm^2. The finding on the optimum steel fibre content for compressive strength is in line with studies by Al-Ameeri (2013) and Rao (2010), which found that steel fibre contents of 0.5% to 1.0%, 0.75%, and up to 3.0% increase the compressive strength of SFRC. Similar findings from studies by Rao (2010) and Al-Ameeri (2013) for 1.0% steel fibre content show a decrease in compressive strength.

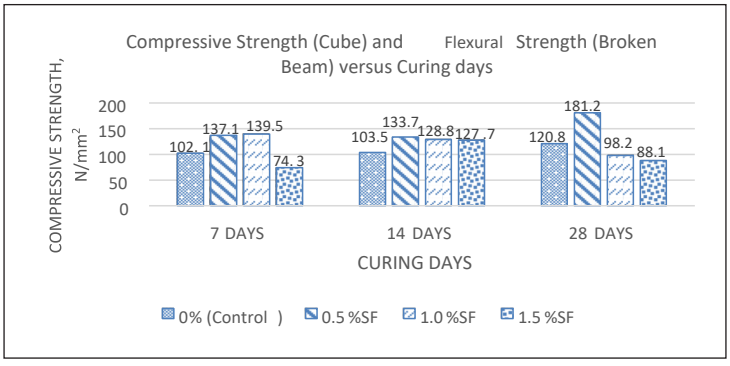

Figure 5. Compressive strength (cube) and flexural strength (broken beam) versus curing days

Figure 6, representing 3 different case studies with loading spans of 102.3 mm, 136.4 mm, or 181.8 mm, shows that the control sample with a reinforcement bar has the best flexural strength compared to those with steel fibre added as an alternative. In comparison to an SFRC with a different volume fraction, the SFRC exhibits an increase in flexural strength as the volume fraction of steel fibre increases. Based on three distinct case studies with loading spans of 102.3mm, 136.4mm, and 181.8mm, a 1.5% steel fibre volume fraction exhibits the highest flexural strength on day 28 compared with other SFRC samples, whereas a 0.5% steel fibre volume fraction exhibits the lowest. The results indicate that a 1.5% steel fibre volume fraction in SFRC yields the highest flexural strength, followed by 0.5% and 1.0%. This finding is in line with studies by Al-Ameeri (2013) and Kumar Athithan et al. (2017). The control sample with a reinforcement bar is much stronger than the steel fibre sample in terms of flexural strength.

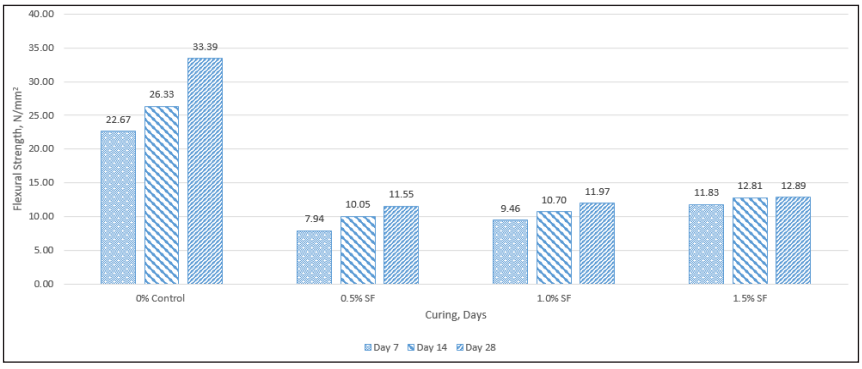

(a)

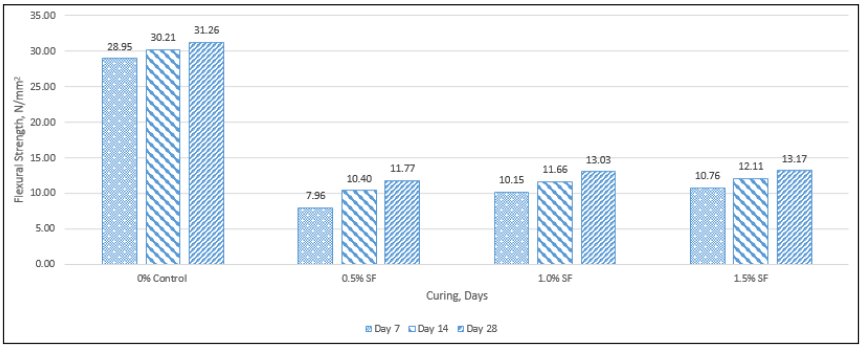

(b)

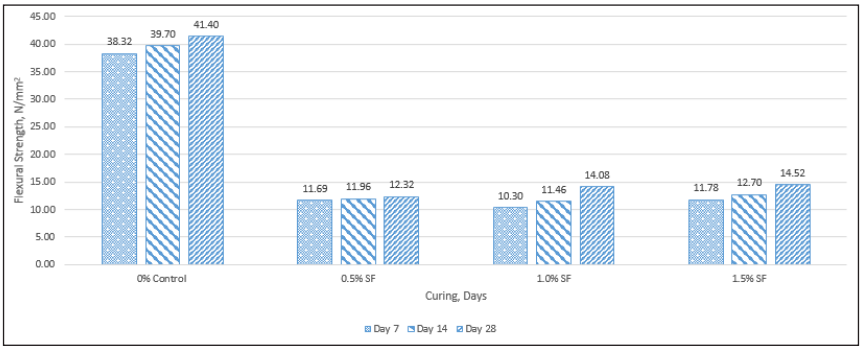

(c)

Figure 6. Tabulation of flexural strength (N/mm^2) with respect to curing days (a) Case 1; (b) Case 2; (c) Case 3

Using the collected experimental dataset, the correlation between steel fibre and the compressive and flexural strengths of SFRC beams has been assessed by performing Linear Regression Analysis and Pearson Correlation. The empirical or correlation equation model obtained for the compressive strength of cubes and beams broken for SFRC beams is presented in Equation 1:

$$fck\ cube\ comp\ BB\ cube = (129.3083) + (-12.9567)Vf \quad [1]$$

Where,
fck cube comp BB cube = Cube and beams broken compressive strength (N/mm^2),
Vf = steel fibre volume fraction.

The empirical or correlation equation model obtained for flexural strength for SFRC beam are pre-sented in Equation 2:

$$flexural\ strength,\ \sigma = (24.5684) + (-11.2783)\ Vf \quad [2]$$

Where,
flexural strength, σ = Flexural strength (N/mm^2),
Vf = steel fibre volume fraction.

The empirical or correlation equation model obtained for compressive strength conversion of rebound number (RN) for SFRC beams is presented in Equation (3):

$$fck\ cube\ comp\ RN = (37.1307) + (-0.0387)Vf \quad [3]$$

Where,
fck cube comp RN = RN conversion compressive strength (N/mm^2),
Vf = steel fibre volume fraction.

Figure 7 shows the test values for compressive strength, flexural strength, and steel fibres, based on a linear regression model. It can be seen from Fig. 7a and 7b that the concrete compressive cube beams broken test and flexural strength test have a moderate correlation with the steel fibre values. This shows that the steel fibre volume fraction has had a significant effect on the concrete during preparation, resulting in both high and low strength. Compared with the concrete compressive strength conversion from rebound number (RN) in Fig. 7c, the result shows a very weak correlation with the steel fibre values. This may be due to inconsistent rebound hammer test results and handling errors during testing.

The results of the linear regression analysis between the test value and the predicted value of SFRC strength are shown in Table 1. As shown in Table 1, a significance test for the slope indicates that the compressive strength of the cube beams and steel fibres is zero, resulting in a t-value of -1.6072. The significance level of this t-test was 0.1173. Since 0.1173 > 0.0500, the hypothesis that the slope is zero is not rejected.

The estimated slope was -12.9567, and the intercept was 129.3083. The lower limit of the 95% confidence interval for the intercept was 113.9834, and the upper limit was 144.6333.

Besides, a significance test for the slope represents flexural strength, and the steel fibre is zero, resulting in a t-value of -5.5115. The significance level of this t-test was 0.1063. Since 0.1063 > 0.0500, the hypothesis that the slope is zero is not rejected. The estimated slope was -11.2783, and the intercept was 24.5684. The lower limit of the 95% confidence interval for the intercept was 20.6784, and the upper limit was 28.4585. In addition, a significance test for the slope indicates that the compressive strength of the rebound number (RN) conversion and steel fibre is significant, resulting in a t-value of 0.0289. The significance level of this t-test was 0.9771. Since 0.9771 > 0.0500, the hypothesis that the slope is zero is not rejected. The estimated slope was -0.0387, and the intercept was 37.1307. The lower limit of the 95% confidence interval for the intercept was 34.5842, and the upper limit was 39.6771.

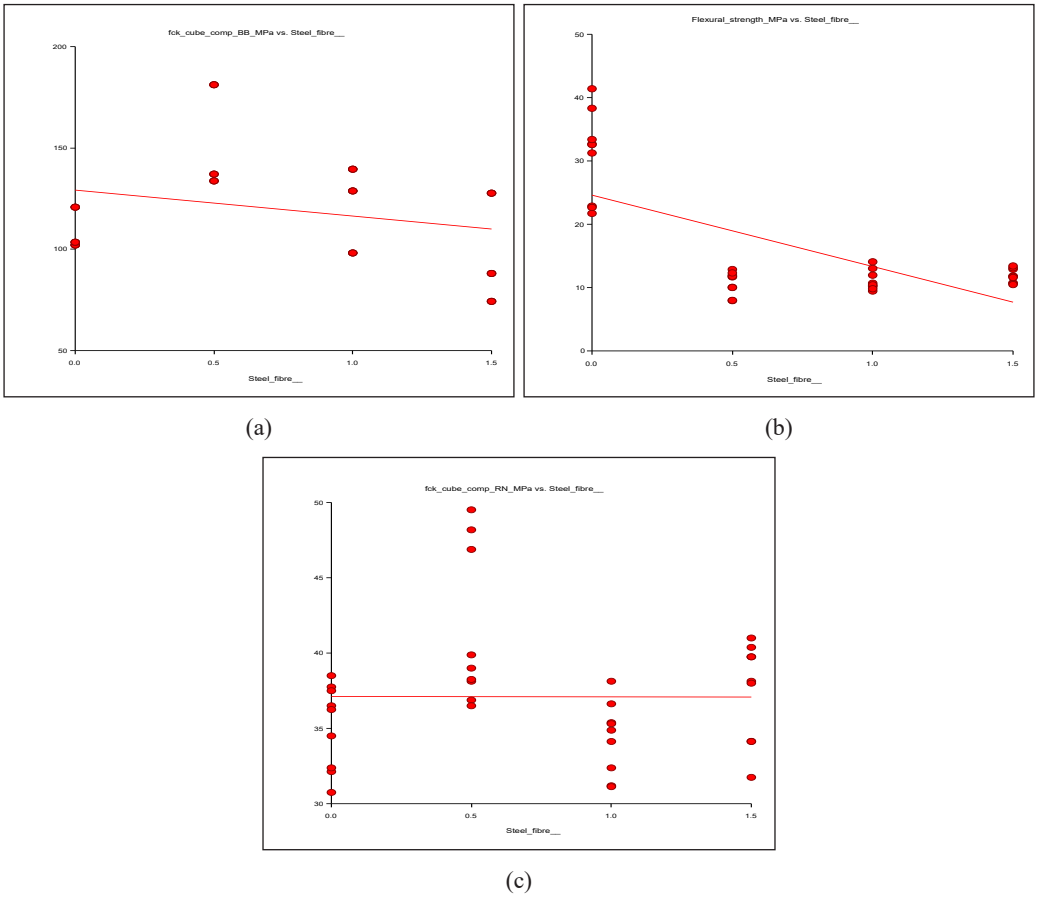

(a) (b)

(c)

Figure 7. Tabulation of test values of the compressive-flexural strength and steel fibre (a) compressive cube beams broken strength; (b) flexural strength; (c) compressive cube RN

Table 1
Result of linear regression-based analysis between test values and predicted values of SFRC strength

	Slope	Intercept	Lower Limit of 95% Confidence Interval (C.I)	Upper Limit of 95% Confidence Interval (C.I)	t-value	Significance Level of t-test	ANOVA	
							Sum of Squares	F-Ratio
Compressive Strength Cube & Beams	-12.9567	129.3083	113.9834	144.6333	-1.6072	0.1173	514870.8	2.5831
Flexural Strength	-11.2783	24.5684	20.6784	28.4585	-5.5115	0.1063	9342.8	30.3762
Compressive Strength RN	-0.0387	37.1307	34.5842	39.6771	-0.0289	0.9771	49555.21	0.0008

CONCLUSION

In conclusion, based on the experimental results, the GPR radargram showed a hyperbolic signature, indicating reflection from the rebar in the reinforced concrete beam, whereas the SFRC sample showed a hazy image, like radio static, with multiple overlapping hyperbolas. The hazy image may represent the uniformity of steel fibre in the SFRC beam. The radargram hazy image is heavier and more sophisticated for a 1.5% steel fibre fraction volume than for a 0.5% steel fibre fraction volume, showing the least.

The results of compressive strength for cube sample and broken beam sample show the same trend of increment in compressive strength for 0.5% steel fibre fraction volume, which for 7, 14, and 28 days are 137.1 N/mm^2, 133.7 N/mm^2, and 181.2 N/mm^2 compared with 1.5% steel fibre fraction volume, which for 7, 14, and 28 days are 74.3 N/mm^2, 127.1 N/mm^2, and 88.1 N/mm^2. Steel fibre fraction volumes of 1.0% and 1.5% can be used to determine the best value for the 0.5% steel fibre fraction volume in terms of strength. In terms of flexural strength, the SFRC exhibits an increase in flexural strength as the volume fraction of steel fibre increases. Based on three distinct case studies, 1.5% steel fibre volume fraction exhibits the most flexural strength on day 28 of any other SFRC sample, whereas 0.5% steel fibre volume fraction exhibits the least. The results indicate that a 1.5% steel fibre volume fraction in SFRC yields the highest flexural strength, followed by 0.5% and 1.0%.

The correlation between compressive strength obtained from the rebound hammer test, cube compressive test, broken beam test, and four-point bending (4PB) flexural strength was successfully analysed using Regression-Based Analysis in NCSS 2021. ANOVA results show that the linear model with sum of squares values of 514870.8 and 9342.8,

and F-ratios of 2.5831 and 30.3762, indicates that the model is significant for compressive cube beam strength and flexural strength. However, the linear model's performance in converting compressive strength to rebound number (RN) is less significant, with an F-ratio of 0.0008 and a sum of squares of 49555.21. The significance levels of the t-test for compressive strength cube beams, flexural strength, and compressive strength RN were 0.1173, 0.1063, and 0.9771, respectively. The hypothesis that the slope is zero is not rejected because the t-test value exceeds 0.0500. The model has fitted the experimental data using the empirical correlation equation model obtained for the compressive strength of cubes and broken beams, flexural strength, and the compressive strength RN conversion for the SFRC beam, as presented in equations 1, 2, and 3.

ACKNOWLEDGEMENT

The authors would like to acknowledge the financial support for this study from the Ministry of Higher Education - Fundamental Research Grant Scheme of 600-IRMI/FRGS 5/3 (178/2019) and other supports from the Institute for Infrastructure Engineering and Sustainable Management (IIESM) and the Faculty of Civil Engineering, Universiti Teknologi MARA (UiTM) Shah Alam, Selangor, Malaysia. These supports are gratefully acknowledged.

REFERENCES

Al-Ameeri, A. (2013). The effect of steel fibre on some mechanical properties of self-compacting concrete. *American Journal of Civil Engineering, 1*(3), 102-110. https://doi.org/10.11648/j.ajce.20130103.14

Bachiri, T., Khamlichi, A., & Bezzazi, M. (2018). Bridge deck condition assessment by using GPR: A review. *MATEC Web of Conferences, 191*, Article 00004. https://doi.org/10.1051/matecconf/201819100004

Briones-Bitar, J., Carrión-Mero, P., Montalván-Burbano, N., & Morante-Carballo, F. (2020). Rockfall research: A bibliometric analysis and future trends. *Geosciences, 10*(10), Article 403. https://doi.org/10.3390/geosciences10100403

Dinh, K., Zayed, T., & Tarussov, A. (2013). GPR image analysis for corrosion mapping in concrete slabs. In *Proceedings of the Annual Conference of the Canadian Society for Civil Engineering* (Vol. 3, pp. 2131–2140). Canadian Society for Civil Engineering.

Gehrig, M. D., Morris, D. V., & Bryant, J. T. (2004). *Ground penetrating radar for concrete evaluation studies* [Technical presentation paper]. Foundation Performance Association.

George, M., & Erdogmus, E. (2009, November). *Use of ground penetrating radar for construction quality assurance of concrete pavement*.

Giannopoulos, A. (2005). Modelling ground penetrating radar by GprMax. *Construction and Building Materials, 19*(10), 755-762. https://doi.org/10.1016/j.conbuildmat.2005.06.007

Harle, S. M. (2019). Experimental investigation on steel fibres in the concrete. *International Journal of Scientific Research in Network Security and Communication, 7*(4), 1-7.

Hasan, M. I., & Yazdani, N. (2016). An experimental and numerical study on embedded rebar diameter in concrete using ground penetrating radar. *Chinese Journal of Engineering, 2016*, Article 9714381. https://doi.org/10.1155/2016/9714381

He, X., Zhu, Z., Lu, G., & Lu, Q. (2009). Bridge management with GPR. In *2009 International Conference on Information Management, Innovation Management and Industrial Engineering* (Vol. 3, pp. 329-332). IEEE. https://doi.org/10.1109/ICIII.2009.387

Hintze, J. L. (2007). *NCSS user's guide I: NCSS statistical system*. NCSS.

Jhatial, A. A., Sohu, S., Bhatti, N. K., Lakhiar, M. T., & Oad, R. (2018). Effect of steel fibres on the compressive and flexural strength of concrete. *International Journal of Advanced and Applied Sciences, 5*(10), 16-21. https://doi.org/10.21833/ijaas.2018.10.003

Kumar Athithan, A. K., Robert Singh, R., & Sri Gomathi, A. B. (2017). Experimental study on steel fibre reinforced concrete in beam-column joint. *International Journal of Civil Engineering and Technology, 8*(8), 599-608.

Lakshmi, K. A., Sangoju, B., Vasanthakumar, & Rahamath, A. (2016). Estimation of rebar radius using ground penetrating radar. *International Journal of Emerging Technology in Computer Science & Electronics, 22*(2), 320-325.

Leucci, G. (2012). Ground penetrating radar: An application to estimate volumetric water content and reinforced bar diameter in concrete structures. *Journal of Advanced Concrete Technology, 10*(12), 411-422. https://doi.org/10.3151/jact.10.411

Liu, H., Lin, C., Cui, J., Fan, L., Xie, X., & Spencer, B. F. (2020). Detection and localization of rebar in concrete by deep learning using ground penetrating radar. *Automation in Construction, 118*, Article 103279. https://doi.org/10.1016/j.autcon.2020.103279

Morcous, G., & Erdogmus, E. (2009). *Use of ground penetrating radar for construction quality assurance of concrete pavement* (Report No. SPR-P1(08) P307). Mid-America Transportation Center, University of Nebraska-Lincoln. https://rosap.ntl.bts.gov/view/dot/24741

Neville, A. M. (2012). *Properties of concrete* (5th ed.). Pearson Education.

Profillidis, V. A., & Botzoris, G. N. (2019). Statistical methods for transport demand modeling. In *Modeling of transport demand* (pp. 163-224). Elsevier. https://doi.org/10.1016/B978-0-12-811513-8.00005-4

Rathod, H., Debeck, S., Gupta, R., & Chow, B. (2019). Applicability of GPR and a rebar detector to obtain rebar information of existing concrete structures. *Case Studies in Construction Materials, 11*, Article e00240. https://doi.org/10.1016/j.cscm.2019.e00240

Razak, N. A., Senin, S. F., & Hamid, R. (2015). Detection of sizes and locations air voids in reinforced concrete slab using ground penetrating radar and impact-echo methods. *Jurnal Teknologi, 74*(3), 63-67. https://doi.org/10.11113/jt.v74.4553

Shamsudin, A. M., Senin, S. F., Hamid, R., & Yusuf, K. (2015). Concrete delaminations location and its severity detection by visual inspection and ground penetrating radar. *Journal of Engineering Science and Technology, 10*(Special Issue on 4th International Technical Conference 2014), 1-12.

Shetty, M. S. (2005). *Concrete technology: Theory and practice* (Multicolour illustrative rev. ed.). S. Chand & Company.

Sultan, A. A., Mashrei, M. A., & Washer, G. A. (2020). Utilisation of Wilcoxon–Mann–Whitney statistics in assessing the reliability of non-destructive evaluation technologies. *Structures, 27*, 780-787. https://doi.org/10.1016/j.istruc.2020.06.024

Sun, H., Pashoutani, S., & Zhu, J. (2018). Nondestructive evaluation of concrete bridge decks with automated acoustic scanning system and ground penetrating radar. *Sensors, 18*(6), Article 1955. https://doi.org/10.3390/s18061955

Van Eck, N. J., & Waltman, L. (2020). *VOSviewer manual* (Version 1.6.16). Universiteit Leiden, Centre for Science and Technology Studies. https://www.vosviewer.com/documentation/Manual_VOSviewer_1.6.16.pdf

Warren, C., & Giannopoulos, A. (2016). Experimental and modelled performance of a ground penetrating radar antenna in lossy dielectrics. *IEEE Journal of Selected Topics in Applied Earth Observations and Remote Sensing, 9*(1), 29-36. https://doi.org/10.1109/JSTARS.2015.2430933

Wiwatrojanagul, P., Sahamitmongkol, R., & Tangtermsirikul, S. (2018). A method to detect lap splice in reinforced concrete using a combination of covermeter and GPR. *Construction and Building Materials, 173*, 481-494. https://doi.org/10.1016/j.conbuildmat.2018.04.027

Zaki, A., Megat Johari, M. A., Wan Hussin, W. M. A., & Jusman, Y. (2018). Experimental assessment of rebar corrosion in concrete slab using ground penetrating radar (GPR). *International Journal of Corrosion, 2018*, Article 5389829. https://doi.org/10.1155/2018/5389829

Zhou, F., Chen, Z., Liu, H., Cui, J., Spencer, B. F., & Fang, G. (2018). Simultaneous estimation of rebar diameter and cover thickness by a GPR-EMI dual sensor. *Sensors, 18*(9), Article 2969. https://doi.org/10.3390/s18092969

Pertanika J. Sci. & Technol. 34 (S2): 51 - 64 (2026)

PERTANIKA JOURNALS

SCIENCE & TECHNOLOGY

Journal homepage: http://www.pertanika.upm.edu.my/

Evaluation of the Causes of On-Farm Food Loss in Cabbage Production: A Case Study in the Large-Scale Farming Group of Hot District, Chiang Mai, Thailand

Pichayapak Channiyamathorn, Suraphol Sreshthaputra*, Ruth Sirisanyaluck, and Juthathip Chalermphol

Department of Agricultural Economy and Development, Faculty of Agriculture, Chiang Mai University, 50200 Chiang Mai, Thailand

ABSTRACT

Food loss at the production stage presents significant economic and environmental challenges, particularly in horticultural systems. This study investigates the extent, causes, and impacts of food loss in cabbage production. Weather variability was identified as the primary driver affecting yield quality. Symptom analysis revealed that 24% of losses were due to produce not meeting size requirements, 23% to excessive leaf trimming, 13% to pest and disease damage, and 6% to stunted growth, resulting in only 34% of total production being marketable. The total loss recorded was 66.58%, equivalent to 3,231.79 kg/rai (1 rai = 0.16 ha), corresponding to an economic loss of approximately 105,033 Baht/rai. In addition, considerable nutrient losses were observed, including energy, carbohydrates, key minerals such as potassium, phosphorus, calcium, and sodium, and vitamin C. These losses indicate substantial inefficiencies in resource utilisation and increased environmental burden. The findings highlight the need for improved production management and targeted interventions to reduce losses. Strengthening farmer awareness and adopting better agronomic practices are essential to enhance productivity, reduce environmental impacts, and support sustainable agriculture and food security.

Keywords: Cabbage loss analysis, farming group, food loss, on-farm food loss

ARTICLE INFO

Article history:
Received: 18 June 2026
Accepted: 05 August 2026
Published: 30 September 2026

DOI: https://doi.org/10.47836/pjst.34.S2.05

E-mail addresses:
ch.pichayapak@gmail.com (Pichayapak Channiyamathorn)
suraphol.s@cmu.ac.th (Suraphol Sreshthaputra)
ruth.si@cmu.ac.th (Ruth Sirisanyaluck)
jutha073@gmail.com (Juthathip Chalermphol)
* Corresponding author

e-ISSN: 2231-8526

© Universiti Putra Malaysia Press

INTRODUCTION

Utilising the entire crop yield could enhance production without increasing land or chemical input usage (Pellegrini & Fernández, 2018). This approach suggests that mitigating farm-level losses may offer a pathway to sustainable intensification, defined as increasing food production without exacerbating environmental impacts (Johnson et al., 2018). Food loss, often unintentional, results from various constraints in agricultural production, such as market conditions or weather effects on produce quality (Gillman et al., 2019). It leads to the waste of resources, including water, land, fuel, fertiliser, and agricultural chemicals, which may be used inefficiently in agricultural processes or during food processing and disposal (Campbell & Munden-Dixon, 2018). Traditionally, efforts to ensure food security have focused on augmenting crop yields, with vegetable producers continually striving to maximise output through improved varieties, tailored fertility programs, precise irrigation, and sophisticated pest and disease management strategies. An alternative approach to augmenting food availability involves reducing losses and enhancing sustainability (Winans et al., 2020). Frequently, produce remains unharvested in fields if it fails to meet market standards or if market prices are too low to justify the cost of harvesting. Like food loss at other stages of the supply chain, farm-level food loss contributes to climate change, pollution, excessive utilisation of water and agricultural chemicals, loss of ecosystem services, and encroachment on critical habitats (Baker et al., 2019).

The Food and Agriculture Organisation (FAO) defines food loss as a decrease in the quantity or quality of food resulting from decisions and actions by suppliers within the supply chain, excluding retailers, food service providers, and consumers. By 2030, it is projected that global food waste at retail and consumer levels, along with post-harvest losses, will be halved per capita across production and supply chains (Carlsen & Bruggemann, 2021; Parfitt et al., 2010). Food loss has significant detrimental effects on the global economy. Food waste is particularly prevalent in middle and high-income countries at the consumption stage. In contrast, in low-income countries, food losses predominantly occur at the early and middle stages of the food chain, rather than at the consumption stage. Globally, production processes account for 24-30% of food loss and waste (FLW), post-harvest losses for 20%, and consumption for 30-35% of the total FLW (Kummu et al., 2012; Lipinski et al., 2013). In low-income countries, overplanting is a notable contributor to food loss. Additionally, in these regions, food losses are often due to inadequate infrastructure, including inefficient equipment and insufficient cold storage, further exacerbating food insecurity. In Southeast Asia, countries like Vietnam, Malaysia, Thailand, the Philippines, and Indonesia experience significant fruit and vegetable losses ranging from 14% to 42%. The primary causes of productivity losses at the post-harvest stage include: (1) storage processes that involve collection during both mature and immature periods, and handling that may cause damage; (2) accelerated trimming and washing processes, where rapid

cleaning can exacerbate injuries to the produce; (3) packaging issues, including losses during sorting and the use of low-quality materials; (4) insufficient cold storage, leading to spoilage; (5) mechanical damage and congestion during transport; and (6) marketplace conditions, where high temperatures can dehydrate the products (Chinwang et al., 2011).

Globally, approximately 70,150,406 tons of cabbage are produced annually. China is the world's largest cabbage producer, producing 34,151,665 tons annually. India follows with an annual production of 9,127,000 tons. Together, China and India account for over 60% of global cabbage production. Thailand ranks 30th, producing 221,679 tons annually. In 2023, Thailand's cabbage yield was about 60,020 tons from a cultivated area of 29,289 rai, averaging 2,943 kg/rai. The average market price for cabbage was 5.31 Baht per kilogram. Chiang Mai Province, as Thailand's second-largest cabbage producer, yielded around 11,620 tons. The Hot District in Chiang Mai is home to the region's largest vegetable farming cooperative, which comprises 30 farmer members and spans 100 rai. This group primarily grows tomatoes, banana peppers, and cabbage, achieving notable yields of approximately 500 tons of cabbage, 400 tons of chillies, and 500 tons of tomatoes per crop cycle. The cooperative manages to conduct 2-3 crop cycles each year, demonstrating impressive production performance (Atlas Big, 2023; Department of Agricultural Extension, 2022).

Despite their achievements, the farming group faces several challenges. They lack the necessary knowledge and resources for implementing technology to control greenhouse conditions. Limited capital restricts their ability to invest in advanced harvesting equipment that could significantly improve production and product quality. Additionally, there is a scarcity of equipment essential for harvesting, storage, and improving product conditions, such as grading and packing. These limitations hinder the group's potential to enhance production efficiency and product quality. Production losses have been identified at various stages, including harvesting, handling, grading, packaging, and storage of agricultural products (Chiang Mai Agricultural Extension Office, 2019).

In Thailand, extensive research has been conducted on on-farm food loss, particularly in vegetable production. However, there remains a lack of precise data on estimating food losses in both quantity and quality. Farmers require additional knowledge, technologies, and models to effectively quantify food losses and implement strategies to prevent and reduce pre-harvest and post-harvest losses. Despite recognising the issue of food loss, many farmers struggle to determine the extent of losses occurring in each production stage.

Therefore, this study was conducted to assess the quantity and quality of cabbage food loss at the farm level. The study aimed to identify the causes of losses in cabbage production and evaluate losses in cabbage quantity and quality. These findings are crucial for improving the efficiency of loss prevention and reducing cabbage production. Furthermore, the results from this study will provide cabbage farmers with insights into production losses, aiding the development of strategies and policies to better handle cabbage and prevent significant losses in Thailand.

METHODOLOGY

Method Approach

This study employed a mixed-method approach using an exploratory sequential design. Mixed-method research integrates qualitative and quantitative methodologies within a single study, combining their findings to deliver a more comprehensive response to the research question. An exploratory sequential design is a specific type of mixed-methods framework in which the quantitative phase of data collection and analysis follows the qualitative phase, enabling systematic exploration and subsequent quantification of the research topic (Creswell & Creswell, 2017).

Study Area

The case study is in the Hot District of Chiang Mai Province, home to the pioneering large-scale Hot farming group. This group is the first of its kind in large-scale vegetable production in the province. It operates over an area of approximately 100 rai (16 hectares). Historically, this group has consistently achieved a yield of about 500 tons of cabbage per crop cycle. With 2-3 crop cycles conducted annually, this farming group offers an excellent opportunity to explore and investigate on-farm food losses (Chiang Mai Agricultural Extension Office, 2019).

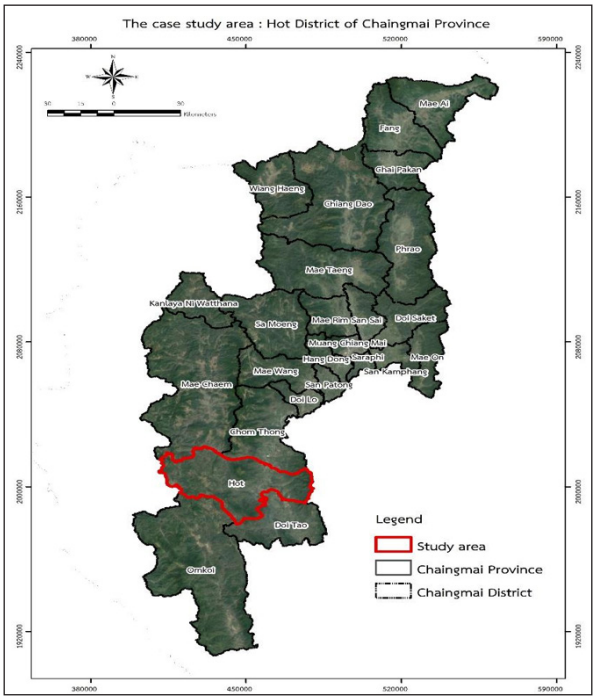

Figure 1. Map of the case study area: The hot district of Chiang Mai Province

Data Collection

The survey methodology combined field visits, observations, questionnaires, in-depth interviews, and focus group discussions to collect data on the cabbage production system, its supply chain, and the factors contributing to losses.

A semi-structured questionnaire and focus group discussions were conducted with all 30 members of the farming groups. This method was instrumental in identifying the causes of loss in cabbage production and understanding how these causes relate to food loss at various stages of the production process. The sample collection from farm levels employed tools, integrating methods to quantify food loss through direct weighing with a measuring device, structured into five steps (Hanson et al., 2016):

1. Initially, samples were selected from 15 representative farms using random duplicate sampling, marking 3 furrows per plot.
2. Farmers were then asked to harvest mature cabbages ready for sale from these marked samples, approximately 10 cabbages per furrow.
3. Harvested cabbage samples were categorised into two groups: those of marketable quality and those of inferior quality.
4. Cabbages of inferior quality were further classified based on the causes of loss, divided into four categories focused on observable symptoms: damage from pests and disease, unmarketable size, small and stunted growth, and trimmed leaves.
5. Finally, the mass of the lost produce was measured and recorded for each category, along with the mass of the good-quality cabbages.

Food Losses Assessment

The percentage of quantity loss was calculated using Equation 1, while the total loss per rai was calculated using Equation 2.

$$Percentage\ of\ the\ quantity\ of\ loss = \frac{total\ weight\ of\ unmarketable\ cabbage\ from\ samples\ x\ 100}{total\ weight\ of\ harvested\ samples} \quad [1]$$

$$Total\ loss\ per\ rai = average\ of\ productivity\ per\ rai\ x\ quantity\ losses\ percent \quad [2]$$

Quality losses, which included economic and nutrient losses, were estimated as follows. Economic losses were calculated using Equation 3.

$$Economic\ losses = market\ price\ per\ kilogram\ x\ the\ weight\ of\ losses\ per\ rai \quad [3]$$

Nutrient losses were estimated using a cabbage nutrient database provided by the Institute of Nutrient, Mahidol University. The nutrient content was compiled per 100-gram edible portion and included the following values: energy (24 kilocalories), carbohydrates (3.24 grams), potassium (236 milligrams), phosphorus (36 milligrams), calcium (34 milligrams), and vitamin C (19 milligrams) (Judprasong et al., 2015). For example, energy loss per rai was calculated using Equation 4.

$$Energy\ losses\ per\ rai = \frac{total\ loss\ per\ rai\ (g) x\ 24kcal}{100\ (g)} \quad [4]$$

Data Analysis

Quantitative data analysis was conducted using descriptive statistics, including frequencies, means, and percentages, utilising IBM SPSS version 26. Qualitative data analysis involved employing content analysis techniques to examine data collected from in-depth interviews and focus group discussions. The findings from these analyses provide a solid basis for formulating policy recommendations to prevent and reduce losses in cabbage production.

The evaluation of practices contributing to food loss during cabbage production was conducted through structured interviews. These interviews addressed fourteen aspects, organised into two phases: production and post-production. The production phase included: (1) production planning, (2) funding and funding sources, (3) sprouts and seeds, (4) cultivation and maintenance, (5) disease and pests, (6) weather variability, (7) natural disasters, and (8) farmers' knowledge and skills. The post-production phase covered: (9) tools and harvesting methods, (10) transportation of produce from the farm to collection and packing sites, (11) Cleanliness and standards of the collecting and packing place, (12) harvest time, (13) workers, and (14) cleaning and trimming of produce before packing. Farmers' adherence to these practices was assessed using a five-point Likert scale, where 5 indicates the highest level of adherence and 1 the lowest. These scores were averaged and compared against a predefined set of interpretative criteria divided into five intervals, each spanning 0.50 points. Average scores were interpreted as follows: 4.51-5.00 represents the highest level of practice, 3.51-4.50 indicates frequent practice, 2.51-3.50 denotes intermediate practice, 1.51-2.50 suggests occasional practice and 1.00-1.50 reflects no practice.

RESULT AND DISCUSSION

Identify Causes of Loss in Cabbage Production

The data presented in Table 1 and Figure 2 illustrate that weather variability significantly impacts cabbage losses among farmers. This variability is evidenced by a practice level of 2.08, indicating only occasional use of climate-control instruments such as hygrometers,

temperature gauges, and rain gauges in their fields. This sporadic use suggests that farmers have limited capacity to mitigate weather-related issues affecting plant growth and crop quality. Moreover, the management of funding and funding sources achieves an intermediate practice level of 3.49. Additional challenges such as natural disasters, cultivation and maintenance, Cleanliness and standards of the collecting and packing place, production plan, farmers' knowledge and skills, workers, diseases and pests, Tools and harvesting method, cleaning and trimming of produce before packaging, harvest time, sprouts and seeds, and Transportation of products from the farm to the collecting and packing place are addressed more frequently. These areas achieve practice levels of 3.64, 3.86, 3.90, 3.93, 4.18, 4.20, 4.26, 4.28, 4.37, 4.38, 4.39, and 4.42, respectively.

During focus group discussions, farmers expressed that during abnormally high temperatures, they need to increase water irrigation to maintain optimal field temperatures. However, if temperatures become uncontrollable, excessive heat can adversely affect cabbage growth, resulting in stunted plants. Additionally, weather variability heightens the risk of plant diseases, which become harder to manage under fluctuating conditions. In some instances, farmers may be forced to destroy crops to prevent the spread of diseases.

Table 1
The level of farmers' practices affecting loss in cabbage production systems

Issues and Procedures	Level of Practice	Meaning of Practice Level	Std. Deviation
1. Weather variability	2.08	occasional practice	0.740
2. Funding and Funding source	3.49	Intermediate practice	0.913
3. Natural disasters	3.64	Frequent practice	0.759
4. Cultivation and maintenance	3.86	Frequent practice	0.635
5. Cleanliness and standards of the collecting and packing place	3.90	Frequent practice	0.598
6. Production plan	3.93	Frequent practice	1.009
7. Farmers' knowledge and skills	4.18	Frequent practice	0.781
8. Workers	4.20	Frequent practice	0.552
9. Diseases and pests	4.26	Frequent practice	0.611
10. Tools and harvesting method	4.28	Frequent practice	0.612
11. Cleaning and trimming of produce before packing	4.37	Frequent practice	0.865
12. Harvest Time	4.38	Frequent practice	0.916
13. Sprouts or Seeds	4.39	Frequent practice	0.714
14. Transportation of products from the farm to the collecting and packing place	4.42	Frequent practice	0.946

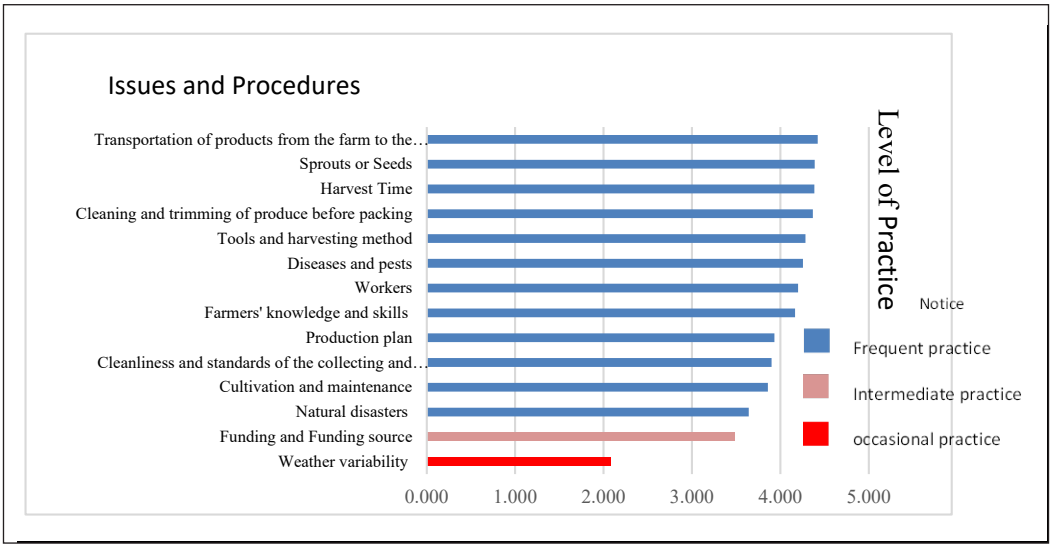

Figure 2. Identify causes of loss in the cabbage production system

The Losses of Cabbage in Terms of Both Quantity and Quality at the Farm Level

The assessment of losses in terms of mass at the farm level during the harvesting stage is presented in Table 2, which indicates that cabbage losses totalled 3,231.79 kilograms per rai, accounting for 66.58% of the yield. Figure 3 identifies the primary causes of these losses through visual inspection: 24% were due to unmarketable size, 23% to trimmed leaves, 13% to pest and disease damage, and 6% to stunted growth. Consequently, only 34% of the total harvested products were of good quality and suitable for sale.

The assessment of cabbage losses considers both economic and nutritional factors. According to the average yield production data presented in Table 3, which amounts to 4,854 kilograms per rai, the evaluation is based on the market price per kilogram, sourced from the Talaadthai market in August 2022, approximately 32.50 Baht per kilogram. Consequently, the economic loss per rai of cabbage is estimated at approximately 105,033 Baht (Talaadthai, n.d.).

Table 4 provides an assessment of nutrient losses per rai, based on the average yield outlined in Table 3, showing a loss of 3,231.79 kg per rai. The results further highlight significant losses of key nutrients, including energy, carbohydrates, potassium, phosphorus, calcium, sodium, and vitamin C. The estimated losses are 775,630.37 kcal/rai, 104,710.10 grams/rai for carbohydrates, 7,627.03 grams/rai for potassium, 1,163.45 grams/rai for phosphorus, 1,098.81 grams/rai for calcium, 807.95 grams/rai for sodium, and 614.04 grams/rai for vitamin C, respectively. These figures underscore the substantial nutrient losses that occur during cabbage production.

Table 2
Mass of cabbage losses at the farm level

Mass of losses	Quantity
Average yield production per rai	4,854 kg/rai
Total sample weight	202.80 kg
Total weight of losses	133.00 kg
Per cent of losses (100 × 133.00 kg)/ 202.80 kg	66.58%
Total weight of losses per rai	3,231.79 kg

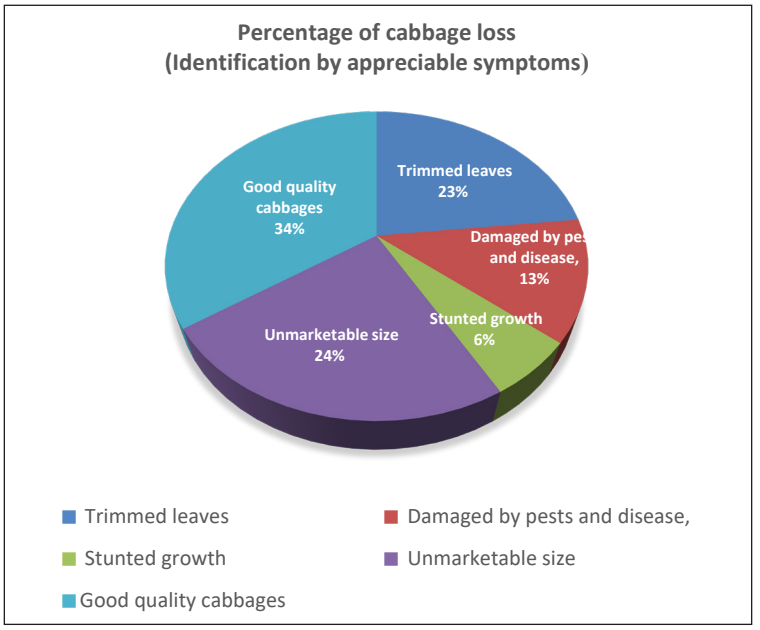

Figure 3. Percentage of cabbage loss, identification by appreciable symptoms

Table 3
Economics of cabbage losses

Economic Losses	Quantity
Average yield production per rai	4,854 kg/rai
The average market price per kilogram (Reference from Talaadthai market in August 2022)	32.50 Baht/kg
Total weight of losses per rai	3,231.79 kg
Economic losses (3,231.79 kg × 32.50 Baht/kg)	105,033 Baht/rai

Table 4
Nutrient of cabbage losses assessment

Nutrients	Detail	Content per 100 g Edible Portion	Nutrient Loss per rai
Energy, by calculation	Calculated by (4 × g protein) + (9 × g fat) + (4 × g CHOAVLDF) + (2 × g dietary fibre) (not include alcohol)	24 Kcal	775,630.37 Kcal
Carbohydrate, available	Calculated by difference: CHOAVLDF = 100 – (weight in grams [water + protein + fat + dietary fiber + ash] in 100 g food)	3.24 g	104,710.10 g
Potassium	AOAC method	236 mg	7,627.03 g
Phosphorus	AOAC method	36 mg	1,163.45 g
Calcium	AOAC method	34 mg	1,098.81 g
Sodium	AOAC method	25 mg	807.95 g
Vitamin C	AOAC - HPLC method	19 mg	614.04 g

Note. Total weight of losses: 3,231.79 kg/rai

Discussion

The data depicted in Fig. 2 indicate that weather variability is the primary factor contributing to cabbage losses at the farm level, largely due to the infrequent use of climate-control tools in the planting area. This variability significantly impacts farming practices, leading to heightened cabbage losses. Correspondingly, other researchers have identified weather variability as a principal cause of food losses across various agricultural sectors, including fruit and vegetable losses (Magalhães et al., 2022) and farm-level crop yield losses in German agriculture (Schmitt et al., 2022). This study aligns with other research examining postharvest management and its impact on the quantity and quality losses of leafy vegetables, revealing that these losses vary with both external and internal factors. External factors identified include temperature, humidity, atmospheric composition, light, gravity, and pests (Boonyakiat et al., 2012). Field data indicate the primary causes of loss, as visually identified: 24% due to unmarketable size, 23% due to trimmed leaves, 13% due to pest and disease damage, and 6% due to stunted growth. Consequently, only 34% of the total products were of good quality and ready for sale. Similarly, a study on postharvest losses of vegetables within the Royal Project Foundation demonstrated that the predominant causes of loss were underutilised parts of vegetables, insect damage, and mechanical injuries (Boonyakiat et al., 2012). Another study, Chompupoung (2017), conducted in the Royal Project Foundation's highland fields identified factors contributing to agricultural losses in three ways: first, losses stem from subpar-quality products, disease infections, insect infestations, weather fluctuations, natural disasters, and the prevalence of recessive species before harvest. The second phase centres on the harvesting process, where product damage

arises from suboptimal harvesting techniques and improper equipment use. Additionally, product deterioration results from untimely harvesting, limited knowledge, and the absence of post-harvest management technology. The final phase occurs post-harvest, during which products sustain bruising due to inadequate packaging methods, container handling, and inefficient transportation from the farm to the packing facility. Both quantitative and qualitative losses in cabbage may affect economic and nutritional value, as well as food safety. Despite awareness of food loss issues, many farmers are unable to quantify losses during production processes.

Within ASEAN countries, the study explored the significance of food loss concerning economic growth. The findings revealed that the Food Loss (FL) value as a percentage of GDP in Cambodia, Laos, Myanmar, and Vietnam (CLMV countries) exceeded that of Indonesia, Malaysia, the Philippines, and Thailand. Thus, it is crucial that economic development strategies extend beyond traditional GDP growth and prioritise sustainability. Nations should adopt inclusive economic growth objectives that address losses in both production and marketing processes. A promising strategy involves adopting a "circular economy for food." To mitigate agricultural product losses, governments should increase investments in research and development of post-harvest technologies and the improvement of logistics systems (Jaroensathapornkul, 2021).

The study investigating strategies employed by maize farmers in Delta State, Nigeria, to mitigate post-harvest losses yielded significant findings. This research examined the methods these farmers adopted to reduce losses. The results revealed that the primary factor contributing to post-harvest losses was a lack of awareness about modern storage facilities (Ovharhe, 2021). It was observed that post-harvest losses were most significant at the storage phase, exacerbated by inadequate extension services, infrequent visits, and the absence of governmental incentives for storage activities. One of the most effective strategies identified for minimising post-harvest losses was the use of storage bags. Numerous researchers have corroborated the efficacy of bags in storing beans, cereals, and legumes (Ikegwu et al., 2022; Uebersax et al., 2022). The study also highlighted significant constraints, including limited institutional support for post-harvest activities and the use of less efficient processing technologies, establishing a significant relationship between these factors. However, a major challenge in recovery efforts remains the variability and unpredictability of natural on-farm food losses. Future studies should concentrate on a critical analysis of the variability and unpredictability of on-farm cabbage loss.

CONCLUSION

This study found that weather variability significantly influences farming practices and is identified as the primary contributor to cabbage losses, with an observed practice level of 2.08. The quantified loss of cabbage per rai was substantial, at approximately 66.58%

(3,231.79 kilograms). Visual observations indicated that 24% of these losses were due to unmarketable sizes, 23% to trimmed leaves, 13% to pests and diseases, and 6% to stunted growth. Consequently, only 34% of the harvested cabbage met the criteria for good quality and market readiness. The associated economic loss was estimated at approximately 105,033 Baht per rai. Additionally, the study highlighted significant nutrient losses, quantifying them as 775,630.37 kcal of energy per rai, 104,710.10 grams of carbohydrates, 7,627.03 grams of potassium, 1,163.45 grams of phosphorus, 1,098.81 grams of calcium, 807.95 grams of sodium, and 614.04 grams of vitamin C. These findings emphasise the profound impact of cabbage losses on both economic and nutritional fronts, underscoring the urgency of addressing and mitigating them. Furthermore, the quality analysis showed that only a minority of the cabbage crop was high-quality and suitable for sale, underscoring the critical need for interventions to improve farming practices and reduce losses. The economic and nutritional losses documented in this research offer valuable insights that can inform the development of strategies to boost cabbage production efficiency and food security. Additionally, this study lays the foundation for raising farmers' awareness of production losses, which can inform targeted training initiatives to prevent and reduce food waste, thereby promoting more sustainable agricultural methods. These efforts contribute to sustainable cabbage cultivation, reduced food wastage, enhanced food security, and a lower environmental footprint, aligning with the global drive for environmental responsibility and sustainable resource management.

ACKNOWLEDGEMENT

This research is supported by the Department of Agricultural Economy and Development, Faculty of Agriculture, Chiang Mai University, Thailand, the Agricultural Research Development Agency (Public Organisation), ARDA Thailand, and the Department of Agricultural Extension (2022), Ministry of Agriculture and Cooperatives.

REFERENCES

Atlas Big. (2023). *World cabbage production by country*. Retrieved September 22, 2026, from https://www.atlasbig.com/countries-cabbage-production

Baker, G. A., Gray, L. C., Harwood, M. J., Osland, T. J., & Tooley, J. B. C. (2019). On-farm food loss in northern and central California: Results of field survey measurements. *Resources, Conservation and Recycling, 149*, 541-549. https://doi.org/10.1016/j.resconrec.2019.03.022

Boonyakiat, D., Poonlarp, P. B., Chuamuangphan, C., & Janta, M. (2012). Postharvest losses on supply chain of vegetables in the Royal Project Foundation. *Agricultural Science Journal, 43*(3 Suppl.), 376-379.

Campbell, D., & Munden-Dixon, K. (2018). On-farm food loss: Farmer perspectives on food waste. *Journal of Extension, 56*(3), Article 23. https://doi.org/10.34068/joe.56.03.23

Carlsen, L., & Bruggemann, R. (2021). The 17 United Nations' sustainable development goals: A status by 2020. *International Journal of Sustainable Development & World Ecology, 29*(3), 219-229. https://doi.org/10.1080/13504509.2021.1948456

Chiang Mai Agricultural Extension Office. (2019). *Information and publications*. Chiang Mai Agricultural Extension Office

Chinwang, U., Siriphanich, J., & Chairat, R. (2011). Enzymatic browning of fresh-cut galangal (*Alpinia siamense* K. Schum) and its relationship to oxidative enzymes. *Journal of the Japanese Society for Horticultural Science, 80*(1), 103-112. https://doi.org/10.2503/jjshs1.80.103

Chompupoung, A. (2017). *Reducing the loss of vegetable productivity at the height land field of the Royal Project Foundation* [Paper presentation]. Seminar on Thai Sustainable Development Perspective on Food Loss and Waste, Bangkok, Thailand.

Creswell, J. W., & Creswell, J. D. (2017). *Research design: Qualitative, quantitative, and mixed methods approaches* (5th ed.). SAGE Publications.

Department of Agricultural Extension. (2022). *Agricultural production information system*. Department of Agricultural Extension. https://production.doae.go.th/service/data-state-product/index

Gillman, A., Campbell, D. C., & Spang, E. S. (2019). Does on-farm food loss prevent waste? Insights from California produce growers. *Resources, Conservation and Recycling, 150*, Article 104408. https://doi.org/10.1016/j.resconrec.2019.104408

Hanson, C., Lipinski, B., Robertson, K., Dias, D., Gavilan, I., Gréverath, P., Ritter, S., Fonseca, J., Van Otterdijk, R., Timmermans, T., Lomax, J., O'Connor, C., Dawe, A., Swannell, R., Berger, V., Reddy, M., Somogyi, D., Tran, B., Leach, B., & Quested, T. (2016). *Food loss and waste accounting and reporting standard*. World Resources Institute.

Ikegwu, T. M., Ezegbe, C. C., Okolo, C. A., & Ofoedu, C. E. (2022). Postharvest preservation technology of cereals and legumes. In M. Ahiduzzaman (Ed.) *Postharvest technology: Recent advances, new perspectives and applications* (pp. 25-42). IntechOpen. https://doi.org/10.5772/intechopen.102739

Jaroensathapornkul, J. (2021). Value of food loss in ASEAN countries and its relationship with economic growth. *International Journal of Agricultural Technology, 17*(1), 115-128.

Johnson, L. K., Dunning, R. D., Gunter, C. C., Bloom, J. D., Boyette, M. D., & Creamer, N. G. (2018). Field measurement in vegetable crops indicates need for reevaluation of on-farm food loss estimates in North America. *Agricultural Systems, 167*, 136-142. https://doi.org/10.1016/j.agsy.2018.09.008

Judprasong, K., Puwastien, P., Rojroongwasinkul, N., Nitithamyong, A., Sridonpai, P., & Somjai, A. (2015). *Thai food composition database* (Online version 2, September 2018). Institute of Nutrition, Mahidol University. https://inmu.mahidol.ac.th/thaifcd/

Kummu, M., de Moel, H., Porkka, M., Siebert, S., Varis, O., & Ward, P. J. (2012). Lost food, wasted resources: Global food supply chain losses and their impacts on freshwater, cropland, and fertiliser use. *Science of the Total Environment, 438*, 477-489. https://doi.org/10.1016/j.scitotenv.2012.08.092

Lipinski, B., Hanson, C., Waite, R., Searchinger, T., & Lomax, J. (2013). *Reducing food loss and waste*. World Resources Institute. https://www.wri.org/research/reducing-food-loss-and-waste

Magalhães, V. S., Ferreira, L. M. D. F., & Silva, C. (2022). Prioritising food loss and waste mitigation strategies in the fruit and vegetable supply chain: A multi-criteria approach. *Sustainable Production and Consumption, 31*, 569-581. https://doi.org/10.1016/j.spc.2022.03.022

Ovharhe, O. J., Emaziye, P. O., Okpara, O., Agoda, S., & Benson, C. O. (2021). Strategies adopted by maize farmers to minimize post-harvest losses in Delta State, Nigeria. *International Journal of Agricultural Technology, 17*(1), 237-256. https://li04.tci-thaijo.org/index.php/IJAT/article/view/5932

Parfitt, J., Barthel, M., & Macnaughton, S. (2010). Food waste within food supply chains: Quantification and potential for change to 2050. *Philosophical Transactions of the Royal Society B: Biological Sciences, 365*(1554), 3065-3081. https://doi.org/10.1098/rstb.2010.0126

Pellegrini, P., & Fernández, R. J. (2018). Crop intensification, land use, and on-farm energy-use efficiency during the worldwide spread of the green revolution. *Proceedings of the National Academy of Sciences, 115*(10), 2335-2340. https://doi.org/10.1073/pnas.1717072115

Schmitt, J., Offermann, F., Söder, M., Frühauf, C., & Finger, R. (2022). Extreme weather events cause significant crop yield losses at the farm level in German agriculture. *Food Policy, 112*, Article 102359. https://doi.org/10.1016/j.foodpol.2022.102359

Talaadthai. (n.d.). *Price information of agricultural products: Cabbage*. Talaadthai https://talaadthai.com/products/cabbage-9726-2397?

Uebersax, M. A., Siddiq, M., Cramer, J., & Bales, S. (2022). Harvesting, postharvest handling, distribution, and marketing of dry beans. In M. Siddiq & M. A. Uebersax (Eds.) *Dry beans and pulses: Production, processing, and nutrition* (2nd ed., pp. 81-104). John Wiley & Sons. https://doi.org/10.1002/9781119776802.ch4

Winans, K., Marvinney, E., Gillman, A., & Spang, E. S. (2020). An evaluation of on-farm food loss accounting in life-cycle assessment (LCA) of four California specialty crops. *Frontiers in Sustainable Food Systems, 4*, Article 10. https://doi.org/10.3389/fsufs.2020.00010

Pertanika J. Sci. & Technol. 34 (S2): 65 - 74 (2026)

PERTANIKA JOURNALS

SCIENCE & TECHNOLOGY

Journal homepage: http://www.pertanika.upm.edu.my/

Influence of Tree Canopy Characteristics on Rainfall Interception, Throughfall and Stemflow in a Tropical Forest

Azinoor Azida Abu Bakar[1]* and Muhammad Khairudin Khalil[2]

[1]Faculty of Civil Engineering, Universiti Teknologi MARA, 40450 Shah Alam, Selangor, Malaysia
[2]Facility Management and GIS Division, Department of Irrigation and Drainage Malaysia, Persiaran Rimba Permai, Cyber 8, 63000 Cyberjaya, Selangor, Malaysia

ABSTRACT

The trees in tropical forests play a crucial role in the ecosystem. Understanding the characteristics of tree canopies and the impact of rainfall interception is vital for the hydrological cycle. Canopy characteristics have been measured at Bukit Lagong Reserved Forest, Kepong, Selangor. To determine interception loss values, daily gross precipitation (PG), throughfall (TF), and stemflow (SF) were measured over 12 months. The tree characteristics determined are tree height (TH), canopy crown diameter (CD), diameter at breast height (DBH), and canopy cover (CC). The results of this study identify the relationships between canopy characteristics and interception loss (IL) in tropical forests. Understanding how tree canopy characteristics influence canopy interception, storage, and throughfall redistribution dynamics is fundamental to advancing the use of trees in water-budget calculations for water management.

Keywords: Canopy characteristics, interception loss, stemflow, throughfall

INTRODUCTION

Tree canopies alter the paths of raindrops by dividing the incoming rainfall into throughfall and stemflow. A portion of the incoming rainfall is captured and temporarily retained on the surfaces of leaves, branches, and stems. Rainfall interception is typically influenced by various factors, including rainfall characteristics (such as amount, intensity, duration, drop size, and raindrop count), micrometeorological conditions, and forest attributes like species of the tree, structure of the canopy (including leaf area index (LAI), crown gap fraction, and stem

ARTICLE INFO

Article history:
Received: 18 June 2026
Accepted: 19 August 2026
Published: 30 September 2026

DOI: https://doi.org/10.47836/pjst.34.S2.06

E-mail addresses:
azinoor@uitm.edu.my (Azinoor Azida Abu Bakar)
khairudinkhalil@water.gov.my (Muhammad Khairudin Khalil)
* Corresponding author

e-ISSN: 2231-8526

© Universiti Putra Malaysia Press

surface area), along with antecedent weather conditions (Livesley et al., 2014). Both rainfall characteristics and the architecture of the forest canopy are recognised as the primary factors influencing rainfall interception by the forest canopy (Crockford & Richardson, 2000; Xiao et al., 2000; Yan et al., 2015).

Numerous studies have investigated the relationship between various forest elements and interception. The influence of forest type on interception loss values has been demonstrated by Abu Bakar and Khalil (2017) and Crockford and Richardson (2000). Abu Bakar et al. (2023) established the connection between canopy cover (CC) and the throughfall (TF) process, while Manfroi et al. (2004) examined the effects of diameter at breast height (DBH) on stemflow (SF). Dietz et al. (2006) studied the impact of tree height (TH) and leaf area index (LAI) on throughfall (TF). Crockford and Richardson (2000) also noted that canopy gaps and larger crown size significantly increase interception loss (IL). Clearly, crown size and canopy gaps are critical factors in determining interception in a forest.

Additional research highlights the significance of canopy cover as a pivotal metric for assessing forest conditions, utilised in investigations related to climate change mitigation, disease monitoring, and forest management (Chappell et al., 2001). Although canopy cover plays a role in rainfall interception, it is also subject to the temporal resolution of rainfall (Yamakura et al., 1986). Regrettably, there remains a dearth of studies focusing on the implications of forest canopy cover for interception, particularly in humid forests. Consequently, this paper seeks to elucidate the relationship between canopy characteristics, such as diameter at breast height (DBH), crown diameter (CD), canopy cover (CC), and tree height (TH), and interception loss in tropical forest ecosystems.

EXPERIMENTAL PROGRAM

Study Area

This study has been carried out in the lowland tropical rainforest situated in the Bukit Lagong Reserved Forest, Selangor, positioned in the peninsula of Malaysia, spanning between 3º 15’ N and 101º 37’ E. The local climate is characterised as tropical and equatorial. For the specific investigation on rainfall interception, a square plot of 20 × 20 m was established. The plot was outlined using PVC pickets and covered an area of 400 m^2. Then it was further subdivided into sub-grids with a 5 m × 5 m interval. Within the plot, trees of the species Mempisang, Kledan, Simpoh, and Keruing, each with a diameter at breast height (DBH) exceeding 10 cm, were recognised, labelled with distinctive markers, and assigned individual numbers, for a total of 20 trees.

Site Measurements

The measurement of TF utilised 25 standard bucket collectors, each equipped with a 225 mm-diameter orifice and a depth of 200 mm. These bucket collectors were strategically positioned at the intersection of the plot beneath the canopy cover, with 5-meter intervals. Daily averages of the data were computed. Due to the dense canopy cover in the forest, the throughfall volume was divided by the collector's receiving area to determine the TF value in depth (mm) (Yusop et al., 2003).

The process of collecting SF involved employing a halved rubber collar spirally wrapped around each carefully selected tree stem. The selection criteria were based on DBH within the plot area, and 15 trees were selected per plot to facilitate installation of the stemflow collar. These accessible trees, with a DBH exceeding 10 cm, were outfitted with a spiral rubber collar designed to channel runoff from the stem into a collecting tank at the collar's end. In this study, the rubber collar was made from PVC hose and firmly attached to the tree stem with nails. Silicone glue was used to fill any gaps between the stem and the collar, ensuring a tight fit. The amount of stemflow (SF) collected was then translated into depth measurements in mm (Bo et al., 1989).

RESULTS AND DISCUSSIONS

Measurement of Gross Rainfall (PG), Throughfall (TF) and Stemflow (SF)

Manual measurements of PG, TF, and SF were conducted over a twelve-month period, spanning from 11 April 2012 to 24 April 2013. Throughout this duration, a total of 94 rainfall events were recorded. In Figure 1, monthly patterns of PG and TF during the study period are illustrated. The wettest season with a cumulative rainfall of 2095.84 mm occurred from October to December 2012. The peak rainfall was observed in November 2012 at 405 mm, while the lowest was recorded in February 2013 with 21 mm.

Regarding TF data, the percentage over PG obtained is 80.96%. TF volume constitutes a significant portion of PG, as it represents rainfall that drips from the CC and is stored in canopy storage. It is important to note that the throughfall (TF) collection bucket positioned at the node of the grid points in the plot may capture rainfall that has not fallen within the canopy. Figure 2 shows the monthly patterns of PG and SF. SF values represent 0.034% of gross rainfall for the 12-month data as shown in Fig. 2. Interception loss (IL) is calculated as the difference between gross precipitation (PG) and net rainfall, which is the sum of throughfall (TF) and stemflow (SF) (Crockford & Richardson, 2000).

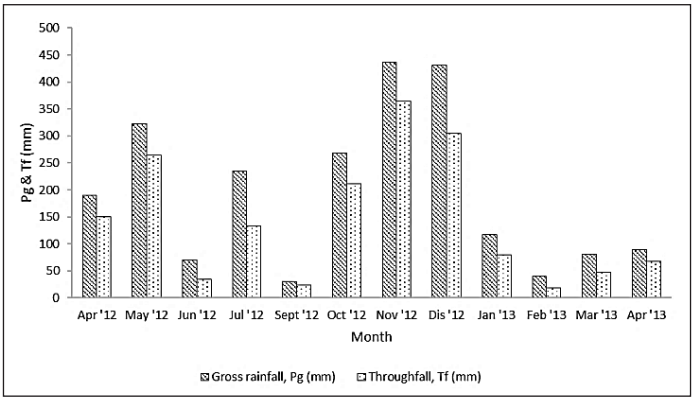

Figure 1. Monthly PG (mm) and TF (mm)

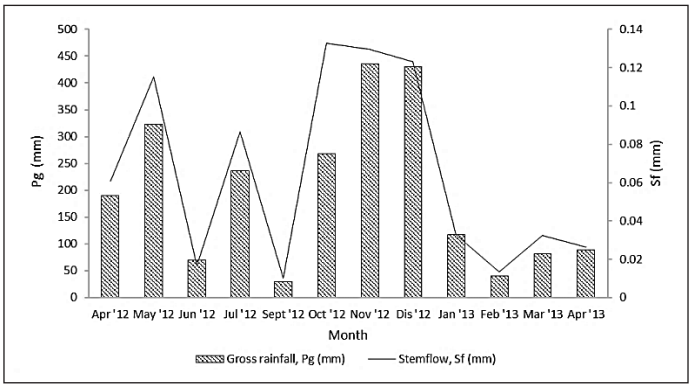

Figure 2. Monthly PG (mm) and SF (mm)

Tree Characteristics

Table 1 presents the descriptive statistics for the three characteristics, including the maximum, minimum, mean, and standard deviation: CD, DBH, TH and CC and consisting of a mix of *Mempisang, Kledan, Simpoh,* and *Keruing* species, were identified within the plot, amounting to a total of 20 trees.

Table 1
Descriptive statistics (mean, min, max and standard deviation) of CD, DBH, TH and CC

	CD (m)	DBH (cm)	TH (m)	CC (%)
Average	5.984	25.98	19.72	95.21
Min	2.11	10.6	10.8	89.53
Max	12.86	44.1	29.8	97.65
Std dev	2.62	11.75	6.54	1.57

The data on canopy CD provide insights into the dimensions of tree canopies in the study area. With an average canopy CD of 5.984 m, it delineates the typical size of tree canopies in the sample. The minimum recorded canopy CD is 2.11 m, representing the smallest observed canopy size in the dataset. Conversely, the maximum observed canopy CD is 12.86 m, indicating the largest tree canopy size recorded in the study area. The standard deviation of 2.62 m indicates the variability of canopy CD around the average. A higher standard deviation points to greater variability among the observed canopy sizes.

The DBH data offers valuable insights into the distribution of tree sizes within the researched area. With an average DBH of 25.98 cm, it represents the typical size of trees in the sample. The minimum recorded DBH of 10.6 cm indicates the smallest diameter observed among the trees in the dataset, showcasing the range of tree sizes. Conversely, the maximum observed DBH of 44.1 cm is the largest recorded for trees in the study area, providing perspective on the upper limit of tree size. The standard deviation of 11.75 cm measures the variability or spread of DBH values around the average. In this context, a higher standard deviation of 11.75 cm suggests greater variability in tree diameters within the dataset. This variability underscores the diversity of tree sizes, contributing to a comprehensive understanding of the size distribution in the studied area.

The dataset on TH offers crucial insights into the vertical dimensions of trees within the study area. With an average TH of 19.72 m, it serves as a representative measure of tree height in the sample. The minimum recorded TH, at 10.8 meters, indicates the shortest height among the trees in the dataset, highlighting the range of vertical dimensions within the studied population. Conversely, the maximum observed tree height of 29.8 m is the tallest recorded in the study area, providing perspective on the upper limit of TH. The standard deviation of 6.54 m quantifies the variability of TH around the average. In this context, a higher standard deviation of 6.54 m indicates greater variability in TH within the dataset. This variability highlights the range of tree heights (TH), aiding a thorough understanding of vertical dimensions in the studied area. The canopy cover (CC) data provide important insights into the extent of vegetation cover in the study area. An average CC of 95.21% indicates the typical percentage of ground area covered by tree canopies in the sample. The minimum recorded CC, at 89.53%, is the lowest observed percentage of ground coverage among areas with trees, underscoring the variability in vegetation density across the study site. On the contrary, the maximum observed CC of 97.65% indicates the highest ground-cover percentage in tree-covered areas, representing the upper limit of vegetation density in the study. The standard deviation of 1.57% quantifies the degree of variability or spread of CC percentages around the average. In this context, a higher standard deviation of 1.57% suggests greater variability in CC within the dataset. This variability underscores the range of vegetation cover percentages, contributing to a comprehensive understanding of canopy spatial distribution across the study area.

Correlation of PG to TF, SF and IL

The impacts of PG, TF, and SF on IL in the study area have been obtained through point correlation analysis. The correlation has been done using linear regression of the data. The correlation analysis indicates that the strongest relationship between TF and PG is given by TF = 0.8352PG – 2.2163, with an R2 of 0.9318. For this equation, TF and PG are in units of depth (mm).

The findings indicate a positive correlation between throughfall (TF) and gross precipitation (PG), with TF increasing as PG increases, as shown in Figure 3. The increase in TF with higher overall rainfall can be attributed to various factors associated with the structure and dynamics of the forest canopy. As rainfall intensity increases, the canopy may become saturated, leading to water overflow. When the canopy reaches its capacity to hold water, excess rainfall drips through the vegetation and reaches the ground as TF.

The CC within the canopy can influence the TF value. Under certain circumstances, leaves might redirect water towards the ground, amplifying TF particularly during intense rainfall events. High CC may limit the direct passage of rainfall to the ground. During low-intensity rainfall, the high CC might reduce water bypassing the leaves and branches, thereby affecting the amount of TF reaching the ground. Studies by Aussenac (1970), Ford and Deans (1978), Herwitz (1986), Johnson (1990), Ovington (1954), and Prebble and Stirk (1980) mentioned that the spatial variability of throughfall (TF) has been found to be associated with the distance from the tree trunk and different canopy characteristics.

The CD of a tree can influence the spatial distribution of TF beneath the canopy. Broader crowns can create a larger coverage area for TF, thereby affecting the distribution pattern on the forest floor. Larger CDs can generate larger canopy gaps, facilitating more direct passage of rainfall to the ground. This, in turn, can affect the ratio of TF to total rainfall in the forest ecosystem.

The results of the correlation analysis reveal the most robust relationship between SF and PG, expressed by the equation SF = 0.0003PG – 0.0005, with an R^2 value of 0.6464, as shown in Figure 4. In this equation, SF and PG are measured in depth units (mm). The findings demonstrate a correlation between SF and PG, with SF tending to increase as PG values rise. The volume of SF is

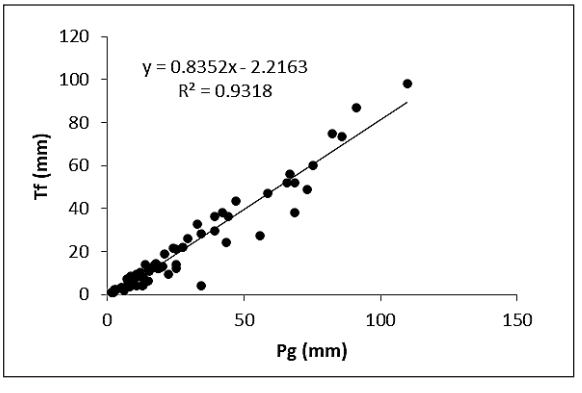

Figure 3. Correlation of TF (mm) with PG (mm)

typically dependent on various factors, including the total amount of rainfall, rainfall intensity, plant growth stages, plant density (Bäse et al., 2012; Lin et al, 2011), branch morphology, and branching architecture (Naharuddin et al., 2017), as well as canopy volume and area (Martinez-Meza & Whitford, 1996). Additionally, meteorological conditions influence SF volume (Levia & Herwitz, 2005).

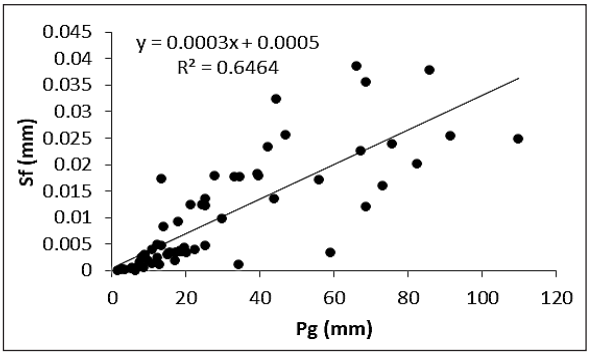

Figure 4. Correlation of SF (mm) with PG (mm)

DBH of a tree can also influence the amount of SF, which is the flow of water down the trunk or stems of a tree during rainfall. Llorens and Domingo (2007) stated that smaller or shorter trees, which are represented by the TH, have also been reported to have lower relative SF. Typically, larger trees with greater DBH exhibit a larger surface area. This expanded surface area provides more space for rainwater interception and directed flow down the trunk, potentially increasing SF. The density of the tree canopy, which is influenced by tree DBH, plays a significant role in determining how much rainwater is captured by the leaves. A denser canopy, often associated with trees of larger DBH, implies a greater number of leaves per unit area. In such cases, a larger leaf surface area is available for intercepting rainfall.

Increased leaf density in a denser canopy increases the likelihood that raindrops are intercepted by the leaves as they fall through the canopy. As a result, more water is collected and funnelled down the stem, thereby increasing the volume of SF. This relationship underscores the importance of considering not only individual tree size but also the overall canopy structure when understanding and predicting the dynamics of SF in a forested environment. Abu Bakar et al. (2021) have investigated the contribution of stemflow to rainfall interception in lowland tropical forest.

The correlation analysis results indicate the strongest connection between IL and PG, as represented by the equation IL = 0.1603PG – 2.2499, with an R^2 value of 0.3142. Both IL and PG are measured in depth units (mm). These findings indicate a correlation between IL and PG, with IL tending to rise as PG increases, as shown in Figure 5.

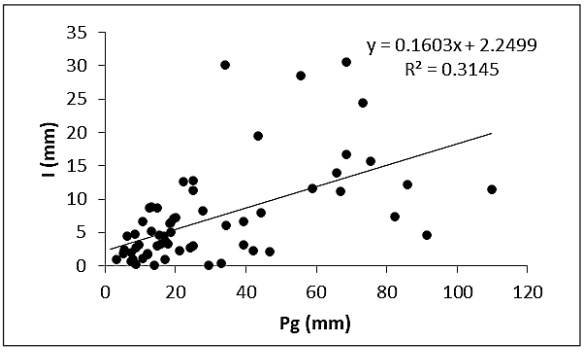

Figure 5. Correlation of IL (mm) with PG (mm)

Larger CDs often correspond to a greater surface area of leaves and branches. This increased surface area provides more space for raindrops to be captured and held by the canopy, leading to higher IL capacity. CD, often associated with a denser canopy, can lead to more effective interception of rainfall. The dense arrangement of leaves and branches provides abundant opportunities for the raindrops to be intercepted.

CC exhibits a close correlation with the Leaf Area Index (LAI), which represents the proportion of total leaf area to ground area. Higher LAI values, indicative of denser canopy cover, indicate a larger leaf surface area for capturing rainfall. This connection implies that a denser canopy, characterised by a higher CC, influences interception loss. Another researcher, Livesley et al. (2014), corroborated that more extensive canopy cover can intercept a significant portion of high-intensity rainfall, whereas thinner or less dense canopy cover is more effective at intercepting smaller showers.

CONCLUSION

This study emphasises the significance of canopy characteristics (CD, DBH, TH, and CC) in governing the extent of interception loss. The findings revealed a range of canopy interception influenced by forest structure and precipitation. The study proposes potential enhancements, including other canopy attributes like leaf area index, canopy storage, and gap fractions in the analysis, as these variables may play pivotal roles in shaping the trajectory of rainfall distribution. In summary, the positive and statistically significant correlation observed between canopy characteristics and interception loss underscores their substantial influence on the hydrological processes studied.

ACKNOWLEDGEMENT

The authors would like to express their sincere gratitude to the Faculty of Civil Engineering, Universiti Teknologi MARA (UiTM), for providing materials and facilities and for the invaluable guidance from the staff. Their support and expertise were instrumental in the successful completion of this research.

REFERENCES

Abu Bakar, A. A., & Khalil, M. K. (2017). Preliminary study on tropical forest canopy interception. *Journal of Engineering and Applied Sciences, 12*(21), 5572-5577. https://doi.org/10.36478/jeasci.2017.5572.5577

Abu Bakar, A. A., Abd Latif, Z., & Lee, W. K. (2023). Comparison of canopy cover effects on rainfall interception loss in tropical forest with homogenous and mixed tree species. *Jurnal Teknologi, 85*(2), 1-9. https://doi.org/10.11113/jurnalteknologi.v85.17661

Abu Bakar, A. A., Lee, W. K., & Abd Latif, Z. (2021). Investigating the role of stemflow in rainfall partitioning in lowland tropical forest. *Journal of Mechanical Engineering, 10*(Special Issue 1), 213-225.

Aussenac, G. (1970). Action du couvert forestier sur la distribution au sol des précipitations. *Annales des Sciences Forestières, 27*(4), 383-399. https://doi.org/10.1051/forest/19700403

Bäse, F., Elsenbeer, H., Neill, C., & Krusche, A. V. (2012). Differences in throughfall and net precipitation between soybean and transitional tropical forest in the southern Amazon, Brazil. *Agriculture, Ecosystems & Environment, 159*, 19-28. https://doi.org/10.1016/j.agee.2012.06.013

Bo, M. W., Tae, H. K., & Kyong, H. K. (1989). Rainfall interception loss from canopy in forest catchment [Conference paper]. *IHP-UNESCO-FRIM Regional Seminar on Tropical Forest Hydrology*, Kuala Lumpur, Malaysia.

Chappell, N. A., Bidin, K., & Tych, W. (2001). Modelling rainfall and canopy controls on net-precipitation beneath selectively-logged tropical forest. *Plant Ecology, 153*(1-2), 215-229. https://doi.org/10.1023/A:1017532411978

Crockford, R. H., & Richardson, D. P. (2000). Partitioning of rainfall into throughfall, stemflow and interception: Effect of forest type, ground cover and climate. *Hydrological Processes, 14*(16-17), 2903–2920. https://doi.org/10.1002/1099-1085(200011/12)14:16/17%3C2903::AID-HYP126%3E3.0.CO;2-6

Dietz, J., Hölscher, D., Leuschner, C., & Hendrayanto. (2006). Rainfall partitioning in relation to forest structure in differently managed montane forest stands in Central Sulawesi, Indonesia. *Forest Ecology and Management, 237*(1-3), 170-178. https://doi.org/10.1016/j.foreco.2006.09.044

Ford, E. D., & Deans, J. D. (1978). The effects of canopy structure on stemflow, throughfall and interception loss in a young Sitka spruce plantation. *Journal of Applied Ecology, 15*(3), 905-917. https://doi.org/10.2307/2402786

Herwitz, S. R. (1986). Infiltration-excess caused by stemflow in a cyclone-prone tropical rainforest. *Earth Surface Processes and Landforms, 11*(4), 401-412. https://doi.org/10.1002/esp.3290110406

Johnson, R. C. (1990). The interception, throughfall and stemflow in a forest in Highland Scotland and the comparison with other upland forests in the U.K. *Journal of Hydrology, 118*(1-4), 281-287. https://doi.org/10.1016/0022-1694(90)90263-W

Levia, D. F., & Herwitz, S. R. (2005). Interspecific variation of bark water storage capacity of three deciduous tree species in relation to stemflow yield and solute flux to forest soils. *Catena, 64*(1), 117-137. https://doi.org/10.1016/j.catena.2005.08.001

Lin, D. J., Zheng, Z. C., Zhang, X. Z., Li, T. X., & Wang, Y. D. (2011). Study on the effect of maize plants on rainfall redistribution processes. *Scientia Agricultura Sinica, 44*(12), 2608-2615. https://doi.org/10.3864/j.issn.0578-1752.2011.12.025

Livesley, S. J., Baudinette, B., & Glover, D. (2014). Rainfall interception and stem flow by eucalypt street trees–The impacts of canopy density and bark type. *Urban Forestry & Urban Greening, 13*(1), 192-197. https://doi.org/10.1016/j.ufug.2013.09.001

Llorens, P., & Domingo, F. (2007). Rainfall partitioning by vegetation under Mediterranean conditions: A review of studies in Europe. *Journal of Hydrology, 335*(1-2), 37-54. https://doi.org/10.1016/j.jhydrol.2006.10.032

Manfroi, O. J., Kuraji, K., Tanaka, N., Suzuki, M., Nakagawa, M., Nakashizuka, T., & Chong, L. (2004). The stemflow of trees in a Bornean lowland tropical forest. *Hydrological Processes, 18*(13), 2455-2474. https://doi.org/10.1002/hyp.1474

Martinez-Meza, E., & Whitford, W. G. (1996). Stemflow, throughfall and channelization of stemflow by roots in three Chihuahuan desert shrubs. *Journal of Arid Environments, 32*(3), 271-287. https://doi.org/10.1006/jare.1996.0023

Naharuddin, Bratawinata, A., Hardwinarto, S., & Pitopang, R. (2017). Canopy interception on tree architecture models of Aubreville, Stone and Leeuwenberg in Lore Lindu National Park Area, Indonesia. *Journal of Biodiversity and Environmental Sciences, 10*(2), 75-88.

Ovington, J. D. (1954). A comparison of rainfall in different woodlands. *Forestry: An International Journal of Forest Research, 27*(1), 41-53. https://doi.org/10.1093/forestry/27.1.41

Prebble, R. E., & Stirk, G. B. (1980). Throughfall and stemflow on silverleaf ironbark (*Eucalyptus melanophloia*) trees. *Australian Journal of Ecology, 5*(4), 419-427. https://doi.org/10.1111/j.1442-9993.1980.tb01266.x

Xiao, Q., McPherson, E. G., Ustin, S. L., Grismer, M. E., & Simpson, J. R. (2000). Winter rainfall interception by two mature open-grown trees in Davis, California. *Hydrological Processes, 14*(4), 763–784. https://doi.org/10.1002/(SICI)1099-1085(200003)14:4%3C763::AID-HYP971%3E3.0.CO;2-7

Yamakura, T., Hagihara, A., Sukardjo, S., & Ogawa, H. (1986). Aboveground biomass of tropical rain forest stands in Indonesian Borneo. *Vegetatio, 68*(2), 71-82. https://doi.org/10.1007/BF00045057

Yan, W., Deng, X., Chen, X., Tian, D., Xiang, W., & Peng, Y. (2015). Long-term variations of rainfall interception in different growth stages of Chinese fir plantations. *Hydrological Sciences Journal, 60*(12), 2178-2188. https://doi.org/10.1080/02626667.2014.964243

Yusop, Z., Cham, S. Y., & Chong, J. H. (2003). Throughfall, stemflow and interception loss of old rubber trees. *Jurnal Kejuruteraan Awam, 15*(1), 24-33. https://doi.org/10.11113/mjce.v15.15656

Pertanika J. Sci. & Technol. 34 (S2): 75 - 88 (2026)

PERTANIKA JOURNALS

SCIENCE & TECHNOLOGY

Journal homepage: http://www.pertanika.upm.edu.my/

Experimental and Finite Element Analysis of Shear Strength in Melunak and Mengkulang Glulam Using Shear Block Test

Nor Jihan Abd Malek[1]*, Rohana Hassan[2], Mohd Nizam Shakimon[3], Nurharniza Abdul Rahman[1], Nazrul Azmi Ahmad Zamri[1], and Khaled M. H. Alreqeb[4]

[1]Faculty of Engineering and Quantity Surveying (FEQS), INTI International University, Persiaran Perdana BBN, Putra Nilai, 71800 Nilai, Negeri Sembilan, Malaysia
[2]Institute for Infrastructure Engineering and Sustainable Management (IIESM), Universiti Teknologi MARA, 40450 Shah Alam, Selangor, Malaysia
[3]Faculty of Engineering, Science and Technology, Kuala Lumpur University Science and Technology, Jalan Ikram-UNITEN, 43000 Kajang, Selangor, Malaysia
[4]Faculty of Engineering, Built Environment and Information Technology, SEGi University, Kota Damansara, 47810 Petaling Jaya, Selangor, Malaysia

ABSTRACT

This study investigates the shear strength parallel to the grain of glued laminated timber (glulam) produced from two Malaysian tropical hardwoods, Melunak (SG5) and Mengkulang (SG5), bonded with a phenol-resorcinol-formaldehyde (PRF) adhesive. The study aimed to determine the shear strength and compare the percentages of wood and glue failures. Twenty block specimens (10 Melunak and 10 Mengkulang), each measuring 50 × 50 × 50 mm, were tested using a universal testing machine. Shear block testing and shear strength evaluation were conducted in accordance with MS 758:2001 and EN 392:1995. Mengkulang recorded a higher average shear strength than Melunak by approximately 2.03 N/mm²; the mean values were 12.9847 N/mm² for Mengkulang and 10.9482 N/mm² for Melunak. Both species exceeded the minimum shear strength requirement of approximately 6 N/mm² specified in MS 758:2001. Post-test observations showed that failure occurred predominantly in the wood rather than along the glue line, indicating strong adhesive bonding. Finite element analysis was also conducted using Abaqus CAE. A three-dimensional model incorporated the specimen geometry, mesh, boundary conditions, material properties, and loading conditions used in the experimental programme. The simulated shear-strength response was close to the experimental results, with a difference of approximately 3%. The combined experimental and numerical

ARTICLE INFO

Article history:
Received: 18 June 2026
Accepted: 18 September 2026
Published: 30 September 2026

DOI: https://doi.org/10.47836/pjst.34.S2.07

E-mail addresses:
norjihan.amalek@newinti.edu.my (Nor Jihan Abd Malek)
rohan742@uitm.edu.my (Rohana Hassan)
nizam@klust.edu.my (Mohd Nizam Shakimon)
nurharniza.rahman@newinti.edu.my (Nurharniza Abdul Rahman)
nazrulazmi.zamri@newinti.edu.my (Nazrul Azmi Ahmad Zamri)
khaled012618@gmail.com (Khaled M.H. Alreqeb)
* Corresponding author

e-ISSN: 2231-8526

© Universiti Putra Malaysia Press

findings demonstrate the shear-strength characteristics and bonding performance of Melunak and Mengkulang glulam.

Keywords: Bonding performance, finite element method, glued laminated timber, shear block test, shear strength

INTRODUCTION

Timber has been significant in environmental interactions and developmental advancements (Buchanan, 2015). Its superior strength-to-weight ratio and adaptability in various structural applications, such as beams, roof trusses, and wall cladding, make it a favoured choice among building materials (Kretschmann et al., 2010). Timber is sourced from various tree species, each with distinct growth rates, structural properties, and durability grades (Zobel et al., 1989). Recent innovations in wood research and design have further expanded the potential uses of timber (Davies et al., 2014).

Glued laminated timber is an engineered wood product consisting of bonded timber laminations (Buchanan & Abu, 2017). It can be fabricated in specific sizes and shapes for structural elements like columns and beams (Dinwoodie, 2000). However, the selection of timber species for lamination requires careful consideration of two key characteristics: susceptibility to glue and dimensional stability under varying atmospheric conditions (Gustafsson et al., 2003). Recent studies have highlighted the importance of understanding the factors influencing the glueing quality of solid wood products in timber construction (Hänsel et al., 2022).

Recent studies have investigated the shear properties of structural-size Malaysian tropical timber using torsional testing in accordance with EN 408:2010 (Mohd Puaad, 2021), while a shear or picture-frame method has also been proposed for determining shear modulus and shear strength (Krüger et al., 2018).

This study addresses this issue by examining the shear strength of two types of Malaysian tropical hardwood: Melunak and Mengkulang. The goal is to determine their shear strength values and compare the percentages of wood and glue failure. The outcomes of this study could offer valuable insights into the performance of these species in glued laminated timber applications, potentially guiding future material selection decisions and aligning with recent efforts by start-ups to make sustainable timber a reality (Xiao, 2007).

LITERATURE REVIEW

Shear strength is an essential property of timber, particularly in structural applications such as glued-laminated timber. Several methods have been proposed and applied to assess and determine the shear strength of various timber species and products.

One method is based on torsional tests, which measure the shear stress and strain in a circular cross-section of timber under torsion. This method is in accordance with the European standard EN 408:2010 (European Committee for Standardisation, 2010). A study utilising this method on selected Malaysian tropical timber revealed that small clear specimens exhibited higher shear strength than structural-size specimens (Mohd Puaad, 2021). This finding suggests that defects such as knots, splits, and checks in larger specimens influence timber's shear strength. Furthermore, the study indicated that the current European standard may not fully accommodate tropical timber species due to their high density and variability (Mohd Puaad, 2021). In addition to these factors, the moisture content of timber also impacts its shear strength. A study by Ravenshorst et al. (2016) determined the shear strength of tropical hardwood timber and found that high-density tropical hardwoods have significantly lower shear strength values compared to softwoods, according to European strength class tables.

Another method is based on shear or picture-frame tests, which measure the shear modulus and shear strength of a rectangular timber cross-section under shear (Krüger et al., 2018). This method is a straightforward way to determine the shear properties of wood, thereby reducing testing time and cost compared to other methods that require separate tests for each property. The method also allows for a more uniform stress distribution in the specimen, which could improve the accuracy and reliability of the results.

Adhesive bonds also influence the shear strength of glued-laminated timber products. Sikora et al. (2018) conducted shear strength and durability testing of adhesive bonds in CLT using two types of adhesives: polyurethane (PUR) and phenol- resorcinol-formaldehyde (PRF). It was found that while PUR specimens had higher shear strength values, PRF specimens demonstrated superior durability in delamination tests, indicating that the choice of adhesive for cross-laminated timber depends on the intended service conditions and performance requirements. The study also highlights the need for further research on the influence of moisture content, temperature, and loading duration on the shear strength and durability of adhesive bonds in cross-laminated timber.

Recent research has also focused on the bending, shear, and compressive properties of cross-laminated timber (CLT) fabricated from black spruce. The study found that increasing CLT thickness while maintaining the same span-to-thickness ratio can slightly reduce the characteristic bending strength of black spruce CLT. For the CLT shear panels, results show that increasing the CLT thickness while maintaining identical span-to-thickness ratios has little enhancement on their characteristic shear strength (He et al., 2020).

In addition, analytical models have also been developed to calculate the shear strength of wood based on its microstructure and fracture mechanics. A study published in Wood Science and Technology (van de Kuilen & Leijten, 2006) discussed the appropriateness of these models and compared them with experimental results. The study found that they

could accurately predict only the shear strength of wood, indicating that there are still gaps in understanding the complex mechanisms underlying wood failure under shear stress. The study also suggests that more experimental data and advanced numerical methods are needed to improve the accuracy and applicability of analytical models for wood shear strength.

The finite element method (FEM) is a numerical technique for simulating the mechanical behaviour of complex structures under various loading conditions. FEM has been widely applied in timber analysis, as it can overcome some of the challenges and limitations of experimental methods, such as the high cost of preparing timber samples, the variability of material properties, and the difficulty of measuring stress and strain distributions. One of the main advantages of FEM over other numerical methods, such as finite-difference or boundary-element methods, is its ability to handle complex geometries and arbitrary boundary and initial conditions (Zienkiewicz et al., 2013). FEM divides the structure into smaller elements with simple shapes, such as triangles or quadrilaterals, and approximates the solution at each element node using interpolation functions.

The global solution is then obtained by assembling all the elements and applying the boundary and initial conditions. This approach allows FEM to capture the detailed features and nonlinearities of timber structures, such as cracks, defects, joints, and anisotropy. However, FEM also has some limitations that must be addressed to ensure its reliability and validity. One of the main challenges is achieving convergence, meaning the solution remains largely unchanged as the mesh is refined or the element size decreases (Bathe, 2014). Convergence is affected by various factors, such as the model's complexity, mesh size, mesh type and shape, material properties, and analysis technique (Monteiro et al., 2020). For example, different mesh sizes can produce significantly different results and stress-strain curves (Chen et al., 2010b). Smaller mesh sizes can improve accuracy but increase computation time (Chen et al., 2010b). Larger mesh sizes can reduce computation time but introduce errors (Chen et al., 2010b). Moreover, some mesh shapes, such as quadrilateral elements, may cause convergence errors due to distortion or singularity (Aicher et al., 2005; Chen et al., 2010b). Therefore, choosing an appropriate mesh size and shape for each problem is crucial.

Another challenge is to select suitable material models and failure criteria for timber structures. Timber is a natural material that exhibits different mechanical behaviours in different loading directions. It is usually ductile in compression and brittle in tension and shear (He et al., 2004). Therefore, most FEM models adopt an orthotropic elasto-plastic behaviour in compression and a brittle elastic behaviour in tension and shear (Ahmad, 2010; Aicher & Dill-Langer, 2003; Aicher & Dill-Langer, 2004; Brandon, 2015; Ceccotti et al., 2002b; He et al., 2004; Shakimon et al., 2016). Some models also assume linear-elastic,

perfectly plastic behaviour in compression (Brandon, 2015). However, these models may only capture some of the nonlinearities and complexities of timber structures. For instance, some models neglect the influence of moisture content, temperature, loading rate, grain angle, or defects on timber properties. Some models also ignore size or scale effects on timber strength (Aicher et al., 2005).

Furthermore, different failure criteria have been proposed for timber structures based on different yield theories or fracture mechanics. For example, some models use the Hill yield criterion (Monteiro et al., 2020), a generalisation of the von Mises yield criterion that accounts for anisotropy (Chen et al., 2010b). Some models use the Hoffman yield criterion (Chen et al., 2010b), based on a quadratic function of stress components (Chen et al., 2010b). However, these criteria may suit only certain timber structures or loading conditions. Therefore, using experimental data, it is necessary to compare and validate different material models and failure criteria for timber structures.

FEM has been applied to various timber structures, such as beams, columns, frames, joints, connections, panels, floors, walls, roofs, bridges, and buildings (Aicher et al., 2005). The structural performance of glued laminated timber beams with round holes has also been investigated experimentally (Okamoto et al., 2021). One specific application is to simulate the shear strength of glulam when loaded parallel or perpendicular to the grain. For example, Ceccotti et al. (2002b) used a three-dimensional solid element model to analyse the shear behaviour of glulam loaded parallel to the grain. The model considered the orthotropic elasto-plastic behaviour of wood and the contact interaction between the laminations. The model was validated by comparing the results with experimental data from Ceccotti et al. (2002a). The model agreed well with the experimental data on load-displacement curves and failure modes. The model also revealed the stress distribution and deformation pattern in the glulam. Aicher and Dill-Langer (2003) used a two-dimensional plane strain element model to analyse the shear behaviour of glulam loaded perpendicular to the grain. The model considered the orthotropic elastic behaviour of wood and the frictional contact between the laminations. The model was validated by comparing the results with experimental data from Aicher and Dill-Langer (2004). The model agreed reasonably with the experimental data regarding load-displacement curves and failure modes.

Therefore, FEM is a valuable and powerful tool for analysing the shear strength of glulam loaded parallel or perpendicular to the grain. However, FEM also has some limitations that must be overcome to improve its accuracy and applicability. Future research should focus on developing more realistic and reliable material models and failure criteria for timber structures and optimising the mesh size and shape for convergence studies. Moreover, more experimental data are needed to validate and calibrate the FEM models for different types of timber structures and loading conditions.

MATERIALS AND METHODS

Experimental Setup

In this study, the Melunak and Mengkulang species were selected as specimens for glued-laminated timber (glulam). These timbers are naturally moderately durable (Ross, 2010), untreated, and suitable for outdoor environmental conditions. Melunak and Mengkulang are hardwoods, with Melunak classified as a light hardwood and Mengkulang as a medium hardwood. General structural use of timber is addressed in MS 544: Part 1: 2001 (Department of Standards Malaysia, 2001b). The glulam specimens were fabricated in accordance with the guidelines provided in MS 758:2001 (Department of Standards Malaysia, 2001a). A total of 20 specimens, 10 each of Melunak and Mengkulang, were prepared to the required dimensions of 50 × 50 × 50mm. This size was based on the minimum requirement stipulated in EN 392:1995 (European Committee for Standardisation, 1995) and BS EN 14080:2013 (British Standards Institution, 2013). The prepared specimens are shown in Figure 1, and a side view of the bonded timber block is shown in Figure 2. To determine the shear block performance on the glue line of each species, a shear block jig and a universal testing machine were used by Davies et al. (2014). The shear block specimens were cut from a glulam beam using a band saw to achieve the required dimensions. The timber specimens were marked on the timber block prior to cutting and placed under the band saw blade for cutting. These timber specimens were preassembled in the UiTM laboratory. The shear block test was performed in accordance with EN 392. (1995), which provided adequate measurements for width > 40 mm to 50 mm and thickness > 40 mm to 50 mm.

The shear block testing equipment is shown in Figure 3. The testing machine was set to apply a load at 9.8 kN/min, ensuring failure would occur within 20 s. Generally, it is anticipated



Figure 1. 50 × 50 × 50mm specimens

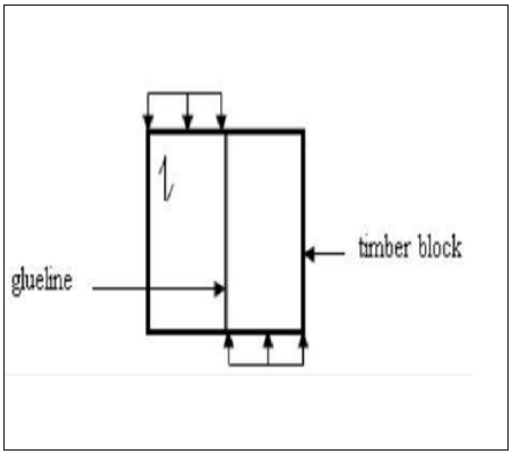

Figure 2. Side view of timber block with glue

that the specimen will fail when the machine applies approximately 15% to 85% of its loading capacity at this calibrated rate, used to determine the appropriate setting. The maximum shear strength (f_V) will be calculated using Equation 1 provided below, with the result rounded to two significant figures.



Figure 3. Shear block equipment

$$f_v = k\frac{F_u}{A}\ (\mathrm{N/mm^2}) \qquad [1]$$

where.

F_u is the ultimate load, in Newton.
A is the sheared area (for a test bar A = bt, and for a drill core A = lt) k is a modification factor (k = 0.78 + 0.0044 t)
It is the thickness, in millimetres.

In addition to shear strength, it is crucial to determine the percentage of wood failure to assess bond quality. This is typically measured through visual examination. If the sheared area is not a simple rectangle, divide it into smaller, measurable shapes (rectangles or squares), calculate the area of each, and sum them. However, it is important to note that the average or individual wood failure percentage of the specimen should not exceed the minimum wood failure percentage as stipulated by EN 392. (1995).

Finite Element Modelling Framework

The finite element model (FEM) of the glulam timber block was meticulously developed using the Abaqus interface. This comprehensive process involved defining the sample geometry, which formed the basis for the model database (.cae file) and an input file. The input file contained the geometry of the glulam timber block sample within its assembly, as shown in Figure 4.

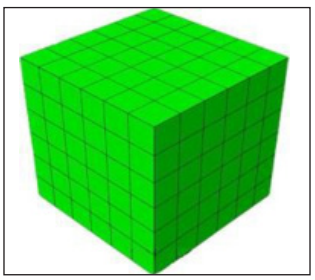

Figure 4. Typical FEM model of the glulam timber block

Material properties were then specified, with the glulam timber block sample defined as an orthotropic material, adhering to Cartesian coordinates with three mutually perpendicular axes of elastic symmetry at each point. A total of nine independent engineering constants were defined, that is, modulus of elasticity E, Poisson's ratio (v) and shear modulus (G) for three orthotropic axes 1(X), 2(Y) and 3(Z) with the value of E1 (10600 N/mm^2) based on MS 544: Part 2: 2001 (Department of Standards Malaysia, 2001c) for glulam timber Mengkulang and Melunak. The values of the independent engineering constants: E2, E3, v21, v31, v32, G12, G23, and G31 were determined from ratios reported by Ahmad (2010) and Green et al. (1999), as shown in Equations 2, 3, and 4 and in Table 1.

$$\frac{E_1}{E_2} = 11.5 \quad [2]$$

$$\frac{E_1}{G_{12}} = 16 \quad [3]$$

$$\frac{V_{12}}{E_1} = \frac{V_{21}}{E_2} \quad [4]$$

Table 1
Values of independent elastic constants for both species

E1 (N/mm^2)	**E2** (N/mm^2)	**E3** (N/mm^2)	**v12** (N/mm^2)	**v13** (N/mm^2)	**v23** (N/mm^2)	**G12** (N/mm^2)	**G13** (N/mm^2)	**G23** (N/mm^2)
10600	848	922	0.015	0.35	0.015	662.5	66.2	441.7

The timber grain directions parallel to the loading direction were modelled by creating material property orientations with the element's stacking direction isoparametric to 1, thereby aligning the timber grain direction with the vertical load direction. The average density of 530 kg/m^3 for both timbers, as it is categorised under the same strength-group block models used. To simplify FEM modelling, the general contact interaction with the selected surface pairs option was used to laminate two timber blocks forming the glulam contact surface, preventing them from intersecting. Four inputs were created to simulate the lamination: tangential behaviour, normal behaviour, cohesive behaviour, and damage. In the tangential behaviour, a friction coefficient of 0.3 was used in the penalty feature to simulate the friction at the timber contact surface. In normal operation, the hard-contact feature was selected to prevent the contact surfaces of the timber blocks from intersecting. The cohesive behaviour was created to simulate the PRF glue used to bond the timber blocks. The stiffness coefficients were specified under uncoupled conditions (to allow only one deformation in one direction) using the stiffness values for a traction (stress) separation

curve in cohesive elements, namely K_{nn}, K_{ss}, and K_{tt}. They represent the traction required to separate two surfaces in normal (nn) and tangential (ss and tt) directions and are calculated using Equations 5 and 6.

$$K_{nn} = \frac{E}{t} \quad [5]$$

$$K_{ss} = \frac{G}{t} = K_{tt} \quad [6]$$

Where;
E is the modulus of elasticity of the cohesive element
G is the shear modulus of the cohesive element
t is the thickness of the cohesive element applied on the contact surfaces

The damage in the contact surface of both sample species was modelled considering the normal strength (T_n) of 7MPa, and shear strength (T_s) of 12MPa from the experimental results. The fixed boundary conditions were applied to the half-bottom surface of the glulam timber block and were partially fixed along the sides of the blocks, with translation in the vertical direction allowed. Shearing under pressure with automatic incrementation was applied to the half-top surface of the glulam timber block to enable the FEM model to be tested until failure. To avoid errors when submitting the FEM model to the Abaqus solver for analysis, small increment sizes of 0.1, 0.1×10^-10, and 0.3 were defined as the initial, minimum, and maximum increment sizes, respectively. The mesh was controlled by specifying global mesh constraints for the two parts of the timber model. An element size of 8 is controlled by setting the global element size for each part based on its overall dimensions. The element type DC3D8R, an 8-node linear hexahedron for 3D stress analysis, was used in the generated meshes. This rigorous process ensures a comprehensive and accurate representation of the glulam timber block samples, facilitating precise analysis and reliable results.

RESULTS AND DISCUSSIONS

The average shear strength value is derived from the shear strength values of 10 test specimens. As depicted in Figure 5, Mengkulang exhibits a higher average shear strength than Melunak, approximately 2.0364 N/mm^2. Furthermore, Melunak's average shear strength is 10.9482 N/mm^2 with a standard deviation of 4.11 and a coefficient of variation of 26.58%, while Mengkulang's average shear strength is determined to be 12.9847 N/mm^2 with a standard deviation of 3.03 and a coefficient of variation of 42.7%. Two types of failure

modes were identified: wood failure and glue failure. Wood failure, which accounted for 100% of the failure surface for both timbers, is shown in Figure 6. However, as shown in Figure 7, Melunak and Mengkulang block specimens exhibited 95% wood failure, with the remaining 5% failing at the glue line. Both types of failures were determined through visual inspections using the proportional method as applied by Zobel et al. (1989). The timber specimen was divided into four quadrants to determine the percentage of failure in either the wood or the glue, with each quadrant representing 25% of the total sheared area. Wood failure was indicated by a brown surface on the timber and a less appealing appearance.

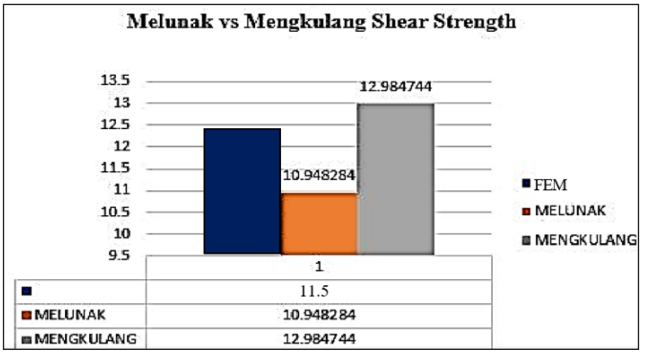

Figure 5. Percentage difference of shear strength of Melunak, Mengkulang, and FEM



Figure 6. Wood failure at 100% for melunak (left), mengkulang (middle) and FEM (right)



Figure 7. Wood failure at 95% and 5% glue failure for Melunak and Mengkulang

CONCLUSION

This research investigated the shear strength of glulam made from two Malaysian wood species: Melunak and Mengkulang. These timbers are naturally durable (Shakimon et al., 2016), untreated, and suitable for outdoor environmental conditions. Melunak and Mengkulang are hardwoods, with Melunak classified as a light hardwood and Mengkulang as a medium hardwood. General structural use of timber is addressed in MS 544: Part 1: 2001 (Department of Standards Malaysia, 2001b). The research objectives were to determine the shear strength values and the wood failure percentages of Melunak and Mengkulang glulam specimens under different loading conditions. The glulam specimens were fabricated in accordance with EN 392:1995 (European Committee for Standardisation, 1995). A total of 20 specimens, 10 each of Melunak and Mengkulang, were prepared to the required dimensions of 50 × 50 × 50mm. This size was based on the minimum requirement stipulated in the guidelines. The shear strength of both specimens was determined in accordance with EN 392:1995 (European Committee for Standardisation, 1995) using a universal testing machine. The average shear strength values were calculated for Melunak and Mengkulang glulam specimens. The results showed that Mengkulang glulam specimens had higher average shear strength than Melunak glulam specimens, approximately 2.0364 N/mm^2. Furthermore, Melunak's average shear strength was 10.9482 N/mm^2 with a standard deviation of 4.11 and a coefficient of variation of 26.58%, while Mengkulang's average shear strength was determined to be 12.9847 N/mm^2 with a standard deviation of 3.03 and a coefficient of variation of 42.7%. Both specimens reached the minimum shear strength of about 6 N/mm^2 specified in MS 758:2001 (Department of Standards Malaysia, 2001a). The results also indicated that both specimens exhibited wood failure rather than glue failure. Wood failure accounted for 100% of the failure surface for both timbers, as shown in Fig. 5. However, as shown in Fig. 6, some specimens exhibited 95% wood failure and 5% glue failure. Both types of failures were determined through visual inspections using the proportional method as assessed in accordance with MS 758:2001 (Department of Standards Malaysia, 2001a). The timber specimen was divided into four quadrants to determine the percentage of failure in either the wood or the glue, with each quadrant representing 25% of the total sheared area. Wood failure was indicated by a brown surface on the timber and a less appealing appearance. The research findings validated the objectives set in this study. They also confirmed the previous studies that conducted similar tests on glulam specimens (Aicher & Dill-Langer, 2003; Ceccotti et al., 2002a). The results demonstrated that the adhesive bond performed excellently against shear loading, allowing the wood to reach its shear strength limit. However, Mengkulang showed a higher average shear strength than Melunak due to its differences in density and grain patterns. The higher density resulted in stronger wood with fewer failures, while the lower density resulted in weaker wood with more failures. Therefore, it can be concluded that to utilise

the full-strength capacity of wood under load and reduce failure in wood, the glue bond should have higher shear stress resistance than wood. Due to strong adhesive bonding, shear failure occurred primarily in the wood rather than at the glue line, indicating good bonding performance of both Melunak and Mengkulang wood species with glue.

ACKNOWLEDGEMENT

The authors would like to acknowledge Universiti Teknologi MARA (UiTM) Shah Alam, INTI International University, IUKL, and SEGi University for their support in accomplishing these research objectives.

REFERENCES

Ahmad, Y. (2010). *Bending behaviour of timber beams strengthened using fibre reinforced polymer bars and plates* [Doctoral thesis, Universiti Teknologi Malaysia].

Aicher, S., & Dill-Langer, G. (2003). Shear strength of glulam perpendicular to grain under short-term loading. *Materials and Structures, 36*(10), 689-698.

Aicher, S., & Dill-Langer, G. (2004). Shear strength of glulam perpendicular to grain under long-term loading. *Materials and Structures, 37*(3), 184-192.

Aicher, S., Dill-Langer, G., & Reinhardt, H. W. (2005). Timber engineering by numerical simulation–State-of-the-art report on modelling issues for solid timber structures in engineering mechanics. *Holz als Roh- und Werkstoff, 63*, 321-333.

Aicher, S., Gustafsson, P.-J., Haller, P., & Petersson, H. (2002). *Fracture mechanics models for strength analysis of timber beams with a hole or a notch: A report of RILEM TC-133* (Report No. TVSM-7134). Division of Structural Mechanics, Lund Institute of Technology.

Bathe, K.-J. (2014). *Finite element procedures* (2nd ed.). Klaus-Jürgen Bathe.

Brandon, D. (2015). *Fire and structural performance of non-metallic timber connections* [Doctoral thesis, University of Bath].

British Standards Institution. (2013). *Timber structures Glued laminated timber and glued solid timber Requirements* (BS EN 14080:2013). https://doi.org/10.3403/30236370

Buchanan, A. (2015). The environmental impact of wood as a building material. *Wood Design Focus, 25*(1), 1-6.

Buchanan, A. H., & Abu, A. K. (2017). *Structural design for fire safety* (2nd ed.). John Wiley & Sons. https://doi.org/10.1002/9781118700402

Ceccotti, A., & Follesa, M. (2002a). Experimental analysis of glued laminated timber beams in bending. *Materials and Structures, 35*(1), 19-27.

Ceccotti, A., Follesa, M., & Lauriola, M. P. (2002b). Numerical simulation of glued laminated timber beams in bending. *Computers & Structures, 80*(20-21), 1567-1575.

Chen, Z., Olofsson, T., Chen, Q., & Li, Q. (2010). Finite element analysis of timber beams strengthened with FRP plates: Convergence study based on mesh size, type and shape effects. *Composite Structures, 92*, 2844-2852.

Davies, G., et al. (2014). Glued laminated timber structures. *Proceedings of the Institution of Civil Engineers – Structures and Buildings, 167*(2), 69-77.

Department of Standards Malaysia. (2001a). *Glued laminated timber Performance requirements and minimum production requirements* (1st rev.; MS 758:2001).

Department of Standards Malaysia. (2001b). *Code of practice for structural use of timber: Part 1: General (first revision)* (MS 544: Part 1: 2001).

Department of Standards Malaysia. (2001c). *Code of practice for structural use of timber: Part 2: Permissible stress design of solid timber (first revision)* (MS 544: Part 2: 2001).

Dinwoodie, J. M. (2000). *Timber: Its nature and behaviour* (2nd ed.). E & FN Spon.

European Committee for Standardization. (1995). *Glued laminated timber Shear test of glue lines* (EN 392:1995).

European Committee for Standardization. (2010). *Timber structures—Structural timber and glued laminated timber-Determination of some physical and mechanical properties* (EN 408:2010).

Green, D. W., Winandy, J. E., & Kretschmann, D. E. (1999). Mechanical properties of wood. In *Wood handbook: Wood as an engineering material* (General Technical Report FPL-GTR-113, pp. 4-1-4-45). U.S. Department of Agriculture, Forest Service, Forest Products Laboratory. https://doi.org/10.2737/FPL-GTR-113

Hänsel, A., Sandak, J., Sandak, A., Mai, J., & Niemz, P. (2022). Selected previous findings on the factors influencing the gluing quality of solid wood products in timber construction and possible developments: A review. *Wood Material Science & Engineering, 17*(3), 230-241. https://doi.org/10.1080/17480272.2021.1925963

He, M., Lam, F., & Foschi, R. O. (2004). Modelling three-dimensional timber structures using solid elements with orthotropic plasticity in ANSYS program. *Computers & Structures, 82*(18-19), 2179-2191.

He, M., Sun, X., Li, Z., & Feng, W. (2020). Bending, shear, and compressive properties of three- and five-layer cross-laminated timber fabricated with black spruce. *Journal of Wood Science, 66*, Article 38. https://doi.org/10.1186/s10086-020-01886-z

Krüger, R., Buchelt, B., & Wagenführ, A. (2018). New method for determination of shear properties of wood. *Wood Science and Technology, 52*(6), 1555-1568. https://doi.org/10.1007/s00226-018-1053-7

Mohd Puaad, M. B. F. (2021). *Shear properties of structural size timber from selected Malaysian tropical timber based on torsional test in accordance with EN 408:2010* [Doctoral thesis, Universiti Teknologi MARA]. UiTM Institutional Repository.

Monteiro, S. R. S., Martins, C., Dias, A. M. P. G., & Cruz, H. (2020). Mechanical performance of glulam products made with Portuguese poplar. *European Journal of Wood and Wood Products, 78*(5), 1007-1015. https://doi.org/10.1007/s00107-020-01569-y

Okamoto, S., Akiyama, N., Araki, Y., Aoki, K., & Inayama, M. (2021). Study on the strength of glued laminated timber beams with round holes: Difference in structural performance between homogeneous-grade and heterogeneous-grade timber. *Journal of Wood Science, 67*, Article 8. https://doi.org/10.1186/s10086-021-01941-3

Ravenshorst, G., Gamper, N., van de Kuilen, J. W. G., & de Vries, P. (2016). Determination of the shear strength of tropical hardwood timber. In J. Eberhardsteiner, W. Winter, A. Fadai, & M. Pöll (Eds.), *WCTE 2016-World Conference on Timber Engineering* (pp. 677-684). Vienna University of Technology.

Ross, R. J. (Ed.). (2010). *Wood handbook: Wood as an engineering material* (General Technical Report FPL-GTR-190). U.S. Department of Agriculture, Forest Service, Forest Products Laboratory. https://doi.org/10.2737/FPL-GTR-190

Shakimon, M. N., Abd Malek, N. J., Hassan, R., & Ahmad, Z. (2016). The finite element modelling of glulam tropical timber beam in bending. *Jurnal Teknologi, 78*(5-5), 75-78. https://doi.org/10.11113/jt.v78.8579

Sikora, K. S., McPolin, D. O., & Harte, A. M. (2016). Shear strength and durability testing of adhesive bonds in cross-laminated timber. *The Journal of Adhesion, 92*(7-9), 758-777. https://doi.org/10.1080/00218464.2015.1094391

van de Kuilen, J. W. G., & Leijten, A. J. M. (2006). Analytical models for the shear strength of wood. *Wood Science and Technology, 40*(8), 647-663.

Xiao, H., Wang, W., & Chui, Y. H. (2007). *Evaluation of shear strength and percent wood failure criteria for qualifying new structural adhesives* (Research Report, Project No. UNB50). University of New Brunswick.

Zienkiewicz, O. C., Taylor, R. L., & Zhu, J. Z. (2013). *The finite element method: Its basis and fundamentals* (7th ed.). Butterworth-Heinemann. https://doi.org/10.1016/C2009-0-24909-9

Zobel, B. J., & van Buijtenen, J. P. (1989). *Wood variation: Its causes and control*. Springer-Verlag. https://doi.org/10.1007/978-3-642-74069-5

Pertanika J. Sci. & Technol. 34 (S2): 89 - 100 (2026)

PERTANIKA JOURNALS

SCIENCE & TECHNOLOGY

Journal homepage: http://www.pertanika.upm.edu.my/

Enhancing Health and Safety Practices by Complying with SOP Requirements at Construction Sites During the Pandemic

Siti Rashidah Mohd Nasir[1]*, Sulaiman Hasim[1], and Eleanna Guan[2]

[1]Faculty of Civil Engineering, Universiti Teknologi MARA, 40450 Shah Alam, Selangor, Malaysia
[2]DAL HCM Sdn. Bhd., Petra Jaya, 93050 Kuching, Sarawak, Malaysia

ABSTRACT

Health and safety issues at the construction sites have arisen due to the spread of COVID-19. This paper aimed to identify the ineffectiveness of health and safety measures implemented by contractors at construction sites during the COVID-19 pandemic and to suggest ways to enhance health and safety practices. Questionnaire surveys were distributed to the Grade 7 contractors in Kuala Lumpur who were affected during the COVID-19 pandemic. Non-probability purposive sampling was used to select experts with experience managing construction projects during the COVID-19 pandemic. Descriptive analysis and mean score rank were conducted for data analysis. The findings of this study show that lack of social distancing, inaccurate body temperature measurement, and irregular 'MySejahtera' check-in were the most ineffective health and safety measures implemented by the contractors during the COVID-19 pandemic. This study sheds light on construction practitioners and on the best health and safety practices for complying with SOP requirements at construction sites during a pandemic.

Keywords: Construction site, COVID-19 pandemic, health and safety

ARTICLE INFO

Article history:
Received: 18 June 2026
Accepted: 25 September 2026
Published: 30 September 2026

DOI: https://doi.org/10.47836/pjst.34.S2.08

E-mail address:
sitir015@uitm.edu.my(Siti Rashidah Mohd Nasir)
sulaiman5603@uitm.edu.my(Sulaiman Hasim)
josephineelena99@gmail.com (Eleanna Guan)
* Corresponding author

INTRODUCTION

The COVID-19 pandemic has affected the health and safety of construction workers on construction sites in Malaysian construction projects and caused fatalities. According to the Ministry of Health Malaysia (2020), 88 confirmed COVID-19 cases were identified in three construction sites, which involved 31 cases consisting of 29 Bangladeshi nationals and 2 Indonesian nationals from the Kuala Lumpur Construction site,

e-ISSN: 2231-8526

© Universiti Putra Malaysia Press

13 clusters from all Bangladeshi nationals at the Setia Alam construction site, and 44 cases detected at the second Kuala Lumpur construction site. The increasing number of COVID-19 cases involving construction sites in Malaysia has been identified, with more than 100 construction sites affected and more than 14,000 construction workers confirmed as positive in COVID-19 clusters (Ibrahim et al., 2022). Construction sites had formed the largest cluster of COVID-19 infections due to a lack of discipline and carelessness in implementing the Standard Operating Procedure (SOP) by both employers and employees; less awareness of the procedures and language barriers contributed to undisciplined attitudes faced by the project manager at the site in educating the foreign workers on the SOP (Ibrahim et al., 2022). According to "The COVID-19 Pandemic" (2020), the Construction Industry Development Board (CIDB) issued warnings to around 800 construction sites for failing to follow the Movement Control Order (MCO) standard operating procedures.

Another primary contributing factor to the rising number of COVID-19 cases in Malaysian construction projects is the movement of construction workers between sites (The Sun Daily, 2022). In the construction industry, the health and safety challenges posed by COVID-19 have led to illnesses, injuries, and fatalities among construction workers, as on-site work is conducted in unhygienic conditions with high exposure to infectious diseases (Olanrewaju et al., 2021). This paper aimed to identify the ineffectiveness of health and Safety practices at construction sites during the pandemic, followed by suggestions to enhance health and safety practices among construction workers in compliance with SOPs to effectively mitigate the spread of airborne viruses. This study is imperative for the construction industry to acknowledge government and health authorities regarding the ineffectiveness of the health and safety measures implemented at construction sites during the pandemic. Thus, addressing effective alternatives and solutions in Health and Safety practices during future pandemics.

LITERATURE REVIEW

On 30 January 2020, the World Health Organisation (WHO) declared COVID-19 a Public Health Emergency of International Concern and, on 11 March 2022, classified it as a global pandemic (Simpeh et al., 2022). The worldwide COVID-19 infection count was 21 million, with 13 million recoveries and 760,000 deaths as of 14th August 2020 (Amoah & Simpeh, 2021). According to the World Health Organisation (WHO), the rise in both case numbers and fatalities was driven by reduced social mobility and inconsistent adherence to proven public health practices (UN News, 2021).

Impact of COVID-19 on the Malaysian Construction Industry

The Ministry of Health (MoH) has found that the main factors driving the spread of COVID-19 on construction sites are crowded, cramped workers' accommodations, lack

of physical distancing, and insufficient personal and environmental hygiene practices among construction workers, especially foreign workers (Ibrahim et al., 2022). During the pandemic, as of 30th June 2019, around 435,002 foreign construction workers at Malaysian construction sites were found to have poor hygiene practices corresponding to their countries of origin (Ibrahim et al., 2022). The situation became worse when the workers were put in temporary small cabins with few amenities and utilities where each cabin accommodated more than ten workers; this issue made the workers difficult to adopt good hygiene and social distancing and thus enhanced the virus transmission more quickly, these housing areas should be sanitised daily, and the commonly used regions in the construction sites had to be sanitised at least three times daily (Ibrahim et al., 2022). In addition, the ineffective implementation of the SOP at construction sites has enhanced the spread of the COVID-19 virus due to a lack of awareness of the COVID-19 disease among workers, who tended to ignore the significance of SOPs, such as non-use of face masks, not maintaining good hygiene, failure to monitor body temperature, and not practising social distancing while working at the construction sites.

Health and Safety Measures On-site Practices During the COVID-19 Pandemic

The nature of work in construction requires operating in groups and confined spaces, which creates a high potential for the spread of COVID-19 on construction sites (Olanrewaju et al., 2021).

Table 1
Health and safety practices incorporating SOP implemented by contractors during COVID-19

Category of Health and Safety Measures	Description	Source (s)
Hygiene and Movement Control	Provide face masks to workers Provide health education to workers regularly Ensure a regular supply of sanitiser Keep social distancing Self-isolation for workers who fall ill or are sick Display health advisory posters and infographics in a language understood by the workers Contractors conduct COVID-19 screening tests daily for all construction workers	Ibrahim et al., 2022; Nnaji et al., 2022; Olanrewaju et al., 2021; Salami et al., 2021
Protective Equipment and Construction Site Monitoring	Sanitise the construction area frequently as scheduled (daily, weekly, monthly) Disinfect contaminated surfaces and objects at the construction site Provide separate housing facilities for workers based on the project works	Ibrahim et al., 2022; Nnaji et al., 2022; Olanrewaju et al., 2021

Table 1 *(continued)*

Category of Health and Safety Measures	Description	Source (s)
	Time slots for construction workers to minimise the number of workers working on the construction site at one time, while working 24 hours a day, to compensate for the reduction of manpower	
	Foods and drinks are provided on sites where workers are not allowed to eat outside during working hours	
COVID-19 Awareness	Instruct construction workers to wear gloves while working	Nnaji et al., 2022; Olanrewaju et al., 2021
	Provide incentives to sick workers so that they will honestly report their medical status	

To minimise the spread of COVID-19 amid rising case numbers at construction sites, the government, in collaboration with the Construction Industry Development Board (CIDB) and the Malaysian National Security Council (NSC), introduced strict SOPs (Ibrahim et al., 2022). Thus, the health and safety measures taken by the contractors were essential to mitigate the spread of COVID-19 at the construction sites. Table 1 lists the health and safety practices that complied with NSC and MoH SOP requirements during the COVID-19 pandemic, as reported by various researchers.

METHODS

The data for this study were collected using a quantitative method, in which questionnaire surveys were distributed to Grade 7 contractors, the highest grade of contractor in the Construction Industry Development Board (CIDB), via social media such as email, WhatsApp, Facebook, and LinkedIn, with no limit on tendering capacity. The respondents were selected from the CIDB list, with the primary selection criterion being ongoing projects in the Kuala Lumpur area during the COVID-19 period. Kuala Lumpur is Malaysia's city centre and is divided into 11 districts: Bukit Bintang, Titiwangsa, Setiawangsa, Wangsa Maju, Batu, Kepong, Segambut, Lembah Pantai, Seputeh, Bandar Tun Razak and Cheras. Kuala Lumpur was chosen in this study for its high number of large-scale ongoing construction projects and the high density of construction workers affected by the COVID-19 pandemic (Anaam & Jailani, 2022). The target respondents are contractors' staff with experience managing the project during the pandemic, i.e., Director, Project Manager, Civil Engineer, Safety and Health Officer, Quantity Surveyor, Site Supervisor, Foreman and others.

A purposive non-probability sampling method was adopted for this study, as there was no equal chance of selecting respondents among Grade 7 contractors at construction sites in Kuala Lumpur (Rahman, 2023). Based on the CIDB Grade 7 contractor list, the

population of contractors who met the criteria was shortlisted to 45. Thus, the required sample size for this study is 40 Grade 7 contractors with ongoing projects during the pandemic (Krejcie & Morgan, 1970).

The questionnaire consists of four sections, i.e., Section A on the respondents' demographic; Section B on the health and safety measures implemented by the contractors during the COVID-19 pandemic; Section C on the effectiveness of health and safety measure practices implemented by contractors during the COVID-19 pandemic; while Section D is the respondents' suggestions to enhance the health and safety practices at the site after the pandemic. However, Section B will not be included in the reporting for this paper.

A 5-point Likert scale was used in Sections C and D of the questionnaire to determine the respondent's degree of agreement and disagreement with the statements provided (Taherdoost, 2019). In Sections C and D, respondent opinion was assessed using the following degree of agreement: 1 – Strongly Disagree; 2 – Disagree; 3 – Moderate; 4 – Agree; 5 – Strongly Agree (Tholibon et al., 2021), while Section C also assesses the respondents' opinion on the degree of effectiveness: 1 – Not at all Effective; 2 – Slightly Effective; 3 – Moderately Effective; 4 – Very Effective; Extremely Effective (Taherdoost, 2019).

The pilot study was conducted with 15 selected experts prior to the full-scale study to assess the questionnaire's reliability. The criteria for selecting the experts for the pilot study include individuals with over 5 years of experience in construction projects to ensure a deep understanding of industry practices; active involvement in managing COVID-19 health and safety measures among construction workers; and knowledge and hands-on experience in handling large construction projects during the pandemic. These criteria are crucial to ensuring that experts can provide valuable insights into health and safety practices, including strategies implemented during this unprecedented period.

Descriptive analysis is conducted to examine the degree of familiarity, frequency, and agreement with a question regarding effective health and safety practices that comply with NSC and MoH requirements at construction sites during the pandemic. While mean score analysis is used to quantify the average responses to questions related to ineffective COVID-19 health and safety measures and suggestions to enhance them, it provides a statistically grounded understanding of these practices.

RESULTS AND DISCUSSION

Demographic Profile

Figure 1 shows the frequency of respondents' job positions: Project Manager (22.50%), Health and Safety Officer and Engineer (20%), Director and Site Supervisor (both at 12.50%), Quantity Surveyor (7.50%), and Site Foreman (5%). The respondents were

directly involved in managing the construction project and monitoring the health and safety measures for construction workers on site during the pandemic. The sample comprises 40 Grade 7 contractors with ongoing projects during the pandemic, meeting the required number of respondents for this study.

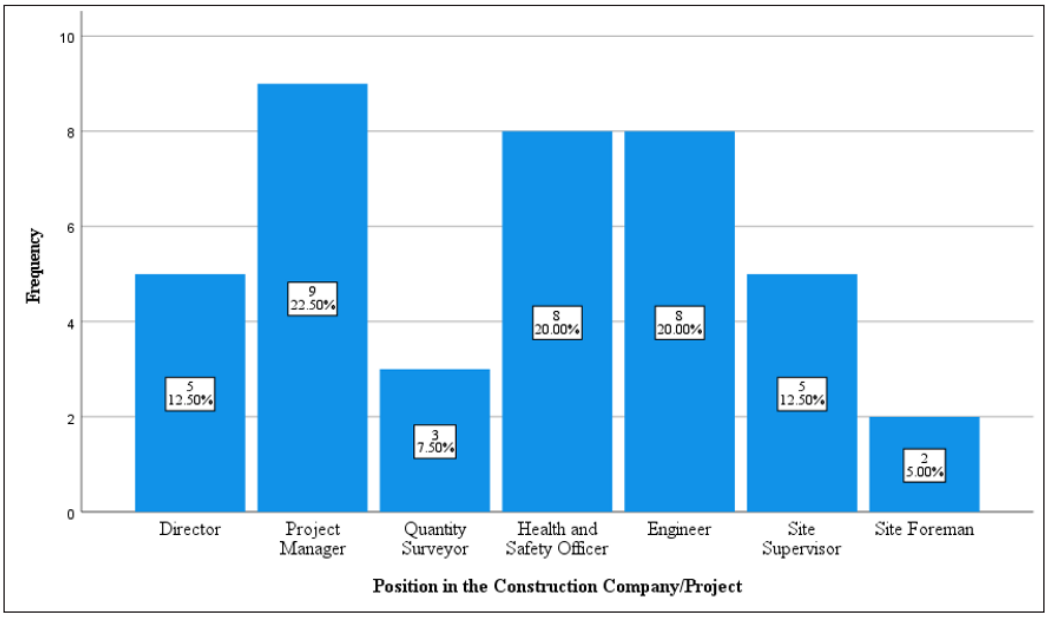

Figure 1. Frequency of respondents based on job position in the construction project

Figure 2 shows the average daily workforce at construction sites by location. The construction projects that had less or equal to 200 workers are as follows: Bandar Tun Razak (22.50%), Bukit Bintang (17.50%), Titiwangsa (12.50%), Cheras (10%), Lembah Pantai and Wangsa Maju (7.50%), Setiawangsa (5%), Segambut (5%), Batu (5%) and Seputeh (2.50%). On the other hand, construction projects with 201 to 300 workers are in Bukit Bintang and Kepong, both at 2.50%.

The data on the average daily workforce in construction sites reflect the intensity and scale of development across various locations. Bandar Tun Razak, leading with 22.50%, showcases rapid construction, including high-rise buildings, public facilities, and infrastructure like the Hospital Kuala Lumpur MRT Station and new highways. Bukit Bintang, at 17.50%, highlights major projects such as the Merdeka 118 building. Titiwangsa (12.50%) is noted for the significant construction of the MRT station amid the COVID-19 pandemic. Cheras (10%) also maintained robust development during the pandemic. Lembah Pantai and Wangsa Maju, each at 7.50%, had several active projects during the pandemic. Setiawangsa, Segambut, and Batu (5% each) are densely populated with residential and housing projects.

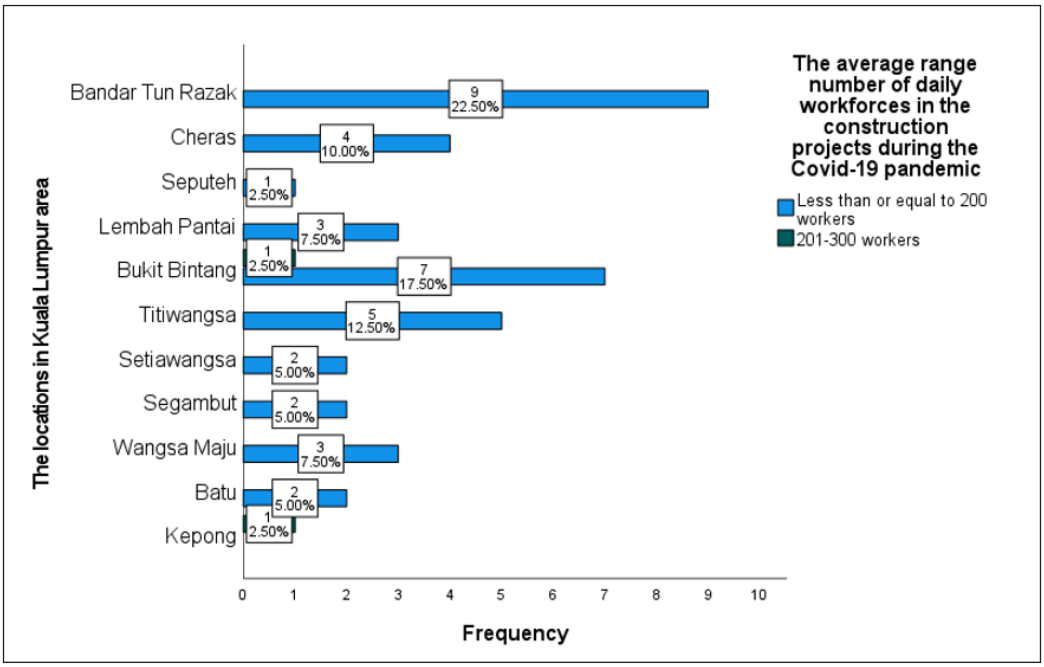

Figure 2. Average daily workforces based on the location of the construction site during the COVID-19 pandemic

In contrast, Seputeh, with the lowest at 2.50%, reflects fewer projects due to its lower population. Lastly, Bukit Bintang and Kepong, each at 2.50%, indicate the presence of larger workforce projects, aligning with their extensive residential developments.

Ineffective Health and Safety Measures at the Construction Site

Table 2 presents an analysis of ineffective COVID-19 health and safety measures practised at construction sites to mitigate the spread of COVID-19. Lack of social distancing and inaccurate body temperature reading received the highest mean score of 4.95 (SD = 0.221).

Figure 3 shows the level of agreement on ineffective health and safety practices. This suggested that 38 respondents (95%) strongly agreed that 'lack of social distancing' is difficult to practice at construction sites, which require heavy work and machinery. This is supported by Chandwani et al. (2021), Pamidimukkala and Kermanshachi (2021), and Shafii et al. (2022), who stated that construction work requires workers to work in confined spaces. 34 respondents (85%) agree that the lack of monitoring of social mobility and movement control among workers (mean score: 4.15, SD = 0.362) leads to a lack of social distancing. Figure 3 shows 36 respondents (90%) and 24 respondents (60%) strongly agree that irregular use of face masks and lack of COVID-19awareness among the construction

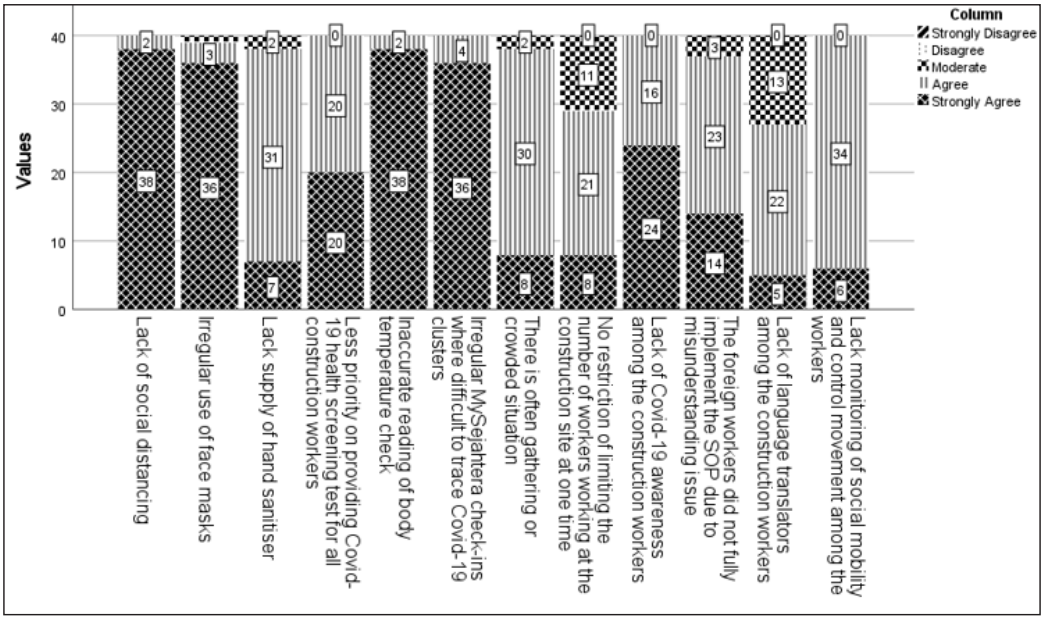

Figure 3. Level of agreement on the ineffective health and safety measure practices

Table 2
Mean score analysis of ineffective COVID-19 health and safety measure practices

Item	Description	Mean	Standard Deviation (SD)
1	Lack of social distancing	4.95	0.221
2	Inaccurate reading of body temperature	4.95	0.221
3	Irregular MySejahtera check-ins had difficulty tracing COVID-19clusters	4.90	0.304
4	Irregular use of face masks	4.88	0.404
5	Lack of COVID-19awareness among construction workers	4.60	0.496
6	Less priority in providing COVID-19health screening tests for all construction workers	4.50	0.506
7	The foreign workers did not fully implement the SOP due to a misunderstanding of the issue	4.28	0.599
8	There are often gatherings or crowded situations	4.15	0.483
9	Lack of monitoring of social mobility and control of movement among the workers	4.15	0.362
10	Lack of supply of hand sanitiser	4.13	0.453
11	No restriction on the number of workers working at the construction site at one time	3.93	0.694
12	Lack of language translators among the construction workers	3.80	0.648

workers, with mean scores of 4.88 (SD = 0.404) and 4.60 (SD = 0.496), respectively, as shown in Table 2, had a significant influence on the spread of COVID-19. Respondents claimed that the workers were reluctant to use face masks while working at the site, even though face mask regulations exist, and were uncomfortable, especially in hot weather and when sweating profusely. This statement was supported by Shafii et al. (2022).

Although body temperature monitoring was mandatory and conducted daily at the construction site entrances, respondents stated that the frequent occurrence of systematic error in the body temperature measuring tool had caused inaccuracy of body temperature which resulted in ineffective health and safety practices at the site as Chen et al. (2022) stated that the discrepancy in body temperature reading is due to the systematic uncertainty of the measuring tool which could not be prevented. Irregular MySejahtera check-ins have difficulty tracing COVID-19 clusters and received the second-highest mean score of 4.90 (SD = 0.304), as shown in Table 2.

Table 2 shows that 36 respondents (90%), as shown in Figure 3 strongly agree that the failure of the construction workers to use the MySejahtera application regularly has a significant effect on the effectiveness of health and safety measures, which contributed to the increasing number of infections, as it is difficult for relevant parties to trace their locations and health status ("Malaysians Should Be More Disciplined," 2020). Figure 3 shows that 20 respondents (50%) agree that the lack of priority in providing COVID-19health screening tests for all construction workers contributed to the ineffective measures. The COVID-19 screening test must be provided to workers to detect asymptomatic cases, as unidentified COVID-19 clusters have been found among construction workers with no symptoms (Ibrahim et al., 2022). This was confirmed by the unidentified clusters with no symptoms at the Damanlela construction site, which had been moving around and spreading COVID-19 as it was transmitted from one site to another, resulting in more than 2,000 workers becoming infected (Ibrahim et al., 2022). In addition, the lack of screening tests is due to their high cost, which has increased project costs (Krishnan, 2021).

Meanwhile, Table 2 shows that the lack of language translators among the construction workers had the least impact on the spread of COVID-19, with a mean score of 3.80 (SD = 0.648), as language translators were unnecessarily required, and the contractors should be responsible for effectively delivering COVID-19 awareness among the construction workers. This shows that the contractors can educate foreign workers on SOP procedures and raise COVID-19 awareness among them (Ibrahim et al., 2022).

Suggestions to Enhance Compliance with SOPs and Health and Safety Practices During the Pandemic

Table 3 shows several suggestions to enhance the health and safety practices compliance with SOP during the pandemic, where all respondents agreed that the contractors should

be entirely restricted to SOP by strictly implementing all the measures at the construction site according to government and MoH requirements, even after the COVID-19 pandemic, with a mean score of 5.00.

According to Olanrewaju et al. (2021), contractors should strictly follow all government guidelines and regulations on construction site safety protocols to avoid being fined or penalised and to be COVID-19 risk-free; other suggestions, such as exposure to health warning signs and regular updates on COVID-19 information were also essential to be implemented so that the construction workers would be more aware of the COVID-19 risk. These mitigation measures were essential to ensure that staff and construction workers worked in healthy conditions and to effectively prevent the spread of COVID-19.

Table 3
Mean score analysis on the suggestions to enhance health and safety practices compliance with SOP during the pandemic

Item	Description	Mean	Standard Deviation
1	The contractors should be entirely restricted to SOP as required by the Government and the Ministry of Health Malaysia (2020)	5.00	0.000
2	Expose health warning signs and infographics as reminders of the COVID-19 risk	5.00	0.385
3	The contractors should provide good hygiene housing facilities and health care to construction workers	5.00	0.501
4	The contractors should adapt the effective health and safety measures implemented by other countries to be applied at the local construction site	5.00	0.597
5	The contractors should routinely update the health information regarding COVID-19 to the workers at the construction site	5.00	0.506

CONCLUSIONS

This paper addresses the lack of health awareness regarding COVID-19 and the transmission of construction workers from site to site, contributing to ineffective health and safety practices at construction sites. Hence, the findings of this study should be duly acknowledged by the relevant authorities on alternative health and safety practices that contractors should implement during the pandemic to maintain hygiene and combat infectious diseases. However, a limitation of this study is its constrained geographic scope, which limits the generalisability of the findings. Future research endeavours would benefit from adopting a more expansive geographical framework, potentially yielding more comprehensive insights. Additionally, the target respondent may not accurately reflect the plurality of experiences and perspectives that exist in the broader population. To address this, subsequent studies should strategically recruit participants from a more diverse array of backgrounds, including varying socioeconomic statuses, professions, and educational

levels, to foster a richer, multidimensional understanding of the attitudes and behaviours surrounding the implementation of health and safety measures amid a pandemic. Such efforts could facilitate a more nuanced comparison of different perspectives and foster a deeper understanding of the multifaceted implications of pandemic responses.

ACKNOWLEDGEMENT

This research was supported by Universiti Teknologi MARA under MyRA research grant [600-RMC/GPM ST 5/3 (047/2021)].

REFERENCES

Amoah, C., & Simpeh, F. (2021). Implementation challenges of COVID-19 safety measures at construction sites in South Africa. *Journal of Facilities Management, 19*(1), 111-128. https://doi.org/10.1108/JFM-08-2020-0061

Anaam, A., & Jailani, J. (2022). The impacts of the pandemic COVID-19 on construction industry in Kuala Lumpur. *Recent Trends in Civil Engineering and Built Environment, 3*(1), 1695-1705. https://doi.org/10.30880/rtcebe.2022.03.01.189

Chandwani, N., Shrigiriwar, M., Jaiswal, S. V., & Dwidmuthe, S. (2021). Knowledge, attitude, and practice (KAP) towards social distancing in pandemic COVID-19 among construction workers in Central India. *Annals of the Romanian Society for Cell Biology, 25*(6), 19746–19757. https://annalsofrscb.ro/index.php/journal/article/view/9839

Chen, A., Zhu, J., Lin, Q., & Liu, W. (2022). A comparative study of forehead temperature and core body temperature under varying ambient temperature conditions. *International Journal of Environmental Research and Public Health, 19*(23), Article 15883. https://doi.org/10.3390/ijerph192315883

COVID-19 pandemic leaves lasting scar on Malaysian construction sector. (2020, December 22). *The Sun Daily*. https://thesun.my/business-news/covid-19-pandemic-leaves-lasting-scar-on-malaysian-construction-sector-FL5782315

Ibrahim, F. S., Esa, M., & Mustafa Kamal, E. (2022). Strategies to minimise the impact of COVID-19 on the construction industry: A case study of construction site clusters in Malaysia. *Construction Economics and Building, 22*(3), 21-42. https://doi.org/10.5130/AJCEB.v22i3.8064

Krejcie, R. V., & Morgan, D. W. (1970). Determining sample size for research activities. *Educational and Psychological Measurement, 30*(3), 607-610. https://doi.org/10.1177/001316447003000308

Krishnan, D. B. (2021, February 2). Reduce COVID-19 test price to encourage screening. *New Straits Times*. https://www.nst.com.my/news/nation/2021/02/662277/reduce-covid-19-test-price-encourage-screening

Malaysians should be more disciplined in using MySejahtera app. (2020, August 4). *The Malaysian Reserve*. https://themalaysianreserve.com/2020/08/04/malaysians-should-be-more-disciplined-in-using-mysejahtera-app/

Ministry of Health Malaysia. (2020, May 26). *Press statement Ministry of Health Malaysia: Updates on the coronavirus disease 2019 (COVID-19) situation in Malaysia*. https://covid-19.moh.gov.my/terkini/052020/

situasi-terkini-26-mei-2020/Kenyataan%20Akhbar%20KPK%20COVID-19%20(26%20Mei%202020)%20-%20EN.pdf

Nnaji, C., Jin, Z., & Karakhan, A. (2022). Safety and health management response to COVID-19 in the construction industry: A perspective of fieldworkers. *Process Safety and Environmental Protection, 159*, 477-488. https://doi.org/10.1016/j.psep.2022.01.002

Olanrewaju, A., AbdulAziz, A., Preece, C. N., & Shobowale, K. (2021). Evaluation of measures to prevent the spread of COVID-19 on the construction sites. *Cleaner Engineering and Technology, 5*, Article 100277. https://doi.org/10.1016/j.clet.2021.100277

Pamidimukkala, A., & Kermanshachi, S. (2021). Impact of COVID-19 on field and office workforce in construction industry. *Project Leadership and Society, 2*, Article 100018. https://doi.org/10.1016/j.plas.2021.100018

Rahman, M. M. (2023). Sample size determination for survey research and non-probability sampling techniques: A review and set of recommendations. *Journal of Entrepreneurship, Business and Economics, 11*(1), 42-62.

Salami, B. A., Ajayi, S. O., & Oyegoke, A. S. (2022). Coping with the COVID-19 pandemic: An exploration of the strategies adopted by construction firms. *Journal of Engineering, Design and Technology, 20*(1), 159-182. https://doi.org/10.1108/JEDT-01-2021-0054

Shafii, H., Mohd Radzi, N. A., Md Yassin, A., & Masram, H. (2022). Implementing COVID-19 standard operation procedure (SOP) in Malaysia construction industry: Challenges and strategies. *International Journal of Property Sciences, 12*(1), 37-53. https://doi.org/10.22452/ijps.vol12no1.3

Simpeh, F., Bamfo-Agyei, E., & Amoah, C. (2022). Barriers to the implementation of COVID-19 safety regulations: Insight from Ghanaian construction sites. *Journal of Engineering, Design and Technology, 20*(1), 47-65. https://doi.org/10.1108/JEDT-03-2021-0153

Taherdoost, H. (2019). What is the best response scale for survey and questionnaire design; review of different lengths of rating scale/attitude scale/Likert scale. *International Journal of Academic Research in Management, 8*(1), 1-10. https://hal.science/hal-02557308/document

Tholibon, D. A., Md Nujid, M., Mokhtar, H., Abd Rahim, J., Abdul Aziz, N. F., & Ahmad Tarmizi, A. A. (2021). Relative importance index (RII) in ranking the factors of employer satisfaction towards industrial training students. *International Journal of Asian Education, 2*(4), 493-503. https://doi.org/10.46966/ijae.v2i4.187

UN News. (2021, July 14). *'Early stages' of COVID third wave, amid Delta surge: WHO chief*. https://news.un.org/en/story/2021/07/1095882

Pertanika J. Sci. & Technol. 34 (S2): 101 - 116 (2026)

PERTANIKA JOURNALS

SCIENCE & TECHNOLOGY

Journal homepage: http://www.pertanika.upm.edu.my/

Strength and Durability Performance of Three-Layered *Leucaena leucocephala* Cement-Bonded Particleboard

Marzuki Ab. Rahman[1], Mohd Fakri Muda[1,4]*, Mohd Razmi Zainudin[1], Muhammad Isha Ismail[1], Farah Wahida Mohd Latib[1], Amminudin Ab Latif[1], Noor Safwan Muhamad[1], Wan Zukri Wan Abdullah[3], Herlien Dwiarti Setio[2], and Mohd Hisbany Mohd Hashim[3,4]

[1]*Faculty of Civil Engineering, Universiti Teknologi MARA Pahang Branch, 26400 Jengka, Pahang, Malaysia*
[2]*Faculty of Civil and Environmental Engineering, Institut Teknologi Bandung, 40132 Bandung, West Java, Indonesia*
[3]*Faculty of Civil Engineering, Universiti Teknologi MARA, 40450 Shah Alam, Selangor, Malaysia*
[4]*3R: Rehabilitation, Repair and Retrofitting Group, Faculty of Civil Engineering, Universiti Teknologi MARA, 40450 Shah Alam, Selangor, Malaysia*

ABSTRACT

A study was conducted to explore the durability of Cement-Bonded Particleboard (CBP) under external shading (free from direct sunlight and rain) and without shading (exposed to natural weathering) conditions prevalent in Malaysia. The three-layered CBP boards were manufactured in the laboratory using *Leucaena leucocephala* (LL) at a wood-to-cement ratio of 1:2.0. The boards were produced to target a density of 1300 kg/m3. All boards were produced using a combination of aluminium sulphate and sodium silicate. The effects of exposure duration and condition on the Modulus of Rupture (MOR), Modulus of Elasticity (MOE), and Internal Bond (IB) were evaluated at 30, 60, 120, and 300 days. The results revealed that the MOR, MOE, and IB values differed significantly across durations and exposures. From this study, LL proved suitable for manufacturing CBP for external exposure.

Keywords: Cement-bonded particleboard, durability, *Leucaena leucocephala*, strength

ARTICLE INFO

Article history:
Received: 18 June 2026
Accepted: 10 August 2026
Published: 30 September 2026

DOI: https://doi.org/10.47836/pjst.34.S2.09

E-mail addresses:
marzukiar@uitm.edu.my (Marzuki Ab. Rahman)
fakri@uitm.edu.my (Mohd Fakri Muda)
razmi74@uitm.edu.my (Mohd Razmi Zainudin)
isha@uitm.edu.my (Muhammad Isha Ismail)
farahwahidaml@uitm.edu.my (Farah Wahida Mohd Latib)
amminudin738@uitm.edu.my (Amminudin Ab Latif)
safwanmuhamad@uitm.edu.my (Noor Safwan Muhamad)
wanz@uitm.edu.my (Wan Zukri Wan Abdullah)
herlien@itb.ac.id (Herlien Dwiarti Setio)
hisbany@uitm.edu.my (Mohd Hisbany Mohd Hashim)
* Corresponding author

INTRODUCTION

In the Cement-Bonded Particleboard (CBP) industry, assessing the long-term performance of wood cement composites,

e-ISSN: 2231-8526

© Universiti Putra Malaysia Press

particularly in warm and humid climates, is crucial. This evaluation is essential to assess the boards' durability and reliability over time. According to the American Society of Testing Materials, ASTM (2017), durability is defined as a material, product, component, assembly, or construction's capacity to remain serviceable as intended with prudent maintenance during the design service life under anticipated internal and external environments. More specifically, Alexander et al. (2017) define durability as the loss (or retention) of mechanical or physical properties after exposure to the ageing process. This statement aligns closely with the findings of Ramage et al. (2017), who suggest that CBP may experience a loss of strength over time due to wood's susceptibility to degradation in highly alkaline environments, similar to cement paste. Therefore, CBP manufactured with cement as the binder may be susceptible to degradation, reducing service life. However, the boards durable in one place may not be durable in another environment (Iraldo et al., 2017). This is probably related to air temperature, relative humidity, rainy weather, and sunshine, which can cause the board to expand and contract. Although modern CBPs have much improved strength properties, the quality, durability, and rising construction costs pose new pressures on researchers and industry. It ensures the durability of construction material in the surrounding environment, especially in the Malaysian climate. Overall, wood-cement composites (such as CBP) present high durability against natural weathering or accelerated ageing, high dimensional stability, and high resistance against fire and biodegradation, such as fungi (Wiejak & Francke, 2021).

The long-term performance of wood-cement composites is influenced by both the inorganic binder (cement) and the organic material (wood). The alkaline nature of Portland Cement (PC) can be particularly damaging to wood, as it can degrade the cellulose cell walls within the cement matrix. However, recent studies suggest that using low-alkaline cement and surface coatings can significantly improve the durability of wood-cement composites. According to a study by Xie et al. (2020), adding surface coatings such as graphene oxide can enhance the mechanical and durability properties of wood-cement composites. Similarly, Wei and Meyer (2015) found that using low-alkali cement can significantly reduce wood degradation in the cement matrix. Note that wood-cement composites have been considered a durable material in severe exposure conditions. Therefore, their long-term stability must also be considered. As an ideal construction material, CBP's durability should be thoroughly tested. Moreover, the use of low-alkaline cement and surface coatings can greatly improve the performance and longevity of wood-cement composites.

Leucaena leucocephala (LL) appears to be a logical choice as a raw material for CBP manufacturing, given the industry's challenges with rubberwood supply. LL offers an alternative raw material and leverages its fast growth rate. Rubberwood is typically available as a by-product from rubber estates after a 25-year economic lifespan (Mead, 2005). Hence, incorporating fast-growing species such as LL can expedite production

compared with woody plants. LL is a leguminous tree species that usually reaches a height of 20 meters with a bole diameter ranging from 5 to 50 cm (Obiakara et al., 2023; Singh et al., 2022). Moreover, it is widely cultivated in tropical and subtropical regions such as Hawaii, Australia, and Southeast Asia. In Malaysia, LL, also known as *petai belalang*, is commonly used as a shading tree due to its rapid growth (the lead tree). *Petai belalang* has been successfully planted at the Malaysian Agricultural Research and Development Institute (MARDI) as part of replanting programs. Additionally, its leaves serve as food for certain animals.

To evaluate the performance of LL CBP, we exposed the specimens to two conditions prevalent in Malaysia: shading (protected from direct sunlight and rain) and non-shading (subjected to natural weathering). The exposure lasted up to 300 days, and no coating was applied to the test specimens. The study focuses on weight changes and the mechanical and physical properties of the CBP over the duration of exposure. Other than that, the evaluation of mechanical and physical properties adheres to the minimum requirements outlined in the Malaysian Standard, MS 544 (2013). This analysis aims to establish the relationship between the durability of LL CBP and environmental factors that may impact its strength properties. These factors are crucial for ensuring the economic viability and efficiency of CBP.

The durability of any building material is influenced by the surrounding environment in which it is utilised. Hence, the mechanical and physical properties of the CBP were assessed at 30, 60, 120, and 300 days of exposure to external conditions, both with and without shading. Consequently, the mechanical tests included determining the Modulus of Rupture (MOR), Modulus of Elasticity (MOE), and Internal Bond (IB), as specified by the standards MS 934 (2013) and MS 544 (2013). Additionally, the physical properties were evaluated, including density and dimensional stability, in terms of the CBP's length, width, and depth, before and after exposure. By studying the interplay between these environmental factors and the mechanical and physical properties of the LL CBP, we can gain valuable insights into its overall durability and performance. This knowledge will help enhance the quality and suitability of CBP for various applications in the construction industry.

METHODOLOGY

Raw Materials Preparation

The wood particles utilised in this study were sourced from 8-year-old LL or *Petai belalang* trees grown in Peninsular Malaysia. To adhere to standard specifications, an ordinary PC was employed as the binder, conforming to the Malaysian Standard, MS 522 (2013) for PC (Ordinary and Rapid Hardening). Cement accelerators, a combination of aluminium

sulphate and sodium silicate, were incorporated at 1.5% and 3% by weight of the cement. Additionally, tap water was used as the mixing medium for all formulations.

The logs, measuring 1.0 m in length with diameters ranging from 30 mm to 150 mm (including branches), were promptly debarked manually using a hammer. Subsequently, the logs were processed into uniform chips using a wood chipper machine. Following conventional particleboard production methods, the chips were further flaked using a knife-ring flaking machine. Note that the wood particles were air-dried for approximately two weeks to achieve a moisture content of 14%-18%. Maintaining this moisture content is vital to prevent fungal infestation, particularly for long-term storage.

After drying, the wood particles were screened to obtain particles of various sizes. Specifically, a screening machine segregated them into fine and coarse particles. The particles retained on the 0.5 mm and 1.0 mm screens were designated fine particles for the surface or outer layer. Meanwhile, those retained on the 2.0 mm screen were categorised as coarse particles for the core layer in producing three-layered CBP specimens. This approach corroborates the findings of previous research, which demonstrated an enhancement in bending strength and stiffness of three-layered boards (Mussi Alencar & de Melo Moura, 2019; Sam-Brew & Smith, 2015). Note that wood particles larger than 5.0 mm were re-flaked using a knife-ring flake machine to obtain smaller particles.

Sample Board Fabrication

The wood particles were carefully placed into the cement board mixer, and precise amounts of chemical additives and water were added. Thorough mixing ensued until a homogeneous consistency was achieved. Subsequently, PC was introduced, and the mixing process continued until complete integration was achieved. The resulting mixture was manually consolidated in the mould, and pressure was applied to compress the board until reaching a thickness of 10 mm. To facilitate proper curing, the boards were securely clamped for 24 hours and then placed in a hardening chamber maintained at 65 ± 3°C. After the designated period, the boards were removed from the moulds and transferred to a curing tank, where they cured for approximately one month. The curing tank maintained a controlled relative humidity of 83% to 96%, which was monitored with a wet-and-dry bulb thermometer and recorded daily. This is to ensure thorough and complete curing of the boards.

Following the curing phase, the CBP panels were carefully trimmed to the prescribed dimensions outlined in the Malaysian Standard for mechanical properties testing. The boards' mechanical properties were assessed per MS 544 (2013). Consequently, the board dimensions were standardised at 450 mm × 450 mm × 10 mm (length × width × thickness), with a targeted density of 1300 kg/m^3. To ensure reliable data, three replicate samples were prepared for testing, resulting in a total of 30 specimen boards. The board sample fabrication is summarised in Figure 1.



Figure 1. Summary of LL CBP fabrication samples

Mechanical Properties Testing

The testing methods for MOR, MOE, and IB evaluate the mechanical properties of CBP. MOR testing measures bending strength by applying force to a board supported at two points until it breaks, indicating its resistance to bending stresses. MOE assesses stiffness by measuring deformation under load and calculating the initial slope of the load-deflection curve. Both properties reveal the material's elastic properties under the flexural stress test, as shown in Figure 2a. Figure 2b shows the IB test, which determines the tensile strength perpendicular to the board's plane by pulling a glued block until the internal bond fails. This test provides insights into the adhesive strength and cohesion within the board.

Method of Analysis

The results obtained from this study were analysed using Analysis of Variance (ANOVA). To assess the impact of the exposure condition, an Independent-Samples T-Test was

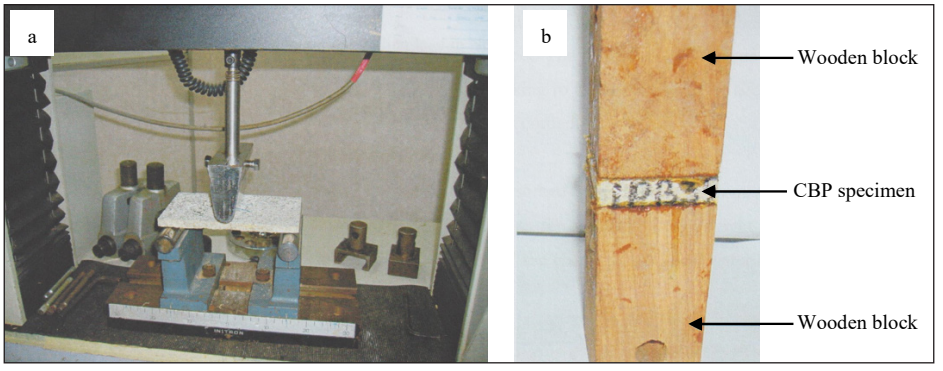

Figure 2. a) Flexural stress test and b) Internal bond test

conducted. Note that the dependent variables were subjected to a significant analysis based on the duration of exposure and exposure conditions. Through these statistical analyses, the study aimed to identify notable variations in the results and draw meaningful conclusions about the effects of exposure duration and conditions on the variables tested.

The performance of LL CBP was assessed by measuring its mechanical properties under different exposure conditions: external exposure with shading and external exposure without shading, and the evaluation period spanned 0, 30, 60, 120, and 300 days. Three essential properties were evaluated to understand the material's behaviour: MOR, MOE, and IB. MOR, represented by Equation 1, serves as a crucial indicator of a material's resistance to bending or flexural stresses, ensuring it remains intact without fracture. On the other hand, Equation 2 is the MOE, also known as Young's modulus, which gauges the material's stiffness and capacity to undergo elastic deformation when subjected to stress. Quantifying the relationship between stress and strain within the linear elastic range offers valuable insights into the material's structural integrity. Additionally, the IB in Equation 3 assesses the adhesive strength binding the particles or fibres within the material by dividing the tensile load, Fmax, by the cross-sectional area, A, of the CBP. This attribute directly influences the material's ability to withstand delamination or separation of its internal layers, ensuring durability and reliability under various conditions.

$$MOR = \frac{3FL}{2bd^2}, \quad [1]$$

$$MOE = \frac{WL^3}{4bd^3\delta}. \quad [2]$$

$$IB = \frac{F}{A} \quad [3]$$

RESULTS AND DISCUSSION

Performance of Exposed CBP

Table 1 and Table 2 present the mean values of the three key mechanical properties of the LL CBP panels exposed to the prevalent weathering conditions in Malaysia. The results are compared to the specifications outlined in the Malaysian Standard MS 544 (2013). These values provide insights into the performance of the LL CBP over the duration of 0 to 300 days. Similarly, Table 3 summarises the mean values of MOR, MOE, and IB for LL CBP panels. Meanwhile, Table 4 provides a comparative analysis of their performance compared to commercial boards. These values serve as references for assessing LL CBP's adherence to the Malaysian Standard MS 544 over time. Note that the data collected in both tables aid in understanding the durability and resilience of LL CBP under external weather conditions. Moreover, it allows for a comprehensive evaluation of its mechanical properties throughout the exposure period.

Effect of Duration Exposure on MOR

The results presented in Table 1 demonstrate a clear correlation between the exposure duration and the LL CBP's mechanical properties. Notably, the MOR of the boards remained relatively stable at the early stages of exposure to external conditions with shading. Furthermore, even after prolonged exposure, the strength properties of the LL

Table 1
Mechanical properties of LL CBP exposed to external conditions, CBP with shading

Duration (days)	MOR: LL CBP (MPa)	MOE: LL CBP (MPa)	IB: LL CBP (MPa)
0	11.76	3506	0.952
30	12.69	3733	0.961
60	11.30	3404	0.822
120	12.21	3462	0.752
300	14.78	4260	0.817
MS544	> 9.0	> 3000	> 0.5

Table 2
Mechanical properties of LL CBP exposed to external conditions, CBP without shading

Duration (days)	MOR: LL CBP (MPa)	MOE: LL CBP (MPa)	IB: LL CBP (MPa)
0	11.76	3506	0.952
30	11.73	3573	0.824
60	10.79	3288	0.620
120	10.74	3584	0.542
300	12.03	3453	0.605
MS544	> 9.0	> 3000	> 0.5

Table 3
Effect of exposure condition on the mechanical properties of LL CBP after 300 days of exposure

Test	Exposure	Mean (MPa)
MOR	Shading	12.55
	Without shading	11.41
MOE	Shading	3673
	Without shading	3481
IB	Shading	0.861
	Without shading	0.708

Table 4
Performance analysis between LL CBP and commercial boards (C-CBP)

Comparisons of LL CBP with Commercial Boards with Shading						
	MOR (MPa)		**MOE (MPa)**		**IB (MPa)**	
Duration (days)	LL CBP	C-CBP	LL CBP	C-CBP	LL CBP	C-CBP
0	11.76	12.09	3506	4318	0.952	0.99
300	14.78	13.88	4260	5917	0.817	1.66
Performance (%)	+ 25%	+14.8%	+21.5%	+37.0%	-15%	+67.7%

Comparisons of LL CBP with Commercial Boards Without Shading						
	MOR (MPa)		MOE (MPa)		IB (MPa)	
Duration (days)	LL CBP	C-CBP	LL CBP	C-CBP	LL CBP	C-CBP
0	11.76	11.66	3506	4696	0.952	1.07
300	12.03	8.06	3453	3260	0.605	0.78
Performance (%)	+ 2.3%	-30.9%	-1.5%	-30.6%	-36.5%	-27.1%

CBP were largely preserved. It is worth noting that during the exposure period, the boards exhibited exceptional resistance to warping, delamination, and twisting, indicating their robustness under external conditions. Figure 3 illustrates the progressive development of MOR in CBP boards exposed to external conditions with and without shading. After 30 days of shading, the MOR of the CBP increased notably, peaking at 300 days of exposure. This remarkable enhancement amounts to approximately 26% relative to the CBP's initial strength. Moreover, the observed increase in MOR is attributed to the continuous hydration of the cement matrix and the hardening process within the CBP. Several studies have previously reported similar strength improvements in CBP due to cement's ongoing hydration and hardening under ambient temperature conditions (Nazerian et al., 2011; Simatupang & Neubauer, 1993; Sudarmanto et al., 2022). It is crucial to note that sustained hydration of cement is facilitated by heat and moisture, especially in warm, humid climates such as those prevalent in Malaysia.

The MOR values decreased until 120 days of exposure, after which they gradually increased. The optimum MOR value of 12.03 MPa was achieved after 300 days of exposure,

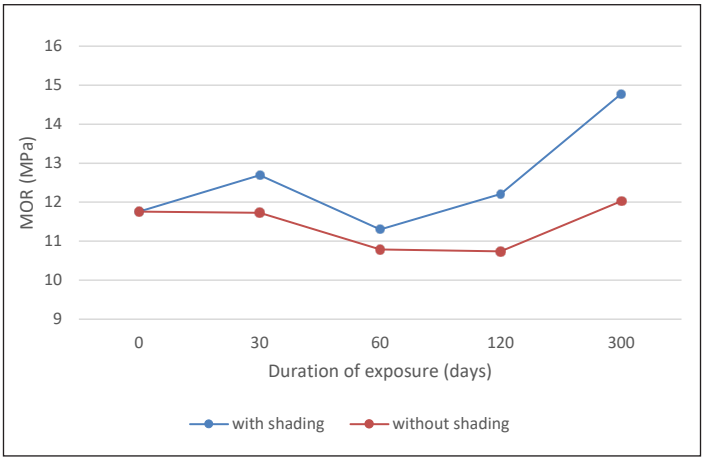

Figure 3. MOR of LL-CBP exposed to external conditions with and without shading for up to 300 days of exposure

representing a modest increase of approximately 2.3% compared to the initial strength. Importantly, this value remained above the 9.0 MPa requirement specified by MS 544. These findings suggest that continuous cement hydration and ongoing hardening contributed to the preservation and slight improvement of the MOR in the CBP. Nevertheless, further investigation is necessary to determine the specific duration for which the MOR might drop below the standard value. Hence, this investigation would provide valuable insights into the potential degradation of CBP's mechanical properties during extended exposure.

Effect of Duration Exposure on MOE

The impact of duration of exposure on the MOE properties of the CBP under external conditions with and without shading from the findings presented in Tables 1 and 2. These tables clearly demonstrate that the duration of exposure influenced the MOE values of the CBP. Notably, the MOE reached its optimum value towards the end of the exposure period. In particular, the maximum MOE was observed in the CBP specimens exposed to external conditions with shading, indicating an approximate 22% increase relative to the initial strength by the end of the exposure period. Figure 4 provides a graphical representation of the MOE development in the CBP specimens exposed to both shading and non-shading conditions.

The mean MOE values exhibited a trend like that of the MOR properties with respect to exposure duration. The MOE of the CBP increased after 30 days of exposure, with the maximum value attained at 300 days of exposure for both shading and non-shading conditions. As previously mentioned, this improvement in MOE is attributable to the cement's continuous hydration and hardening within the CBP. However, for CBP exposed to external conditions with shading, the MOE initially declined after 30 days of exposure.

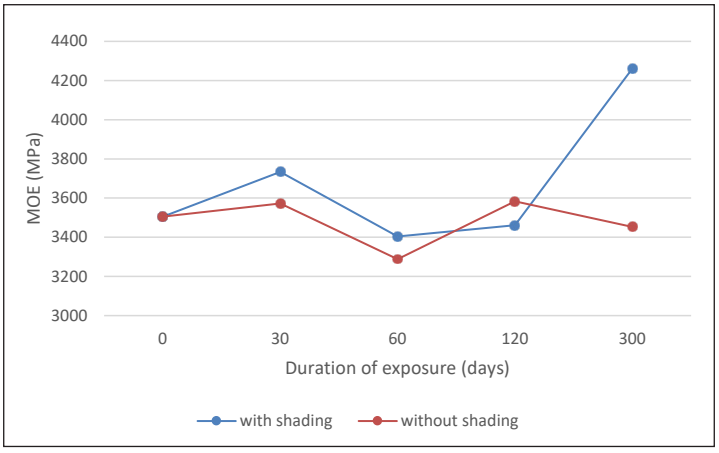

Figure 4. MOE of LL-CBP exposed to external conditions with and without shading for up to 300 days of exposure

Nevertheless, the CBP eventually reached a constant MOE value after 300 days of exposure. On the other hand, for boards exposed to external conditions without shading, the MOE values showed significant differences over the duration of exposure. The maximum MOE value exceeded the Malaysian Standard requirement after 120 days of exposure, representing an increase of approximately 19.5%. Importantly, the MOE mean values remained above the minimum requirement specified by the Malaysian Standard (3000 MPa) throughout the entire exposure period. These results indicate that the LL CBP specimens possess resistance to weathering exposure in the Malaysian climate.

The exposure conditions significantly affect the MOE strength properties of LL CBP, as presented in Table 3. CBP exposed that those with shading recorded higher MOE values than those without shading. The deterioration in MOE for the unshaded exposure may be attributed to the higher temperature, wetting, and humidity in Malaysia's climate. These environmental conditions can significantly impact the physical and mechanical properties of CBP materials. Studies, such as those conducted by Liu et al. (2024), have shown that alkaline wood fibres can degrade the cement matrix, a process exacerbated by moisture, thereby accelerating these processes. This interaction can compromise the stiffness and structural integrity of CBP, as evidenced by reduced MOE values. Further, the cyclic nature of wetting and drying, combined with high temperatures, leads to repeated expansion and contraction of the CBP, resulting in micro-cracking and weakening of the cement-wood bond. This phenomenon has been documented by Yu et al. (2016) and Yilmaz et al. (2015), who note that wood-cement composites, such as LL-CBP, exposed to environmental heat will experience a decline in properties over time. However, the research results for both shaded and unshaded specimens still exceeded the required minimum standard of 3,000 MPa under MS 544.

Effect of Duration Exposure on IB

The effect of duration exposures on IB of LL CBP is provided in Tables 1 and 2. The tables indicated that the mean IB attained was significantly lower compared to that of commercial CBP. The DMRT also indicates that the interaction between IB and duration was highly significant at a 5% significance level. Figure 5 shows a significant decrease in IB of up to 13.7% relative to the initial IB during the first 60 days of exposure under shading conditions. The IB value decreased continuously to 0.75 MPa (21%) relative to the initial IB after 120 days of the exposure test. Additionally, the same trend was observed for specimens exposed to external conditions without shading. The IB value decreased after exposure, and the drop was significantly greater than in those exposed to shading conditions. The IB value gradually decreased to 0.54 MPa, or about 43% of the initial IB, within 120 days of exposure. This may be due to mechanical stress on the binder induced by the particles' swelling forces, which caused poor binding between cement and wood particles under the alternating hot and rainy weather in Malaysia. Furthermore, the stress was probably induced by the tensile force applied to the specimens. According to Melichar et al. (2022) and Pakhomova et al. (2023), the cyclic occurrence of rain and hot weather can induce stress and movement between wood particles and cement. This phenomenon involves alternating tensile and compressive forces in the cement paste and wood particles, potentially compromising the wood particles' effectiveness as reinforcing materials and, consequently, affecting the long-term durability of the composite. Nevertheless, the IB of the LL CBP remained higher than or equivalent to the MS standard requirement of 0.5 MPa for IB after exposure to both environments for up to 300 days.

Table 3 indicates the significant effect of exposure conditions on the IB property of LL CBP. CBP exposed without shading had lower IB values compared to those exposed with

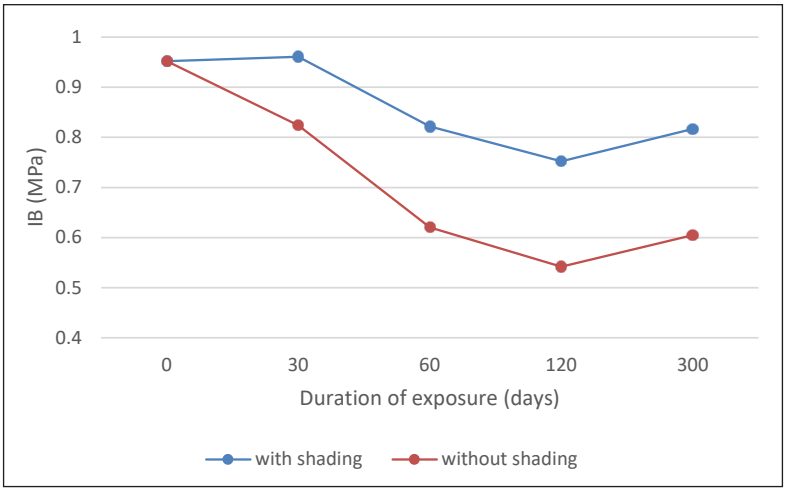

Figure 5. IB of LL CBP exposed to external conditions with and without shading for up to 300 days of exposure

shading. This indicates that weathering substantially impacts the bonding between cement and wood particles. Malaysia's extremely hot and humid climate may cause mechanical stress on the binder, leading to poor binding and reduced strength over time. However, even after 300 days of exposure, the IB values remained above the required MS 544 standard of 0.5 MPa under both shaded and unshaded conditions.

Stereo Compound Microscope Analysis

The effect of A: a microstructural study was used to corroborate the physical characteristics of CBP specimens. The surface morphology of the CBP specimens subjected to external exposure, with and without shading, was evaluated using a stereo compound microscope. The effects of external exposure with and without shading conditions on the LL CBP specimens' physical appearances are exhibited in Figure 6b, Figure 6d, and Figure 6f. The figures illustrate that the CBP specimens underwent morphological changes during and after exposure, particularly under external shading conditions. Hence, the most common degradation phenomenon is the self-debonding of the cement matrix and wood particles at the top surface of the boards, which had been exposed to external conditions without shading. This is probably due to the loss of cement grains from the surface caused by the alternating expansion and contraction of the cement matrix during exposure. Close observation of the board surface with a stereo compound microscope revealed distinct morphologies on the surfaces of CBP specimens exposed to the two conditions. Moreover, the roughening of the external surface without shading was probably due to the loss of cement from the board surface after prolonged exposure to alternating rain, heat, and wind.

For the CBP specimens exposed to shading conditions (Figure 6a, Figure 6c, and Figure 6e) There was a very minimal physical change on the surface and cross-section compared to those exposed without shading conditions. The specimens exposed to this condition always remained dry and grey in colour (the colour of cement). However, a similar CBP exposed to external conditions without shading was noticed to be faded. It is probably due to excessive alternate wetting and drying (Figure 6b) during rain and sunshine. Another common feature is fungal attack. Normally, a fungal attack can be observed with a microscope or by manual inspection. However, after 300 days of exposure, it was discovered that the fungus failed to attack the LL CBP specimens. This was mainly due to the high alkalinity of the CBP specimens (pH of 11.13 to 11.38), a major drawback for fungal development. Therefore, determining the CBP pH is important, as it may influence fungal attack and finishing characteristics of the CBP. In this study, the pH of CBP was tested using a pH meter.

In an earlier study, Kartal et al. (2001) confirmed that the high alkalinity (pH 11.3) and sodium silicate admixture in the CBP mixture were a major factor in improving resistance against insect and fungal attacks. The microphotograph from the stereomicroscope also suggests a dual mechanism of fibre fracture and fibre pullout failure in the LL

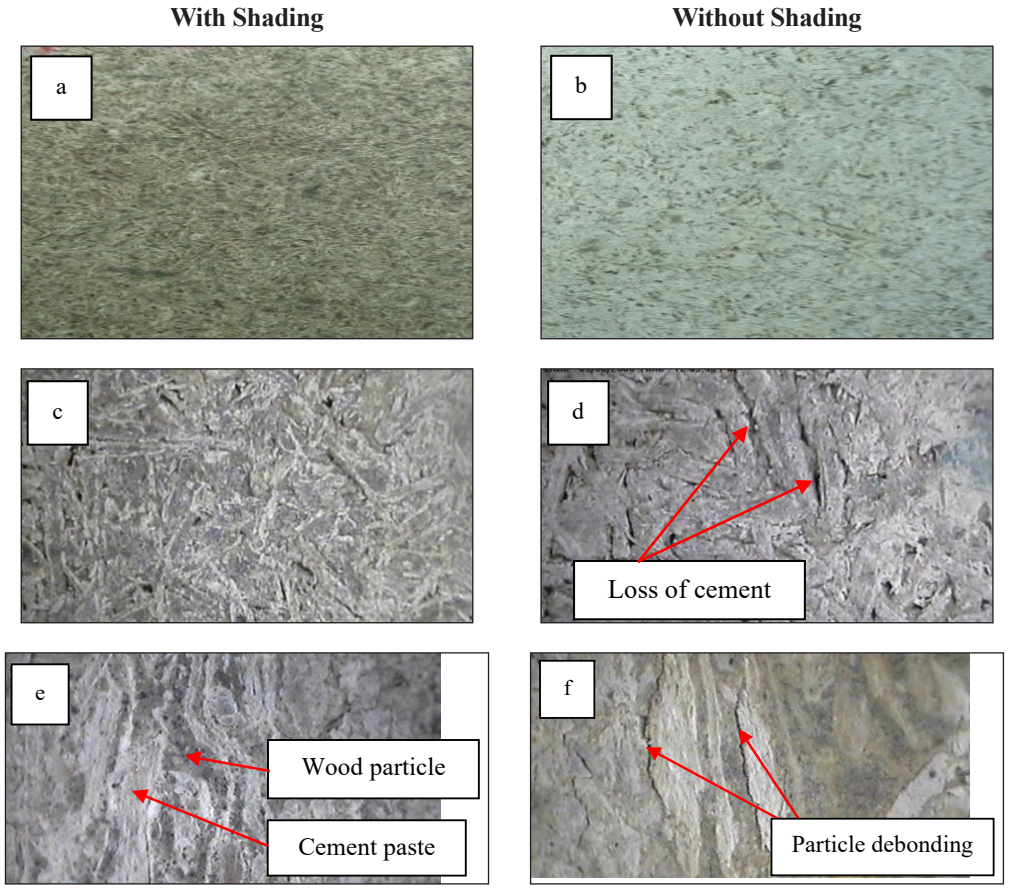

Figure 6. Detailed surface morphology observations on CBP samples exposed to both shaded and unshaded conditions. The top surface of samples a, b, c, and d is a cross-section of the samples, while e and f were examined at a 2× magnification level

CBP specimen (shaded), subjected to a mechanical properties test. It is observed that the test CBP specimens failed due to both failures of the fibre-to-fibre bond (fibre fracture) and fibre-to-cement matrix (fibre pullout) bond, as displayed in Figure 7 and Figure 8. At lower cement percentages, the failure mechanism was primarily attributed to fibre pullout, while at higher cement percentages, fibre fracture became the predominant cause of failure. Furthermore,



Figure 7. A close observation of CBP specimens demonstrating fibre fracture and fibre pullout after being subjected to a bending strength test (magnification 4.5×)

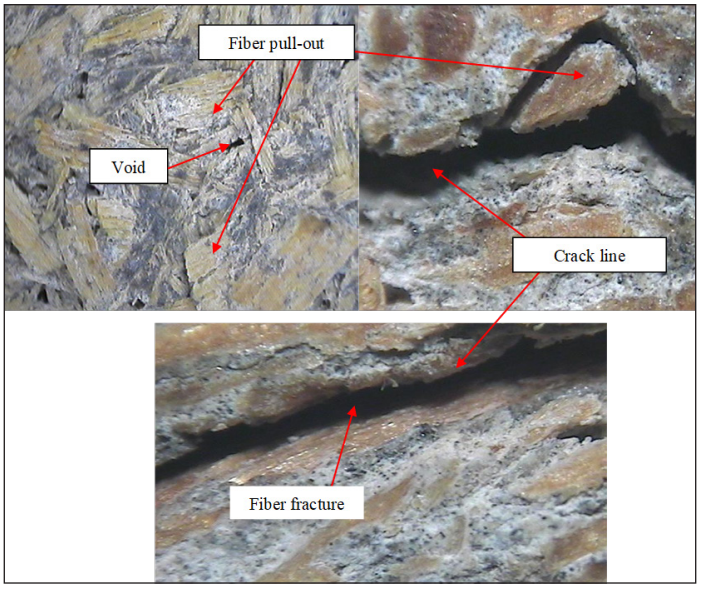

Figure 8. Typical surface of fibre fracture and fibre pullout failure for CBP specimen under IB test (magnification 4.5×)

a detailed analysis of the test specimens' surfaces unequivocally reveals that fibre pullout was the primary fracture failure mode, as depicted in Figure 7. Thus, the microphotograph provides a valuable visual confirmation of various mechanisms present in CBP materials.

CONCLUSION

This study highlights the potential of utilising the fast-growing species LL as an alternative particle source in CBP manufacturing. The results demonstrate that incorporating LL into CBP improved weather resistance under natural Malaysian conditions for up to 300 days. LL CBP showed a significant increase in MOR and MOE after prolonged exposure, particularly under shaded conditions, where it exhibited minimal physical deterioration and superior resistance to environmental stresses compared to unshaded conditions. The findings suggest that LL CBP, despite the challenges posed by high temperatures and moisture in unshaded environments, maintains its structural integrity and performance, attributed to the continuous hydration and hardening of the cement matrix. However, to comprehensively understand the impact of exposure duration on mechanical and physical properties, further research is recommended as follows:

1. Adhesive Optimisation: Optimise the adhesive formulations used in CBP manufacturing with LL particles. Different adhesives may influence the bonding strength and overall performance of the CBP. Hence, finding the most suitable adhesive for this specific material is essential.

2. Finite Element Analysis (FEA): Utilise FEA simulations to model the behaviour of LL-based CBP under different loading scenarios. FEA can provide valuable insights into stress distribution, failure mechanisms, and deformation patterns, optimising material design and engineering.
3. Cost Analysis: Perform a comprehensive cost analysis to assess the economic feasibility of using LL CBP compared to conventional particleboard materials. Understanding the production costs and market competitiveness will facilitate its integration into the industry.

ACKNOWLEDGEMENT

This research was supported by the College of Engineering, UiTM Cawangan Pahang, Malaysia, as well as the services and facilities provided by UiTM Cawangan Pahang to carry out the laboratory work.

REFERENCES

Alexander, M. G., Bentur, A., & Mindess, S. (2017). *Durability of concrete: Design and construction*. CRC Press. https://doi.org/10.1201/9781315118413

Iraldo, F., Facheris, C., & Nucci, B. (2017). Is product durability better for environment and for economic efficiency? A comparative assessment applying LCA and LCC to two energy-intensive products. *Journal of Cleaner Production, 140*, 1353-1364. https://doi.org/10.1016/j.jclepro.2016.10.017

Kartal, S. N., & Clausen, C. A. (2001). Leachability and decay resistance of particleboard made from acid extracted and bioremediated CCA-treated wood. *International Biodeterioration & Biodegradation, 47*(3), 183-191. https://doi.org/10.1016/S0964-8305(01)00047-6

Liu, J., Li, Y., Jin, C., Lin, H., & Yang, B. (2024). Exploring the influence and mechanisms of functionalized nanoscale wood fibre on the electromagnetic transmission performance of OPC paste. *Construction and Building Materials, 420*, Article 135621. https://doi.org/10.1016/j.conbuildmat.2024.135621

Mead, D. J. (2005). Forests for energy and the role of planted trees. *Critical Reviews in Plant Sciences, 24*(5-6), 407-421. https://doi.org/10.1080/07352680500316391

Melichar, T., Bydžovský, J., Brožovský, J., & Vacula, M. (2022). Structural, physical and mechanical changes of cement-bonded particleboards during sudden fluctuations in temperature and moisture. *Journal of Wood Science, 68*, Article 3. https://doi.org/10.1186/s10086-021-02004-3

Mussi Alencar, J. B., & de Melo Moura, J. D. (2019). Mechanical behaviour of cross-laminated timber panels made of low-added-value timber. *Forest Products Journal, 69*(3), 177-184. https://doi.org/10.13073/FPJ-D-18-00037

Nazerian, M., Gozali, E., & Ghalehno, M. D. (2011). The influence of wood extractives and additives on the hydration kinetics of cement paste and cement-bonded particleboard. *Journal of Applied Sciences, 11*(12), 2186-2192. https://doi.org/10.3923/jas.2011.2186.2192

Obiakara, M. C., Olubode, O. S., & Chukwuka, K. S. (2023). Climate change and the potential distribution of the invasive shrub, *Leucaena leucocephala* (Lam.) De Wit in Africa. *Tropical Ecology, 64*(4), 698-711. https://doi.org/10.1007/s42965-023-00294-w

Pakhomova, E., Emelyanov, S., Yartsev, V., Danilov, V., & Monastyrev, P. (2023). The influence of climatic ageing on the performance of wood-based panels. *Civil Engineering Journal, 9*(6), 1491-1508. https://doi.org/10.28991/CEJ-2023-09-06-015

Ramage, M. H., Burridge, H., Busse-Wicher, M., Fereday, G., Reynolds, T. P. S., Shah, D. U., Wu, G., Yu, L., Fleming, P., Densley-Tingley, D., Allwood, J., Dupree, P., Linden, P. F., & Scherman, O. (2017). The wood from the trees: The use of timber in construction. *Renewable and Sustainable Energy Reviews, 68*, 333-359. https://doi.org/10.1016/j.rser.2016.09.107

Sam-Brew, S., & Smith, G. D. (2015). Flax and hemp fibre-reinforced particleboard. *Industrial Crops and Products, 77*, 940-948. https://doi.org/10.1016/j.indcrop.2015.09.079

Simatupang, M. H., & Neubauer, A. (1993). Manufacture and properties of rapid-hardening cement-bonded particleboards made by carbon-dioxide injection: Influence of cement strength class. *Holz als Roh- und Werkstoff, 51*(5), 309-311. https://doi.org/10.1007/BF02663800

Singh, P., Tewari, A., & Pandey, V. (2022). Changes in growth pattern and rhizospheric soil biochemical properties of a leguminous tree species *Leucaena leucocephala* under long-term exposure to elevated ozone. *3 Biotech, 12*(7), Article 152. https://doi.org/10.1007/s13205-022-03215-1

Sudarmanto, Juwono, A. L., Subyakto, Budiman, I., Lubis, M. A. R., Kusumah, S. S., Kusumaningrum, W. B., & Adi, D. S. (2022). Effect of cold-water treatment and hydrothermal carbonization of oil-palm-trunk fibres on compatibility with cement for the preparation of cement-bonded particleboard. *Wood Material Science & Engineering, 17*(6), 979-988. https://doi.org/10.1080/17480272.2021.1983871

Wei, J., & Meyer, C. (2015). Degradation mechanisms of natural fibre in the matrix of cement composites. *Cement and Concrete Research, 73*, 1-16. https://doi.org/10.1016/j.cemconres.2015.02.019

Wiejak, A., & Francke, B. (2021). Testing and assessing method for the resistance of wood-plastic composites to the action of destroying fungi. *Materials, 14*(3), Article 697. https://doi.org/10.3390/ma14030697

Xie, W., Guo, S., Liu, Y., Chen, R., & Wang, Q. (2020). Organic-inorganic hybrid strategy based on ternary copolymerization to prepare flame retardant poly(methyl methacrylate) with high performance. *Composites Part B: Engineering, 203*, Article 108437. https://doi.org/10.1016/j.compositesb.2020.108437

Yilmaz, M., Tokyay, M., & Yaman, I. O. (2016). Cement production by cement-bonded wood particleboard wastes. *Advances in Cement Research, 28*(4), 233-240. https://doi.org/10.1680/jadcr.15.00023

Yu, Y., Hou, J., Dong, Z., Wang, C., Lu, F., & Song, P. (2016). Evaluating the flammability performance of Portland cement-bonded particleboards with different cement-wood ratios using a cone calorimeter. *Journal of Fire Sciences, 34*(3), 199-211. https://doi.org/10.1177/0734904116630758

Pertanika J. Sci. & Technol. 34 (S2): 117 - 137 (2026)

PERTANIKA JOURNALS

SCIENCE & TECHNOLOGY

Journal homepage: http://www.pertanika.upm.edu.my/

Review Article

The Use of Lignin as Bio-Binder for Sustainable Asphalt Pavement-A Recent Review

Amminudin Ab Latif[1]*, Mohd Fakri Muda[1,3], Noor Safwan Muhamad[1], Marzuki Ab. Rahman[1], Muhammad Isha Ismail[1], Mohd Razmi Zainudin[1], Farah Wahida Mohd Latib[1], and Wan Zukri Wan Abdullah[2]

[1]Faculty of Civil Engineering, Universiti Teknologi MARA Pahang Branch, 26400 Jengka, Pahang, Malaysia
[2]Faculty of Civil Engineering, Universiti Teknologi MARA, 40450 Shah Alam, Selangor, Malaysia
[3]3R: Rehabilitation, Repair and Retrofitting Group, Faculty of Civil Engineering, Universiti Teknologi MARA, 40450 Shah Alam, Selangor, Malaysia

ABSTRACT

Lignin, a natural biopolymer predominantly derived from the pulp and paper industry, offers a promising alternative to petroleum-based asphalt binders for its sustainability and performance-enhancing properties. This review aims to consolidate research on the use of lignin as a bio-binder, focusing on its ability to enhance the mechanical and environmental performance of asphalt mixtures. Key findings indicate that lignin-modified asphalt exhibits enhanced thermal stability, increased rutting resistance, and improved anti-ageing properties, all of which contribute to longer-lasting pavements. However, challenges remain in optimising lignin's content, balancing mechanical properties such as fatigue life and low-temperature cracking, and ensuring compatibility with various asphalt binders. Future research should focus on these challenges while investigating the large-scale feasibility and long-term performance of lignin-modified asphalt under diverse environmental conditions. This review concludes that lignin offers considerable potential for developing sustainable asphalt pavements, aligning with global efforts to reduce carbon emissions and reliance on fossil fuels in road construction.

Keywords: Asphalt, bio-binder, lignin, pavement

ARTICLE INFO

Article history:
Received: 18 June 2026
Accepted: 22 September 2026
Published: 30 September 2026

DOI: https://doi.org/10.47836/pjst.34.S2.10

E-mail addresses:
amminudin738@uitm.edu.my (Amminudin Ab Latif)
fakri@uitm.edu.my (Mohd Fakri Muda)
safwanmuhamad@uitm.edu.my (Noor Safwan Muhamad)
marzukiar@uitm.edu.my (Marzuki Ab. Rahman)
isha@uitm.edu.my (Muhammad Isha Ismail)
razmi74@uitm.edu.my (Mohd Razmi Zainudin)
farahwahidaml@uitm.edu.my (Farah Wahida Mohd Latib)
wanz@uitm.edu.my (Wan Zukri Wan Abdullah)
* Corresponding author

INTRODUCTION

In general, the term 'lignin' refers to wood, particularly trees, and is a significant plant component. Lignin is widely available in the

e-ISSN: 2231-8526

© Universiti Putra Malaysia Press

natural world and ranks among the most prevalent plant polymers globally, after cellulose. Industries such as paper and pulp are the main sources of lignin. There is potential to utilise lignin in power generation plants via combustion. Lignin has been identified in various plant species and in tree biomass. For example, straw, flax, cotton, jute, hemp, as well as pulp and wood bark (Watkins et al., 2015). As per existing literature, the pulp and paper sector produces around 50 million tons of lignin each year, and this output is projected to experience additional expansion in the coming times (Collins et al., 2019).

Lignin is a crucial constituent of plant cell walls, enabling plants to maintain adequate firmness and rigidity, as shown in Figure 1. Lignin is a complex phenolic polymer composed of three alcohol monomers, known as simply alcohol, coniferyl alcohol, and p-coumaroyl alcohol. It possesses functional groups like methoxy, carboxyl, carbonyl, and hydroxyl. The degradation process can produce advanced lignin derivatives, such as binders and surfactants. Lignin degradation can occur through thermal, chemical, or enzymatic means. Various techniques for extracting lignin use chemical solvents such as ethanol, acetic acid, acetone, propanol, and methanol to separate lignin from plant sources. Lignin is a by-product utilised in the pavement construction industry as an asphalt modifier to improve pavement performance. Asphalt is a dark, cement-like substance that exhibits a wide range of consistencies, from solid to semi-solid under typical atmospheric conditions. It mainly consists of hydrocarbons. Asphalt is also known as a bituminous material because of its hydrocarbon composition. Asphalt is widely utilised in highway and road constructions, parking lots, and airport runways. Normally, asphalt is employed as a binder between the aggregates to form an asphalt mixture. Virgin asphalt is produced from crude oil or petroleum-based products. The production of virgin asphalt and pavement-laying works contributed to greenhouse gas emissions. Many researchers have been investigating pavement construction methods and materials for energy conservation, asphalt pavement

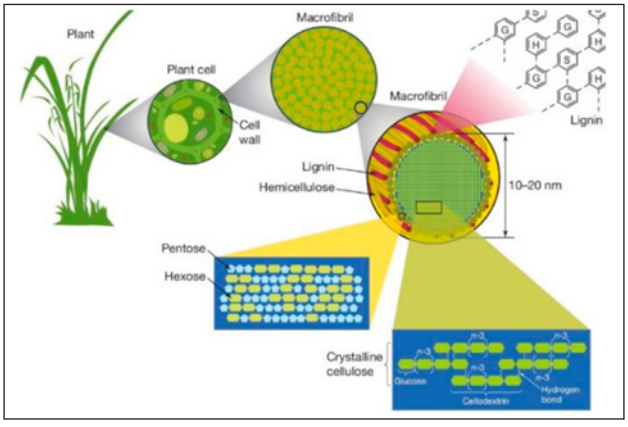

Figure 1. Lignin structure in the plants' cell walls (Yao et al., 2022)

recycling, carbon emissions reduction, and incorporating new materials as modifiers in asphalt binders to reduce greenhouse gas emissions.

Developing a modified asphalt binder incorporating lignin reduced waste, providing environmental, economic, and social benefits (Cheng et al., 2020). Previous research revealed that applying lignin as an asphalt additive material enhanced asphalt pavement performance related to water damage resistance and cracking resistance (Abdelsalam et al., 2020).

Based on various sources, the lignin incorporation into regular asphalt is capable of enhancing oxidation reactions and increasing fatigue life by approximately 8% (Gao et al., 2020). Here, a separate investigation has revealed that the incorporation of lignin into asphalt exhibits a notable enhancement in its anti-ageing properties, thereby leading to an extended service life of pavement (Cai et al., 2022). Furthermore, a previous study also investigated the impact of two lignin products, specifically lignin fibre and lignin powder, on the performance of the asphalt mixture (Zhang et al., 2020) . Thus, the asphalt mixture containing lignin powder has enhanced various aspects of mechanical performance, including rutting, ravelling, thermal stability, abrasion resistance, fatigue cracking resistance, and moisture susceptibility.

Certainly, partially replacing bitumen with lignin offers a compelling and ecologically viable solution. Moreover, the substantial volume of lignin production provides researchers with a notable opportunity to explore the potential uses of lignin within the realm of asphalt technology(Min et al., 2013; Sun et al., 2017).

The aim of this study is to consolidate the significant findings of previous research on the application of lignin obtained from paper pulp industries for incorporation into asphalt binders and mixtures. The study also examined the improvements in the chemical, mechanical, and environmental properties of asphalt mixtures and binder when lignin is incorporated into the asphalt content. Moreover, the utilisation of lignin-modified asphalt is gaining significant interest among researchers worldwide, as it offers an opportunity to enhance the performance of asphalt pavements while simultaneously minimising waste generated by the pulp industry. In the Malaysian context, there remains ongoing debate among industry stakeholders regarding the implementation of lignin as a bio-binder in asphalt materials and mixtures. The research's findings contribute to the research community by providing valuable insights on effectively navigating the available literature and promptly addressing emerging challenges and issues related to the employment of lignin-modified asphalt pavement as a bio-binder.

EXTRACTION PROCESS OF LIGNIN

The lignin's purity will vary based on the extraction, the additive used, and the isolation method (Yin et al., 2021). Conventionally, lignin is acquired as a secondary product from

the wood and paper production sectors. It can be found in differing proportions within numerous plant varieties and can be categorised into three primary types, relying on their origin and chemical makeup: hardwood lignin, softwood lignin, and grass lignin (Boeriu et al., 2014). Lignin can be extracted from wood using various chemical processes, including:

i. Kraft pulping: This process is widely employed for the industrial manufacture of lignin. It entails treating wood chips with sodium hydroxide and sodium sulphide to dissolve lignin and hemicelluloses, leaving the cellulose fibres intact. Subsequently, the resulting lignin-rich substance, known as black liquor, is isolated and utilised as a fuel by being burned in the recovery boiler.

ii. Sulphite pulping: By combining sulphur dioxide and heat, this procedure dissolves the lignin, ultimately leaving the cellulose fibres unaffected. The lignin-rich waste liquor is either burned as fuel or further processed to extract lignin.

iii. Organosolv pulping: This process uses an organic solvent, such as ethanol or methanol, to dissolve the lignin and hemicelluloses, leaving behind cellulose fibres. The solvent enriched with lignin is isolated, and the recovery of lignin is accomplished through either precipitation or distillation techniques.

Each of these processes has its own set of strengths and weaknesses. The process selection depends on the desired end-use of the lignin and the type of wood being processed.

The most widely used industrial lignin is kraft lignin. Among the many uses for kraft lignin are as a fuel, binder, dispersant, and in the synthesis of other compounds. Concerns about the long-term economic and environmental viability of burning lignin for energy recovery have recently led to a rise in the popularity of organosolv lignin, which is derived from the waste product of the biofuel manufacturing process. As a possible supply of high-value fuels and chemicals, it is being observed instead. This sulphur-free form of lignin is perceived as a more environmentally friendly option. The different types and characteristics of lignin are summarised in Table 1. Meanwhile, Figure 2 illustrates the physical properties of kraft lignin powder from the hardwood, dried at room temperature and oven dried.

Table 1
Types and characteristics of lignin

Lignin	Sulfur (%)	Ash (%)	PH	Acids (%)	Purity	Moisture (%)
Lignosulfonate (Aro & Fatehi, 2017)	3-5.8	4-8	2-12	4-6	Moderate/ low	5.8
Kraftlignin (Arapova et al., 2020)	1-3	2-6	13	4.1-6	High	3-6
Organosolv (Khandelwal, 2019)	0	0-0.5	-	7-8	High	7.5
Soda Lignin (Rodríguez et al., 2010)	0	0-0.5	11-13	-	Moderate	2.5-5

Physical and Chemical Properties of Lignin

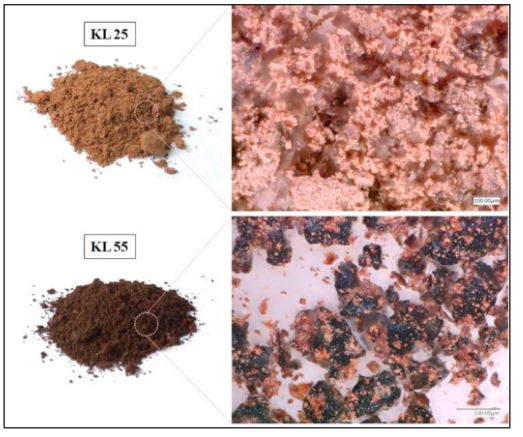

Figure 2. Kraft lignin extracted from the hardwood was dried at room temperature (25 °C) and oven-dried at 55 °C.Adapted from (Gordobil et al., 2021)

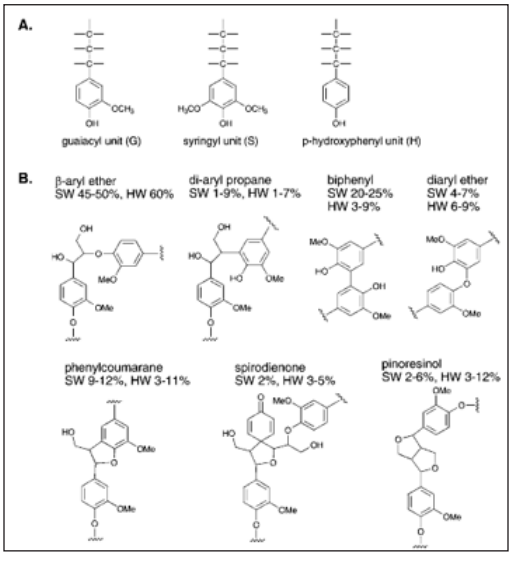

Figure 3. The structural unit in the lignin. A) Structure of G, H, and S monomeric units. B) Structure of chemical linkage (SW, softwood; HW, Hardwood). Adapted from (Bugg et al., 2012)

One type of complex organic polymer formed from phenylpropanoid monomers is lignin. Guaiacyl, syringyl, and p-coumaroyl alcohols are the main sources of these monomers, which are three condensed aromatic monomers. Lignin is an essential component of plant cellular structure, contributing to the rigidity and strength of the cell wall. This polymer constitutes approximately 15-35% of the total weight of dry wood. Lignin is a significant constituent of various plant materials, including but not limited to straw, hemp, and flax. Furthermore, lignin comprises a diverse array of structural components interconnected by various chemical bonds. The prevailing linkages observed in this context are acetyl, coumaroyl, and phenylpropyl. The structural makeup of lignin has a considerable impact on its reactivity and properties. Figure 3 depicts the structural unit identified in lignin. Lignin is comprised of a complex network of interconnected aromatic heteropolymers and phenylpropanoid aryl-C3 units. These units are connected through various ethers as well as C-C bonds. Lignin constitutes around 15-30% of the dry weight of lignocellulose. Moreover, it is synthesised through the radical polymerisation of guaiacyl (G) units derived from the precursor coniferyl alcohol, syringyl (S) units from precursor p-sinapyl alcohol, as well as p-hydroxyphenyl (H) units from precursor p-coumaryl alcohol. Other than that, the G:S:H units ratio ranges depending on the species and whether it is a softwood or hardwood, generally leading to G-type lignin in softwoods and GS-type lignin in hardwoods. The most prevalent linkage is the ß-aryl ether, which involves an ether linkage to another aryl unit at the C2 of the

C3 chain. This linkage constitutes about 45-50% of units in softwoods and around 60% in hardwoods.

Furthermore, the physical properties of lignin can be divided into solubility, dispersity index, and thermal properties (Calvo-Flores, 2020). The dispersion index serves as a parameter to characterise polymers and gauge the distribution of molecular weights. Concurrently, soluble lignin and its derivatives exhibit notable dispersion characteristics, ranging from 2.5-3.0 to 10-11, depending on the lignin source (Kong et al., 2023). Recently, the thermal properties of lignin can be categorised depending on the parameters of glass transition temperature (TG) (Jin et al., 2023; Pe et al., 2023). The glass TG refers to a parameter employed to describe the transition of amorphous or semicrystalline polymers from a solid, glassy state to a more fluid and rubbery state. The thermal degradation temperature range of lignin has been determined to be 200-500 ℃.

LIGNIN IN ASPHALT

Asphalt is black in colour and made up of hydrocarbons. It is a cementitious material and semisolid at room temperature. It is also known as a bituminous substance. Asphalt can be classified as a thermoplastic material because its consistency changes with temperature fluctuations. When heated sufficiently, it softens, and at a certain temperature, it becomes liquid. Various types of asphalt are used in pavement work, such as penetration-grade, performance-grade, and polymer-modified asphalt. Figure 4 displays the typical penetration of asphalt and polymer-modified asphalt in liquid conditions after heating to a certain temperature (Tauste-Martínez et al., 2022). When it cools, asphalt hardens and holds the particles together. Generally, the currently used asphalt is manufactured through the refinery process of crude oil. Modern refinery equipment permits asphalt production for specific applications, as illustrated in Figure 5. As a result, various types of asphalt are manufactured for purposes such as road construction, waterproofing, roofing, and diverse applications. Other than that, in pavement engineering, asphalt serves as a binder that binds the aggregates within asphaltic layers. Moreover, earlier studies have indicated that lignin holds promising potential in roles such as an asphalt emulsifier, extender, modifier, and coupling agent (Khater et al., 2021) .



Figure 4. Penetration and polymer-modified asphalt (Tauste-Martínez et al., 2022)

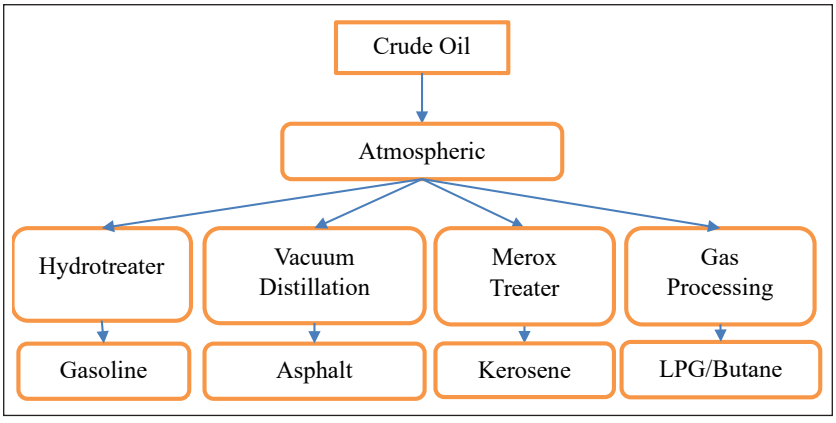

Figure 5. Schematic diagram of asphalt production (Al-Moubaraki & Obot, 2021)

Lignin Modified Asphalt and Mixtures

Recently, investigations into incorporating lignin into asphalt binders have become increasingly popular due to its abundance, low production cost, and potential to enhance the mechanical and physical properties of asphalt pavement. Furthermore, Cheng et al. (2020) found that the anti-rutting performance and thermal stability of lignin-modified asphalt increase with increasing lignin content up to 12%. Simultaneously, introducing lignin into the asphalt binder has the capability to slow down oxidation reactions, diminish asphalt fatigue life, enhance elastic properties, elevate viscosity, and enhance the resistance of the asphalt binder to permanent deformation (Gao et al., 2020).

Lignin can be introduced into the asphalt binder as a modifying agent. It's important to note that asphalt binder properties typically encompass elasticity, viscosity, and plasticity. The performance of asphalt mixtures is closely tied to the behaviour of the asphalt binder employed. Assessing asphalt binder properties involves examining aspects such as temperature sensitivity, resistance to cracking, moisture susceptibility, fatigue endurance, and resistance to ageing. Numerous studies have been conducted to explore the impact of lignin on asphalt and its mixtures. Table 4 summarises the research findings on the physical, mechanical, chemical, and environmental properties of lignin-modified asphalt. Based on the analysis of 30 research papers retrieved from the Scopus database with "lignin AND Asphalt AND binders AND mixture AND pavement" searching keywords, the studies on evaluating the performance of lignin-modified asphalt binder and mixtures can be categorised into 20 clusters, including cracking, rutting, viscosity, and others, as depicted in Figure 6. The primary focus of most researchers was the assessment of rutting performance, followed by fatigue, ageing, and environmental impact. Meanwhile, a brief study of permanent deformation, rheological properties, viscosity, elastic properties, and resilience modulus. Therefore, further research is necessary to evaluate the performance of

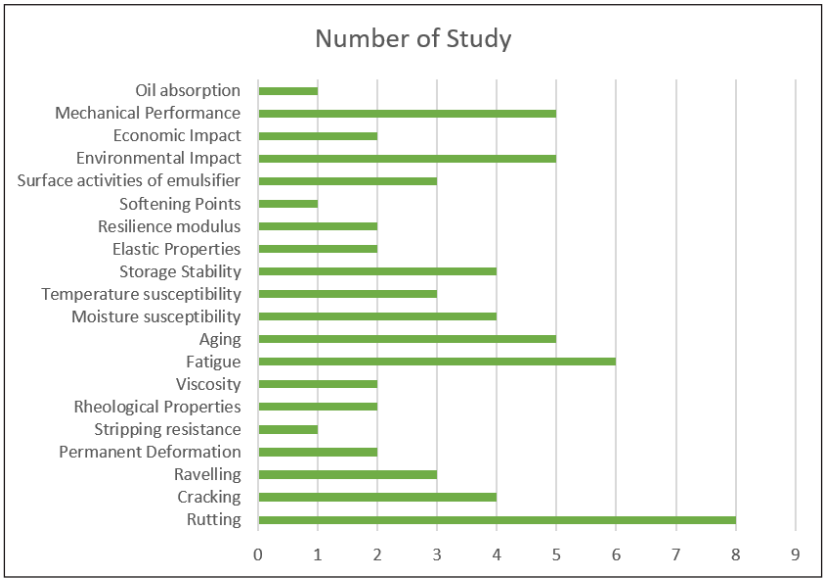

Figure 6. Performance evaluation of lignin-modified asphalt binder and mixtures

lignin-modified asphalt and mixtures, particularly with respect to permanent deformation, viscosity, and rheological properties of the lignin-modified asphalt binder and mixtures. The research also necessitated expansion to encompass the economic and environmental aspects.

Lignin as Emulsifier and Coupling Agent in Asphalt

An emulsifier is a substance that aids in mixing two or more immiscible substances, such as oil and water, by lowering surface tension and stabilising the mixture. Consequently, emulsifiers form a layer around small droplets of one liquid, allowing them to disperse without separating throughout the other liquid.

Lignin can be utilised as an asphalt emulsifier, helping to mix and stabilise asphalt with water to form an emulsion. In the construction industry, this is commonly used for road paving and roofing applications. Many researchers have investigated water-based emulsions to reduce carbon emissions in asphalt production industries. Thus, Yuliestyan et al. (2017, 2022) discovered that cationic kraft lignin exhibited the most effective emulsification properties in the development of bitumen emulsions. Additionally, compared with unmodified asphalt, the residue from bitumen modified with kraft lignin exhibited improved characteristics in viscous flow and linear viscoelasticity. Another noteworthy advancement involved the development of a new cationic asphalt emulsifier based on tetraethylene pentaamine/formaldehyde-modified lignin amine. This emulsifier, synthesised from alkali lignin, tetraethylenepentamine, as well as formaldehyde, yielded positive outcomes, showcasing favourable surface activity and satisfactory emulsification effects (Chen et al., 2017).

Conversely, the utilisation of both Low-Density Polyethene (LDPE) and lignin as coupling agents in asphalt mixtures resulted in an enhancement in Marshall stability by up to 89.5%. Moreover, integrating lignin as a coupling agent for both LDPE and asphalt could address the limitations of asphalt plastic technology and help tackle plastic waste. The experiments were further extended to incorporate Polyethene (PE) and Polypropylene (PP) into the original asphalt, utilising lignin as the intermediary coupling agent. This addition of lignin notably influenced asphalt in terms of penetration index, ductility, and hardness properties (Putra et al., 2017). Based on a summary of thirty (30) cited articles from the Scopus database using the search keywords "lignin AND Asphalt AND binders AND mixture AND pavement," it was found that only four (4) studies have evaluated the performance of lignin-based emulsifiers. These 4 studies found that the lignin-based emulsifier demonstrated excellent surface activity and improved emulsification, making it suitable for road pavement applications. However, the authors suggested that further research is needed to enhance the performance of lignin emulsifier in various asphalt pavement projects and under extreme environmental conditions.

Experimental Method

The experimental methods for incorporating lignin into asphalt mixtures typically begin with selecting appropriate materials, including the asphalt binder and the lignin additive. In most studies, researchers use a base asphalt binder as a control for comparison. Lignin, which can be derived from various sources, including the pulp and paper industry, is incorporated into the asphalt binder at different proportions. Common lignin contents range from 2% to 15% by weight of the binder, depending on the study's specific objectives (Cheng et al., 2020). The mixture of lignin and asphalt is achieved through a physical blending process, ensuring that the lignin is evenly distributed within the binder. Table 2 provides an overview of the blending criteria for lignin and asphalt.

Once the lignin-modified asphalt binders are prepared, they undergo a series of rheological and mechanical tests to assess their performance. Rheological tests such as the Dynamic Shear Rheometer (DSR) and Rotational Viscosity (RV) tests are frequently employed to evaluate the high-temperature stability and flow characteristics of the modified asphalt. The DSR test measures the complex shear modulus (G*) and phase angle (δ), which indicate the material's resistance to deformation and its elastic behaviour under stress. In addition, mechanical performance tests are conducted to evaluate the modified asphalt mixtures' resistance to various forms of distress. These tests include low-temperature bending tests to assess cracking resistance, Marshall Immersion tests to evaluate water stability, and freeze-thaw splitting tests to measure the asphalt mixture's durability under cyclic freezing and thawing. The findings from these tests help to determine the optimal lignin content and its effects on different performance aspects of the asphalt binder. Ageing

Table 2
The optimum blending criteria between lignin and asphalt

Lignin Source	Base Bitumen	Lignin State	Lignin Content (% by weight)	Mixing Temperature (°C)	Mixing Timing (min)	Mixing speed (rpm)	Mixer Type	Reference
Organosolv	70/100	Powder	10	163	30	3000	High shear mixer	Vishtal & Kraslawski, 2011
Kraft corn stalk	60/70	Powder	5	160	60	4000	High shear radial	Xu et al., 2021
Waste from corncobs	160/220	Powder	5-10	150	60	6000	High shear mixer	Norgbey et al., 2020
Black liquor from softwood, kraft lignin, rice hulls	PG 67-22	Powder	2-4	180	60	12000	High shear mixer	Arafat et al., 2019

tests are performed to simulate the long-term behaviour of lignin-modified asphalt under real-world conditions. The Rolling Thin Film Oven Test (RTFOT) and Pressure Ageing Vessel (PAV) are commonly used to simulate short-term and long-term ageing, respectively. These ageing processes expose the asphalt binder to elevated temperatures and oxygen, mimicking the effects of environmental exposure over time. The results of these ageing tests are critical in understanding how lignin influences the oxidative stability and overall longevity of the asphalt mixture. The combination of these experimental methods provides a comprehensive understanding of the potential benefits and limitations of using lignin as a bio-additive in asphalt pavements. According to the previous study, the research primarily focused on evaluating the performance of asphalt binders and mixtures with respect to typical mechanical and physical properties. These properties include rutting, cracking, fatigue, ageing, moisture susceptibility, and other aspects of mechanical performance. Nevertheless, it has been discovered that there is a deficiency in research regarding the impact of lignin on asphalt binder and mixtures in terms of permanent deformations, rheological characteristics, viscosity, elastic properties, resilience modulus, oil absorption, and economic impact.

Future Research Directions on Lignin -Based Asphalt Binders and Mixtures

Lignin has great potential as a sustainable additive for improving the properties of asphalt binders due to its advantageous anti-ageing and antioxidant properties. However, there are still challenges regarding its compatibility, optimal composition, and effects on various mechanical properties. Future research should prioritise addressing these difficulties by conducting thorough investigations into the long-term performance, economic viability,

and environmental consequences of lignin. Based on the research findings in Table 4, the studies should be clustered into the specific research areas outlined in Table 3.

Table 3
Research clusters for future research on lignin-based asphalt binders and mixtures

Research Cluster	Research Focus	Key Area for Further Study
Long-Term Durability & Performance	Investigate lignin's effects on the durability of asphalt binders and mixtures under various environmental and traffic conditions.	Long-term performance in different climates and traffic loads.
Mechanical Properties & Rheology	Optimise lignin content and its interactions with asphalt to improve rheology while balancing fatigue life and other mechanical properties.	Optimal lignin content for balancing mechanical properties and fatigue life impact.
Lignin Compatibility & Interaction	Explore methods to improve lignin compatibility with various asphalt types and additives.	Chemical interaction with anti-rutting agents. Emulsifier stability in different systems.
Environmental & Economic Feasibility	Evaluate the scalability, cost-effectiveness, and environmental impact of lignin-modified asphalt in large-scale applications.	Large-scale feasibility and environmental benefits. Cost analysis of lignin-based binders.
Composite Systems & Fibre-Reinforced Asphalt	Study lignin in combination with other materials such as diatomite, glass fibres, and bio-oils to optimise performance under varied conditions.	Fibre reinforcement optimisation. Impact of composite systems on performance
Sustainability & Bio-based Additives	Explore the potential of lignin and other bio-based materials to further reduce the environmental impact of asphalt production and application.	Integration with other sustainable additives. Environmental impact reduction strategies.

Table 4
Summary of the research findings related to the performance of lignin-modified asphalt

No.	Author	Performance Evaluation	Findings	Future Research
1	Cheng et al., 2020	1	Lignin improves thermal stability up to 12% of asphalt mass, beyond which there is no significant benefit.	Investigate the effects of lignin on asphalt's long-term durability under various environmental conditions

Table 4 (*continued*)

No.	Author	Performance Evaluation	Findings	Future Research
2	Abdelsalam et al., 2020	2	Diatomite improves water resistance; lignin fibre enhances anti-cracking performance. Combined, they improve overall asphalt performance.	Explore the long-term durability and economic feasibility of using diatomite-lignin composites in different climates.
3	Gao et al., 2020	4, 7, 8	Lignin increases the viscosity and elastic components of asphalt, improving resistance to permanent deformation, but may reduce fatigue life if used excessively	Study the optimal lignin content to balance the benefits of improved rheology against the potential reduction in fatigue life.
4	Cai et al., 2022	9	Lignin improves anti-ageing performance and high-temperature stability but raises issues with asphalt compatibility.	Investigate methods to enhance lignin compatibility with various asphalt types.
5	Zhang et al., 2020	1, 2, 3	Lignin powder improves overall mechanical performance; lignin fibre enhances rutting and thermal cracking resistance but degrades other properties.	Focus on optimising the balance between different mechanical properties when using lignin fibre in asphalt mixtures.
6	Batista et al., 2018	11, 14	Lignin enhances resistance to thermal cracking and improves high-temperature performance, with 4 wt.% lignin showing optimal resistance to weathering ageing.	Further explore the effects of varying lignin types and contents on the long-term performance of asphalt binders under different environmental stresses.
7	Abdelsalam et al., 2020 and Yue, et al., 2021	10, 11	The addition of 0.30% lignin fibre and 0.30% glass fibre improved water stability, low-temperature stability, and overall quality of the bituminous mix.	Further investigation into the long-term effects of lignin and glass fibre composites on pavement performance
8	Zhao et al., 2011	11	EHL improved the penetration index, increased the softening point, and reduced the brittle point, enhancing the temperature susceptibility of asphalt.	Explore the potential of combining EHL with other polymers for further enhancing asphalt properties.
9	Yu et al., 2021	6, 7, 8, 11, 12	The addition of soda lignin powder reduced temperature sensitivity, increased viscosity, enhanced rutting and fatigue performance, but slightly reduced low-temperature cracking performance	Investigate the environmental impact and economic feasibility of large-scale use of soda lignin-modified asphalt.

Table 4 (*continued*)

No.	Author	Performance Evaluation	Findings	Future Research
10	Xue et al., 2022	11, 13	Lignin improved high-temperature performance, while waste engine oil enhanced low-temperature flexibility; however, excessive lignin reduced stiffness	Optimise the ratio of lignin to waste engine oil for achieving balanced high- and low-temperature performance in asphalt binders
11	Shi et al., 2016	12, 16	The new lignin emulsifier exhibited excellent surface activity and satisfactory emulsification effect, with improved storage stability compared to conventional emulsifiers	Explore the potential for large-scale application of this lignin-based emulsifier in various asphalt pavement projects.
12	Chen et al., 2017	12, 16	The modified lignin emulsifier demonstrated excellent surface activity and improved emulsification, making it suitable for road pavement applications such as chip seal and tack coat.	Investigate further modifications to enhance the performance of lignin emulsifiers under extreme environmental conditions
13	Yao et al., 2022	11	Lignin-modified asphalt exhibits increased viscosity and hardness, with improved high-temperature resistance, though low-temperature crack resistance may be reduced	Further research is needed to optimise lignin's use in pavement engineering, particularly to enhance low-temperature crack resistance.
14	Yue et al., 2022	18	The use of diatomite-lignin composites resulted in minimal negative environmental impacts, making them a viable alternative for improving asphalt pavement performance.	Investigate ways to further reduce the environmental impact of composite admixtures in asphalt, potentially integrating other sustainable materials.
15	Xu et al., 2017	1	Wood lignin improved high-temperature rutting performance and ageing resistance but negatively impacted the fatigue life of the asphalt binder.	Explore methods to mitigate the negative effects of lignin on the fatigue life of asphalt while retaining its anti-ageing benefits.
16	Arafat et al., 2019	1, 2, 9	Lignin-modified asphalt demonstrated improved high-temperature performance and oxidative ageing resistance, with enhanced cracking resistance and flexibility index	Further research on the scalability of lignin use in hot mix and warm mix asphalt processes, particularly in different climatic conditions.

Table 4 (*continued*)

No.	Author	Performance Evaluation	Findings	Future Research
17	Duarte Mendonça et al., 2022	10, 14	Lignins from Pinus and Eucalyptus improved the resilience of asphalt mixtures and reduced moisture susceptibility, with 3% Pinus lignin showing the best mechanical performance	Further study on the long-term durability and performance of lignin-modified asphalt mixtures in different environmental conditions.
18	Peng et al., 2020	5, 19	Lignin-based polyurethane modified asphalt binder (LPUA) exhibited improved tensile strength and adhesion properties during UV ageing, with satisfactory performance under water exposure.	Explore other lignin-based compounds to further enhance the durability and adhesion properties of asphalt binders under various environmental conditions.
19	Wu et al., 2022	1	An anti-rutting agent (ARA) improved the performance of lignin-fibre-reinforced asphalt mixtures, particularly in maintaining performance under ageing.	Further explore the chemical interactions between lignin fibres, anti-rutting agents, and asphalt to optimise the long-term performance of asphalt mixtures.
20	Kou et al., 2020	6, 13	Basalt fibre enhanced the physical properties, while lignin fibre improved the rheological properties. The best fibre mix ratio was 1:2 (basalt).	Study the long-term durability and performance of MFRA under different environmental conditions and traffic loads.
21	Xin et al., 2016	13	Lignin-based epoxy resin improved the elastic behaviour of asphalt binder at elevated temperatures, making it a viable alternative to conventional epoxy.	Further optimise the formulation of lignin-based epoxy systems for broader applications in sustainable pavement materials.
22	Liu et al., 2013	13, 16	Higher surface activity of emulsifiers reduced particle size and improved storage stability.	Investigate other lignin derivatives to further improve emulsion stability and performance.
23	Luo et al., 2019	1, 2, 3, 17, 19	Lignin fibres improve low-temperature performance; glass fibres enhance high-temperature resistance. Composite modification improves overall performance	Further research on composite modifications to optimise performance across all conditions.
24	Chen et al., 2017	13, 16	The synthesised emulsifier demonstrated good surface activity and satisfactory emulsification, with improved storage stability.	Explore different lignin sources and chemical modifications to enhance emulsifier performance.

Table 4 (*continued*)

No.	Author	Performance Evaluation	Findings	Future Research
25	Luz et al., 2021	1, 8, 9	Incorporating lignin improved fatigue lifespan, rutting resistance, and delayed short-term ageing.	Investigate the long-term performance of these modified binders under different climatic conditions.
26	Khadim & Ahmad, 2024	6	Lignin improved physical properties, decreased asphaltene content, and increased aromatic content. 2. Rheological characteristics were enhanced, with optimum performance at 10% lignin.	Explore the long-term environmental impact and durability of lignin-modified asphalt in real-world conditions.
27	Yuliestyan et al., 2018	NA	Successfully prepared reduced-temperature asphalt mixes that met French design requirements.	Explore optimisation of mix design parameters for different RAP sources and environmental conditions.
28	Cai et al., 2024	9	Lignin improved rutting resistance and maintained molecular weight balance during ageing, especially with enzymatic lignin.	Further research on optimising lignin types and dosages to enhance long-term asphalt performance across different climates.
29	Hu et al., 2022	NA	Quercetin exhibited superior anti-ageing activity compared to lignin due to higher phenolic hydroxyl content.	Modify lignin's structure to enhance its anti-ageing properties and compare with other natural antioxidants.
30	Wu & Hou, 2024	1	Bio-oil reduced stiffness and brittleness, improved fatigue resistance, and enhanced adhesion and moisture resistance. 2. Improved flexibility and thermal crack resistance at low temperatures.	Investigate the scalability and economic feasibility of bio-oil usage in large-scale asphalt production and application

Note.

1	Rutting	11	Temperature susceptibility
2	Cracking	12	Storage Stability
3	Ravelling	13	Elastic Properties
4	Permanent Deformation	14	Resilience modulus
5	Stripping resistance	15	Softening Points
6	Rheological Properties	16	Surface activities of emulsifier
7	Viscosity	17	Environmental Impact
8	Fatigue	18	Economic Impact
9	Aging	19	Mechanical Performance
10	Moisture susceptibility	20	Oil absorption

CONCLUSION

This paper reviewed the potential of lignin as a sustainable resource for use in asphalt materials. The utilisation of lignin as bio-binders in asphalt mixtures was assessed through laboratory experiments. Based on the cited literature, using lignin as a modifier, extender, or bitumen replacement is a viable alternative. This is because its utilisation appears to ensure performance on par with or superior to that of standard reference materials. Overall, this review demonstrates the significant potential of lignin as a sustainable bio-binder for asphalt pavement, offering both environmental and technical advantages. Specifically, lignin-modified asphalt has been found to enhance thermal stability, increase resistance to rutting and deformation, and provide superior anti-ageing properties, thereby extending pavement service life. These findings align with global efforts to reduce greenhouse gas emissions and transition towards more sustainable construction materials, as lignin offers a renewable alternative to traditional petroleum-based asphalt binders. Additionally, lignin's ability to enhance asphalt's oxidation resistance can slow the ageing process, further boosting the longevity of asphalt pavements.

However, several technical challenges remain that need to be addressed before the widespread adoption of lignin in asphalt mixtures. One of the primary concerns is lignin's compatibility with asphalt, particularly when optimising its concentration in the binder. While high lignin content can improve certain properties like rutting resistance and viscosity, it may also reduce the binder's fatigue life and low-temperature cracking resistance. This trade-off underscores the need for careful balance in lignin content to avoid compromising essential mechanical properties. Moreover, the chemical interactions between lignin and other additives, such as anti-rutting agents, require further exploration to ensure stable, consistent performance across different environmental and traffic conditions.

ACKNOWLEDGEMENT

This study was not supported by any grants from funding bodies in the public, private, or not-for-profit sectors.

REFERENCES

Abdelsalam, M., Yue, Y., Khater, A., Luo, D., Musanyufu, J., & Qin, X. (2020). Laboratory study on the performance of asphalt mixes modified with a novel composite of diatomite powder and lignin fibre. *Applied Sciences, 10*(16), Article 5517. https://doi.org/10.3390/app10165517

Al-Moubaraki, A. H., & Obot, I. B. (2021). Corrosion challenges in petroleum refinery operations: Sources, mechanisms, mitigation, and future outlook. *Journal of Saudi Chemical Society, 25*(12), Article 101370. https://doi.org/10.1016/j.jscs.2021.101370

Arafat, S., Kumar, N., Wasiuddin, N. M., Owhe, E. O., & Lynam, J. G. (2019). Sustainable lignin to enhance asphalt binder oxidative ageing properties and mix properties. *Journal of Cleaner Production, 217*, 456-468. https://doi.org/10.1016/j.jclepro.2019.01.238

Arapova, O. V., Chistyakov, A. V., Tsodikov, M. V., & Moiseev, I. I. (2020). Lignin as a renewable resource of hydrocarbon products and energy carriers (A review). *Petroleum Chemistry, 60*(3), 227-243. https://doi.org/10.1134/S0965544120030044

Aro, T., & Fatehi, P. (2017). Production and application of lignosulfonates and sulfonated lignin. *ChemSusChem, 10*(9), 1861-1877. https://doi.org/10.1002/cssc.201700082

Batista, K. B., Padilha, R. P. L., Castro, T. O., Silva, C. F. S. C., Araújo, M. F. A. S., Leite, L. F. M., Pasa, V. M. D., & Lins, V. F. C. (2018). High-temperature, low-temperature and weathering ageing performance of lignin modified asphalt binders. *Industrial Crops and Products, 111*, 107-116. https://doi.org/10.1016/j.indcrop.2017.10.010

Boeriu, C. G., Fiţigău, F. I., Gosselink, R. J. A., Frissen, A. E., Stoutjesdijk, J. H., & Peter, F. (2014). Fractionation of five technical lignins by selective extraction in green solvents and characterisation of isolated fractions. *Industrial Crops and Products, 62*, 481-490. https://doi.org/10.1016/j.indcrop.2014.09.019

Bugg, T. D. H., Ahmad, M., Hardiman, E. M., & Rahmanpour, R. (2012). ChemInform abstract: Pathways for degradation of lignin in bacteria and fungi. *ChemInform, 43*(9). https://doi.org/10.1002/chin.201209276

Cai, M., Cheng, C., Luo, J., Ma, X., Wang, T., & Li, X. (2024). Effect of thermal oxygen ageing on rheological properties and chemical structure of lignin-modified asphalt. *Journal of Materials in Civil Engineering, 36*(9). https://doi.org/10.1061/JMCEE7.MTENG-18135

Cai, M., Zhao, X., Han, X., Du, P., Su, Y., & Cheng, C. (2022). Effect of thermal oxygen ageing mode on rheological properties and compatibility of lignin-modified asphalt binder by dynamic shear rheometer. *Polymers, 14*(17), Article 3572. https://doi.org/10.3390/polym14173572

Calvo-Flores, F. G. (2020). Lignin: A renewable raw material. In S. Hashmi & I. A. Choudhury (Eds.), *Encyclopedia of renewable and sustainable materials* (pp. 102–118). Elsevier. https://doi.org/10.1016/B978-0-12-803581-8.11517-6

Chen, M., Shi, L.-S., Tian, F., Xing, Y.-N., & Hui, Y.-J. (2017). Synthesis of triethylenetetraamine/formaldehyde modified lignin amine asphalt emulsifier and its investigation by online FTIR spectrophotometry. In I.-Z. Chen & Q. Li (Eds.), *Advanced materials and energy sustainability: Proceedings of the 2016 International Conference on Advanced Materials and Energy Sustainability (AMES2016)* (pp. 315-322). World Scientific. https://doi.org/10.1142/9789813220393_0040

Cheng, C., Sun, W., Hu, B., Tao, G., Peng, C., Tian, Y., & Wu, S. (2020). Analysis of the mechanism and effectiveness of lignin in improving the high-temperature thermal stability of asphalt. *Journal of Renewable Materials, 8*(10), 1243-1255. https://doi.org/10.32604/jrm.2020.012054

Collins, M. N., Nechifor, M., Tanasă, F., Zănoagă, M., McLoughlin, A., Stróżyk, M. A., Culebras, M., & Teacă, C. A. (2019). Valorisation of lignin in polymer and composite systems for advanced engineering applications–A review. *International Journal of Biological Macromolecules, 131*, 828-849. https://doi.org/10.1016/j.ijbiomac.2019.03.069

Duarte Mendonça, A. M. G., Melo Neto, O. de M., Rodrigues, J. K. G., Batista de Lima, R. K., Silva, I. M., & Marques, A. T. (2023). Characterisation of modified asphalt mixtures with lignin of pinus and eucalyptus woods. *Australian Journal of Civil Engineering, 21*(2), 253-264. https://doi.org/10.1080/14488353.2022.2089376

Gao, J., Wang, H., Liu, C., Ge, D., You, Z., & Yu, M. (2020). High-temperature rheological behaviour and fatigue performance of lignin modified asphalt binder. *Construction and Building Materials, 230*, Article 117063. https://doi.org/10.1016/j.conbuildmat.2019.117063

Gordobil, O., Herrera, R., Poohphajai, F., Sandak, J., & Sandak, A. (2021). Impact of drying process on kraft lignin: Lignin-water interaction mechanism study by 2D NIR correlation spectroscopy. *Journal of Materials Research and Technology, 12*, 159-169. https://doi.org/10.1016/j.jmrt.2021.02.080

Hu, D., Gu, X., Wang, G., Zhou, Z., Sun, L., & Pei, J. (2022). Performance and mechanism of lignin and quercetin as bio-based anti-ageing agents for asphalt binder: A combined experimental and ab initio study. *Journal of Molecular Liquids, 359*, Article 119310. https://doi.org/10.1016/j.molliq.2022.119310

Jin, X., Li, X., Liu, X., Du, L., Su, L., Ma, Y., & Ren, S. (2023). Simple lignin-based, light-driven shape memory polymers with excellent mechanical properties and wide range of glass transition temperatures. *International Journal of Biological Macromolecules, 228*, 528-536. https://doi.org/10.1016/j.ijbiomac.2022.12.098

Khadim, A., & Ahmad, N. (2024). Evaluating the effect of paper waste lignin in hot mix asphalt. *Engineering Research Express, 6*(2), Article 025105. https://doi.org/10.1088/2631-8695/ad3f72

Khandelwal, M. (2019). *Carbon footprint of lignin modified asphalt mix: A tree to gate LCA assessment* [Master's thesis, Utrecht University].

Khater, A., Luo, D., Abdelsalam, M., Ma, J., & Ghazy, M. (2021). Comparative life cycle assessment of asphalt mixtures using composite admixtures of lignin and glass fibres. *Materials, 14*(21), Article 6589. https://doi.org/10.3390/ma14216589

Khater, A., Luo, D., Abdelsalam, M., Yue, Y., Hou, Y., & Ghazy, M. (2021). Laboratory evaluation of asphalt mixture performance using composite admixtures of lignin and glass fibres. *Applied Sciences, 11*(1), Article 364. https://doi.org/10.3390/app11010364

Kong, L., Dai, L., & Wang, Y. (2023). Enhancing aromatic hydrocarbon formation via catalytic depolymerization of lignin waste over Ru/WOx/N-C catalyst. *Fuel, 332*, Article 126263. https://doi.org/10.1016/j.fuel.2022.126263

Kou, C., Wu, X., Xiao, P., Liu, Y., & Wu, Z. (2020). Physical, rheological, and morphological properties of asphalt reinforced by basalt fibre and lignin fibre. *Materials, 13*(11), Article 2520. https://doi.org/10.3390/ma13112520

Liu, Z. G., Zong, L., Zhao, L. L., & Xie, X. M. (2013). Preparation and storage stability of asphalt emulsions made from modified lignin cationic asphalt emulsifiers. *Applied Mechanics and Materials, 357-360*, 781-785. https://doi.org/10.4028/www.scientific.net/AMM.357-360.781

Luo, D., Khater, A., Yue, Y., Abdelsalam, M., Zhang, Z., Li, Y., Li, J., & Iseley, D. T. (2019). The performance of asphalt mixtures modified with lignin fibre and glass fibre: A review. *Construction and Building Materials, 209*, 377-387. https://doi.org/10.1016/j.conbuildmat.2019.03.126

Luz, P. M. S. G., Ziegler, C. R., Mendonça, A. M. G. D., & Rodrigues, J. K. G. (2021). Rheological evaluation of PG 64-22 asphalt binder modified with lignin of pinus and eucalyptus woods. *Materials and Structures, 54*(4), Article 166. https://doi.org/10.1617/s11527-021-01757-z

Min, D.-Y., Smith, S. W., Chang, H.-M., & Jameel, H. (2013). Influence of isolation condition on structure of milled wood lignin characterised by quantitative 13C nuclear magnetic resonance spectroscopy. *BioResources, 8*(2), 1790-1800. https://doi.org/10.15376/biores.8.2.1790-1800

Norgbey, E., Huang, J., Hirsch, V., Liu, W. J., Wang, M., Ripke, O., Li, Y., Takyi Annan, G. E., Ewusi-Mensah, D., Wang, X., Opoku, P. A., & Nkrumah, P. N. (2020). Unravelling the efficient use of waste lignin as a bitumen modifier for sustainable roads. *Construction and Building Materials, 230*, Article 116957. https://doi.org/10.1016/j.conbuildmat.2019.116957

Pe, J. A., III, Mun, J. S., & Mun, S. P. (2023). Thermal characterisation of kraft lignin prepared from mixed hardwoods. *BioResources, 18*(1), 926-936. https://doi.org/10.15376/biores.18.1.926-936

Peng, C., Huang, S., You, Z., Xu, F., You, L., Ouyang, H., Li, T., Guo, C., Ma, H., Chen, P., & Dai, J. (2020). Effect of a lignin-based polyurethane on adhesion properties of asphalt binder during UV ageing process. *Construction and Building Materials, 247*, Article 118547. https://doi.org/10.1016/j.conbuildmat.2020.118547

Putra, W. N., Syahwalia, R., Hendrasetyawan, B. E., Giovanni, S. C., & Chalid, M. (2017). Comparison study of polyethylene and polypropylene addition on asphalt with lignin as coupling agent. *Macromolecular Symposia, 371*(1), 140-143. https://doi.org/10.1002/masy.201600066

Rodríguez, A., Sánchez, R., Requejo, A., & Ferrer, A. (2010). Feasibility of rice straw as a raw material for the production of soda cellulose pulp. *Journal of Cleaner Production, 18*(10-11), 1084-1091. https://doi.org/10.1016/j.jclepro.2010.03.011

Shi, L.-S., Wang, T.-Y., Chen, M., Li, D.-M., & Ma, C.-F. (2016). Synthesis of aminoethylpiperazine/formaldehyde modified lignin amine asphalt emulsifier and its investigation by online FTIR spectrophotometry. In *Proceedings of the 4th 2016 International Conference on Material Science and Engineering (ICMSE 2016)* (pp. 133–138). Atlantis Press. https://doi.org/10.2991/icmse-16.2016.23

Sun, D., Sun, G., Du, Y., Zhu, X., Lu, T., Pang, Q., Shi, S., & Dai, Z. (2017). Evaluation of optimized bio-asphalt containing high content waste cooking oil residues. *Fuel, 202*, 529-540. https://doi.org/10.1016/j.fuel.2017.04.069

Tauste-Martínez, R., Hidalgo, A. E., García-Travé, G., Moreno-Navarro, F., & Rubio-Gámez, M. C. (2022). Influence of type of filler and bitumen on the mechanical performance of asphalt mortars. *Materials, 15*(9), Article 3307. https://doi.org/10.3390/ma15093307

Vishtal, A. G., & Kraslawski, A. (2011). Challenges in industrial application of technical lignins. *BioResources, 6*(3), 3547-3568. https://doi.org/10.15376/biores.6.3.3547-3568

Watkins, D., Nuruddin, M., Hosur, M., Tcherbi-Narteh, A., & Jeelani, S. (2015). Extraction and characterisation of lignin from different biomass resources. *Journal of Materials Research and Technology, 4*(1), 26-32. https://doi.org/10.1016/j.jmrt.2014.10.009

Wu, Q., & Hou, G. (2024). The impact of bio-oil on the structure, rheology, and adhesion properties of lignin-modified asphalt. *Materials Research Express, 11*(6), Article 065101. https://doi.org/10.1088/2053-1591/ad55ad

Wu, X., Easa, S., Kang, A., Xiao, P., Fan, Z., & Zheng, X. (2022). Performance evaluation of lignin-fibre reinforced asphalt mixture modified by anti-rutting agent. *Construction and Building Materials, 346*, Article 128152. https://doi.org/10.1016/j.conbuildmat.2022.128152

Xin, J., Li, M., Li, R., Wolcott, M. P., & Zhang, J. (2016). Green epoxy resin system based on lignin and tung oil and its application in epoxy asphalt. *ACS Sustainable Chemistry & Engineering, 4*(5), 2754-2761. https://doi.org/10.1021/acssuschemeng.6b00256

Xu, C., Wang, D., Zhang, S., Guo, E., Luo, H., Zhang, Z., & Yu, H. (2021). Effect of lignin modifier on engineering performance of bituminous binder and mixture. *Polymers, 13*(7), Article 1083. https://doi.org/10.3390/polym13071083

Xu, G., Wang, H., & Zhu, H. (2017). Rheological properties and anti-ageing performance of asphalt binder modified with wood lignin. *Construction and Building Materials, 151*, 801-808. https://doi.org/10.1016/j.conbuildmat.2017.06.151

Xue, X., Gao, J., Wang, J., & Chen, Y. (2022). Evaluation of high-temperature and low-temperature performances of lignin–waste engine oil modified asphalt binder and its mixture. *Materials, 15*(1), Article 52. https://doi.org/10.3390/ma15010052

Yao, H., Wang, Y., Liu, J., Xu, M., Ma, P., Ji, J., & You, Z. (2022). Review on applications of lignin in pavement engineering: A recent survey. *Frontiers in Materials, 8*, Article 803524. https://doi.org/10.3389/fmats.2021.803524

Yin, C., Wang, M., Ma, Q., Bian, H., Ren, H., Dai, H., & Cheng, J. (2021). Valorisation of rice straw via hydrotropic lignin extraction and its characterisation. *Molecules, 26*(14), Article 4123. https://doi.org/10.3390/molecules26144123

Yu, J., Vaidya, M., Su, G., Adhikari, S., Korolev, E., & Shekhovtsova, S. (2021). Experimental study of soda lignin powder as an asphalt modifier for a sustainable pavement material. *Construction and Building Materials, 298*, Article 123884. https://doi.org/10.1016/j.conbuildmat.2021.123884

Yue, Y., Abdelsalam, M., Khater, A., & Ghazy, M. (2022). A comparative life cycle assessment of asphalt mixtures modified with a novel composite of diatomite powder and lignin fibre. *Construction and Building Materials, 323*, Article 126608. https://doi.org/10.1016/j.conbuildmat.2022.126608

Yuliestyan, A., Gabet, T., Marsac, P., García-Morales, M., & Partal, P. (2018). Sustainable asphalt mixes manufactured with reclaimed asphalt and modified-lignin-stabilized bitumen emulsions. *Construction and Building Materials, 173*, 662-671. https://doi.org/10.1016/j.conbuildmat.2018.04.044

Yuliestyan, A., García-Morales, M., Moreno, E., Carrera, V., & Partal, P. (2017). Assessment of modified lignin cationic emulsifier for bitumen emulsions used in road paving. *Materials & Design, 131*, 242-251. https://doi.org/10.1016/j.matdes.2017.06.024

Yuliestyan, A., Partal, P., Navarro, F. J., Martín-Sampedro, R., Ibarra, D., & Eugenio, M. E. (2022). Emulsion stabilization by cationic lignin surfactants derived from bioethanol production and kraft pulping processes. *Polymers, 14*(14), Article 2879. https://doi.org/10.3390/polym14142879

Zhang, Y., Wang, X., Ji, G., Fan, Z., Guo, Y., Gao, W., & Xin, L. (2020). Mechanical performance characterization of lignin-modified asphalt mixture. *Applied Sciences, 10*(9), Article 3324. https://doi.org/10.3390/app10093324

Zhao, Z. D., Xie, Y., Cheng, X. S., Jin, Y. Q., & Xu, M. Y. (2011). Research on enzymatic hydrolysis lignin modified petroleum asphalt. *Advanced Materials Research, 306-307*, 1080-1083. https://doi.org/10.4028/www.scientific.net/AMR.306-307.1080

REFEREES FOR THE PERTANIKA

JOURNAL OF SCIENCE & TECHNOLOGY

Vol. 34 (S2) 2026

The Editorial Board of the Pertanika Journal of Science and Technology wishes to thank the following:

Abdul Rahman Saili
(UiTM, Malaysia)

Anis Azmi
(UKM, Malaysia)

Azinoor Azida
(UiTM, Malaysia)

Azlinda Saadon
(UiTM, Malaysia)

Balqis binti Md Yunus
(UiTM, Malaysia)

Eeydzah Aminudin
(UiTM, Malaysia)

Khairil Azman Masri
(UMPSA, Malaysia)

Low Wen Pei
(INTI, Malaysia)

Mazlina Binti Mohamad
(UiTM, Malaysia)

Neni Kartini Che Mohd Ramli
(UiTM, Malaysia)

Niraku R Ahmad
(UTP, Malaysia)

Norisham Binti Ibrahim
(UiTM, Malaysia)

Nur Izzati Ab Rani
(UiTM, Malaysia)

Nurlaila Ismail
(UiTM, Malaysia)

Nurul Hidayah Mohd Kamaruddin
(UTHM, Malaysia)

Nurul Izzatul Lydia Za'ba
(SEGi, Malaysia)

Shahrul Azwan Shakrani
(UniMAP, Malaysia)

Suzana Ramli
(UiTM, Malaysia)

Wael Abdelhafeez Mohamed Abdelhameed
(ASU, Bahrain)

ASU : *Applied Science University*
INTI : *INTI International University*
SEGi : *SEGi University*
UiTM : *Universiti Teknologi MARA*
UKM : *Universiti Kebangsaan Malaysia*
UMPSA : *Universiti Malaysia Pahang Al-Sultan Abdullah*
UniMAP : *Universiti Malaysia Perlis*
UTHM : *Universiti Tun Hussein Onn Malaysia*
UTP : *Universiti Teknologi PETRONAS*

While every effort has been made to include a complete list of referees for the period stated above, however if any name(s) have been omitted unintentionally or spelt incorrectly, please notify the Chief Executive Editor, *Pertanika* Journals at executive_editor.pertanika@upm.edu.my

Any inclusion or exclusion of name(s) on this page does not commit the *Pertanika* Editorial Office, nor the UPM Press or the university to provide any liability for whatsoever reason.

Enhancing Health and Safety Practices by Complying with SOP Requirements at Construction Sites During the Pandemic 89
Siti Rashidah Mohd Nasir, Sulaiman Hasim, and Eleanna Guan

Strength and Durability Performance of Three-Layered Leucaena Leucocephala Cement-Bonded Particleboard 101
Marzuki Ab. Rahman, Mohd Fakri Muda, Mohd Razmi Zainudin, Muhammad Isha Ismail, Farah Wahida Mohd Latib, Amminudin Ab Latif, Noor Safwan Muhamad, Wan Zukri Wan Abdullah, Herlien Dwiarti Setio, and Mohd Hisbany Mohd Hashim

Review Article 117
The Use of Lignin as Bio-Binder for Sustainable Asphalt Pavement - A Recent Review
Amminudin Ab Latif, Mohd Fakri Muda, Noor Safwan Muhamad, Marzuki Ab. Rahman, Muhammad Isha Ismail, Mohd Razmi Zainudin, Farah Wahida Mohd Latib, and Wan Zukri Wan Abdullah

Pertanika Journal of Science & Technology
Vol. 34 (S2) 2026

Content

Preface xi
Rohana Hassan, Mohd Fadzil Arshad, and Fauzi Baharudin

Removal of Methylene Blue Using Durian Peel: A Column Experiment 1
Jurina Jaafar, Nur Azwa Zulkefli, Zulhafizal Othman, Siti Rashidah Mohd Nasir, Shariff Ibrahim, and Nur Qudus

Self-Healing Ability of Steel Fibre Asphalt Mixture Using Microwave Heating and Semi-Circular Bending Test 15
Ekarizan Shaffie, Fionna Shiong, Ahmad Kamil Arshad, Mohd Khairul Afzan Mohd Lazi, Muhammad Ibrahim Khalili Abd Rahim, and Ramadhansyah Putra Jaya

Hybrid Solar PV-Micro-Hydro System for Sustainable Electrification of Remote Communities in Arunachal Pradesh, India 29
Somila Hashunao, Taken Nguri, A.S Shimreiwung, Ngayaiwon Hashunao, and Ram Krishna Mehta

Correlation Between Compressive and Flexural Properties in Steel Fibre Reinforced Concrete (SFRC) Beam Using Regression Analysis 37
Md Yushairi Kamarul Effendy Mohd Yusof, Anizahyati Alisibramulisi, Muhd Norhasri Muhd Sidek, Nadiah Saari, and Suraya Hani Adnan

Evaluation of the Causes of On-Farm Food Loss in Cabbage Production: A Case Study in the Large-Scale Farming Group of Hot District, Chiang Mai, Thailand 51
Pichayapak Channiyamathorn, Suraphol Sreshthaputra, Ruth Sirisanyaluck, and Juthathip Chalermphol

Influence of Tree Canopy Characteristics on Rainfall Interception, Throughfall and Stemflow in a Tropical Forest 65
Azinoor Azida Abu Bakar and Muhammad Khairudin Khalil

Experimental and Finite Element Analysis of Shear Strength in Melunak and Mengkulang Glulam Using Shear Block Test 75
Nor Jihan Abd Malek, Rohana Hassan, Mohd Nizam Shakimon, Nurharniza Abdul Rahman, Nazrul Azmi Ahmad Zamri, and Khaled M.H. Alreqeb

Pertanika Editorial Office, Journal Division,
Putra Science Park,
1st Floor, IDEA Tower II,
UPM-MTDC Center,
Universiti Putra Malaysia,
43400 UPM Serdang,
Selangor Darul Ehsan
Malaysia

http://www.pertanika.upm.edu.my
Email: executive_editor.pertanika@upm.edu.my
Tel. No.: +603- 9769 1622

http://penerbit.upm.edu.my
Email: penerbit@upm.edu.my
Tel. No.: +603- 9769 3606

e-ISSN 2231-8526